IN VITRO AND *IN VIVO* CHARACTERIZATION OF A CELL SOURCE FOR BONE TISSUE ENGINEERING APPLICATIONS: PRIMARY BONE MARROW STROMAL CELLS OVEREXPRESSING THE OSTEOBLAST-SPECIFIC TRANSCRIPTIONAL ACTIVATOR RUNX2/CBFA1

A Dissertation
Presented to
The Academic Faculty

by

Benjamin Allen Byers

In Partial Fulfillment
of the Requirements for the Degree
Doctor of Philosophy in Bioengineering
George W. Woodruff School of Mechanical Engineering

Georgia Institute of Technology
December 2003

IN VITRO AND _IN VIVO_ CHARACTERIZATION OF A CELL SOURCE FOR BONE TISSUE ENGINEERING APPLICATIONS: PRIMARY BONE MARROW STROMAL CELLS OVEREXPRESSING THE OSTEOBLAST-SPECIFIC TRANSCRIPTIONAL ACTIVATOR RUNX2/CBFA1

Approved by:

Dr. Andrés J. García, Advisor

Dr. Julia E. Babensee

Dr. Barbara D. Boyan

Dr. Robert E. Guldberg

Dr. Joseph M. LeDoux

Dr. Grace K. Pavlath

Date Approved: December 8, 2003

To my wife and family for your support, faith, and love

ACKNOWLEDGEMENTS

I express my most sincere gratitude to my advisor, Dr. Andrés J. García, for his integral role in guiding my development and maturation as a student, independent researcher, and person. He provided tremendous opportunities to make the most of my graduate career, and I am eternally grateful for the 'constant but subtle pressure' that motivated me to strive for perfection and success. We began our relationship as 'rookies' in different phases of our lives, an aspiring new assistant professor with no students or laboratory and a green graduate research assistant who really had no idea what he wanted to do. In the end, I could not have imagined a more ideal situation. Our personalities, objectives, and life passions were quite remarkably similar, and our differences provided the spice to make us an even stronger and more productive team. As one of his first students, it was truly a unique and special experience to be involved from the beginning and observe the profound success he enjoyed in the early stages of his career. Reflecting on the past five and half years, I marvel at my good fortune in being blessed with a mentor who has been so dedicated, supportive, understanding, and encouraging. Most of all, however, I value our friendship, which will last a lifetime.

I gratefully acknowledge the support and dedication of my dissertation committee for their contributions in the development of this research and my maturation as a scientist: Dr. Robert E. Guldberg for sharing his expertise in sterile surgical technique and micro-CT and devoting extensive time during some rather lengthy days of surgery; Dr. Barbara D. Boyan for providing resources and scientific expertise and insight which strengthened my work, attitude, and professional development; Dr. Grace K. Pavlath for

the willingness to collaborate and provide an engineer with excellent training in plasmid cloning and retroviral transduction techniques; Dr. Joseph M. LeDoux for many helpful discussions and providing an extra centrifuge which shortened those seemingly never ending days of retroviral transduction; and Dr. Julia E. Babensee for stimulating discussion and scientific direction.

I gratefully acknowledge funding support from the National Institutes of Health (R01-EB003364), the Georgia Tech/Emory NSF Engineering Research Center on Tissue Engineering (EEC-9731643) and the Emory-Georgia Tech Biomedical Technology Research Center which were instrumental in the completion of this work.

I also express extensive appreciation to all of those individuals who were influential in the completion of this work: Dr. Gerard Karsenty for providing the Runx2/Cbfa1/Osf2 sequence and a 'frustratingly incomplete' plasmid map; Dr. T.J. Murphy for helpful cloning discussions during my time at Emory University; Dr. Harish Radhakrishna for multiple 'molecular biology' conversations; Dr. Zvi Schwartz for his scientific expertise, early morning and late night conversations, and introducing me to 'the dental tool'; Dr. Don Ranly for his devoted consultation and histomorphometry training; Dr. Dietmar Hutmacher for providing the fused deposition-modeled polycaprolactone scaffolds and introducing me to Kobe beef; Steve Woodard and Johnafel Crowe for outstanding technical support in flow cytometry over the years; Dr. Laura O'Farrell for overseeing, consulting, and assisting in animal surgeries; Cherry Forkey and Kelly Winn for providing an outstanding environment for animal surgery (except for the occasional poor selection of music), unyielding devotion during long, frustrating, and stressful days of surgery, and unparalleled post-operative animal care;

and Tracey Couse for her spirited guidance and assistance in histology and immunohistochemistry, stimulating political discussions, and informative conversations on U.S.-Canadian immigration laws.

Several individuals contributed significantly to my scientific development and personal growth while at Georgia Tech, which was truly a unique institution to pursue a graduate education. I specifically thank Dr. Robert M. Nerem, Director of the Petit Institute for Bioengineering and Bioscience and the Georgia Tech/Emory Center for the Engineering of Living Tissues, for his incomparable devotion to student development, commitment to providing remarkable scientific resources and facilities in the bioengineering community at Georgia Tech, and personal encouragement and support of my active participation in GTEC; all of the IBB and GTEC staff, especially Donna Brown for her patience, guidance, friendship and Sally Gerrish for her support, friendship, and never-ending desire to discuss Indiana University basketball or the next big 'Bob Knight fiasco'. Finally, I would like to thank Dr. Ward O. Winer and Dr. Bill Wepfer of the George W. Woodruff School of Mechanical Engineering for enabling me to contribute to and benefit from such a wonderful engineering program and, perhaps of equal importance, agreeing to provide additional travel support to a then second year graduate student so that he could travel to the World Congress of Biomaterials in Kona, Hawaii in order to meet his soul mate.

My colleagues and friends in the García lab made this experience truly special by contributing to my growth in the lab and in life. At one point or another, each of them assisted in the successful completion of my dissertation research. Whether it was a massive media change during one of my many trips north of the border or opening up yet

another pair of sterile gloves during surgery, I couldn't have done it without them. I'm eternally grateful for their dedication and support, and I wish them all the utmost happiness and success in their careers and more importantly their personal lives. There are so many memories which we share, and because I am proudly 'disagreeably verbose', it would remiss to not include a short message thanking each of them personally: Benjamin Keselowsky (forever known as B.K.), who would have thought Andrés would draft two guys with same name in his first year as an advisor? We started together, struggled together, became great friends, and our musical duets at the far end of the bench and in the culture room remain lasting memories which I will definitely long for in the next phase of my career and beyond. Nate Gallant, whenever comic relief was required but more frequently when it was wholly inappropriate, he never failed to come through in the clutch. I thank him for being such a wonderful friend, dedicated and motivated weight lifting partner, and the ideal 'last call power drinker'. Catherine Reyes, whom I had the extreme privilege of sitting 'behind' and working beside for so many years, our conversations about science, Catholicism, and life-in-the-universe will be forever remembered. She provided me the ultimate honor as a friend by reading at my wedding, and I will always cherish her involvement in our special day. Kristin Michael, I sincerely appreciate her way of making me and everyone in the lab feel comfortable and special, whether it was randomly treating us to Krispy Kreme and OJ or organizing the day's lunch run to Jersey Mike's, she always gave so much of herself to make the rest of us feel great. Jeff Capadona, what can I say about a chemist, a country music buff, and a Cubs fan…that's three strikes, right? In all seriousness, I extend my sincere gratitude for how helpful he was on a couple of late night, last minute FT-IR phone calls and being

such a great person to be around. Charlie Gersbach (Chuckles, but more affectionately know as Chuck E. Pooh) will forever be my 'Runx2 brother' and confidant. I will never forget the multitude of Runx2 discussions over Rocky Mountain Brew, wings, chicken tender salads, and an occasional entire slice of pizza eaten in one bite. It was an honor and a privilege working with him on this project, and I leave Tech knowing that Runx2 will prosper in his more than capable hands. I express my sincere gratitude for his unyielding assistance and dedication to the cause throughout the last few years. Jenn Phillips (the 'self-anointed' Queen of Runx2), in the lifetime of a Ph.D. project our overlap was unfortunately brief; however, I enjoyed every fad diet, silly nickname (C. Elegans), and especially the stimulating scientific conversations. I'm grateful that she, too, is carrying the Runx2 research torch, as her dedication and professionalism are remarkable. Sean Stephansson was perhaps the best and most devoted Undergraduate Research Scholar I could have ever hoped to mentor and befriend. Finally, I extend my utmost gratitude to Lindsay Bryant, the lab caregiver, organizer, and sometimes even enforcer and peacemaker, who made our lives much less complicated. She was and always will be a dear friend and blessing in every since of the word, and I truly appreciate all that she did each day to absorb stresses and make everything function so smoothly.

Acknowledgements must also be given to those members of the Guldberg lab, Wing 2D, and the IBB who contributed so diligently to my work and graduate school experience: Angel Duty for coaching me in the art of subcutaneous implantation and countless other techniques; Natasha Case for meaningful hours of scientific conversation and late night research fests; Blaise Porter for being an outstanding confocal microscopy consultant, devoted friend and roommate, and a wonderful co-supporter of Georgia Tech

athletics…we'll always have Joe Hamilton and the Kelly Campbell end around; the "Big Three", Srin Nagaraja, Angela S.P. Lin (Geela), and Galen Robertson (G-Rob), for their tireless micro-CT assistance; Geela (president), Srin (vice-president), and Catherine (treasurer) who along with myself (secretary) comprised the Procrastination Corner, perhaps the most amazing, entertaining, and poorly lit work environment in the entirety of the IBB; Craig Duvall and Chris Gemmiti for additional micro-CT support, stimulating sports conversations, Super Bowl parties, and pick-up games; and Blaise Porter (again) and Bryan Marshall for giving a 'homeless' married guy space for his 'couch-bed' for the final five months and relentlessly applying pressure until a finally made it to a Thrashers game (a 4-1 loss to the Leafs, but we did get a knit cap, that did fit, although snuggly!).

Throughout my undergraduate education in Chemical Engineering at Rose-Hulman Institute of Technology, a variety of talented individuals gave of themselves to educate and motivate me toward great things, specifically Dr. Samuel F. Hulbert, Dr. Noel E. Moore, Dr. Carl F. Abegg, Dr. Ronald S. Artigue, Dr. Jerry A. Caskey, Dr. Stuart M. Leipziger, Dr. M. Hossein Hariri, and Dr. Mark D. Ball. Two outstanding internship mentors, Brian Cognata of Pfizer, Incorporated and Gary Solbrekken of Intel Corporation, I reflect in appreciation of their 'burdening' me with great responsibility, continuously challenging me as they prepared me for the future and gave me the freedom to grow as an engineer. I owe much gratitude to the men of the Rose Tech Chapter of Triangle Fraternity for late night study sessions and pool tournaments in undergrad, but more importantly I'm eternally indebted for their F, S, & C. Dr. Chris Litteken and Dr. Nick Bosco, I thank for providing the initial motivation and friendship which instigated my decision to attend graduate school. Finally, I thank all of the teachers at Southridge

High and Middle Schools and Holland Elementary School for pushing me, educating me, and sending me into the world well-prepared to tackle life's big challenges.

My family, who I shared this work and experience with mostly from afar, was a source of great strength and inspiration, and I express my sincere love and gratitude for all of their support over the years. My grandparents, Carl and Lu Byers and the late Jack Ellis and Joann Ellis Bacon, I'm so grateful for everything they did for me over the years, and I was very fortunate to be the oldest grandchild in order to have so many years of receiving their love and affection. My younger brothers, James Andrew and Dustin Leigh, and sister-in-law, Jennifer, I thank for many happy memories growing up and sharing recent family moments and experiences. I'm so proud of all that they have done so far and will continue to do in the future. My little sister and apple of my eye, Amber Lynn, I will always cherish the opportunities I had to take you on backyard camping trips, and it has been so amazing to see you grow up, even though I have been away from home for so long.

My parents have given so much of themselves throughout my life in support of my growth, maturation, and education, and I owe them more gratitude, love, and respect than I can ever describe in words. I'm grateful to my Dad and 'Wicked-Step-Mother', Frank and Terri Byers, for their devotion to always making that roundtrip drive to pick me up and take me home on the weekends so that I could always be a part of family activities, being so supportive in all of my life's endeavors, and treating me with a great deal of respect and dignity. They continuously supported my diversity through camping and hunting trips and adventures in lawn mowing (some more successful than others) and insisted that I keep trying to ride that bike no matter how intensely I resisted. I learned a

great deal during my summertime employment at Frank's Heating & Air Conditioning, but I must say the motivation I gained to work hard in school so that someday I could use my brains rather than my brawn (ha-ha) was far and away the most invaluable. Finally, my Mom and Step-Dad, Linda and Dan Buening, who have been a truly blessing with their love and support throughout all of my years of education at every level. I will always cherish how hard my mother worked when I was growing up, placing my interests and commitments unselfishly ahead of her own. In addition to understanding that I really did have to do homework in front of the television in order to acquire the proper amount of background noise, I thank her for putting me in Boy Scouts and Little League and sticking with me through high school sports, driving me around when the weather was too cold to deliver newspapers on my bike, and doing all that she could to send me on the trip to Europe after completing high school. Quite simply, she provided me with unlimited experiences and opportunities to grow up and learn while doing it. None of what I have accomplished in life to this point would have been possible without her, and this dissertation is a tribute to her hard work as much as it is my own.

I am forever indebted to my best friend and wonderful wife, Dolores, for the unconditional love and support that she provided during our intertwined progression toward the completion of our doctoral programs. As I write these words, I reflect on how we overcame the most challenging phase of our lives, which included eight hundred some miles of separation, nearly four years of religious daily phone conversations and numerous trips to Hartsfield and Pearson, joyous reunifications, and tearful and often painful goodbyes. We definitely put our professional aspirations and previous commitments ahead of our own perhaps more selfish personal preference of just being

together. She is a true inspiration to me, and I've come to admire so much about her through this experience we have shared. In addition to diligently completing her own dissertation research, she masterfully planned our wedding day to the finest detail. She was a scientific sounding board, a tough critic when she had to be, but always my biggest supporter through thick and thin. A more perfect story could not have been scripted, and who would have ever thought that a happenstance encounter at a beachside lounge at a conference in Hawaii and the ensuing discussion over serum and cell culture techniques would blossom into such a perfect friendship, partnership, and lifelong, loving relationship. Our graduate school days enabled us to experience many outstanding places and locations together, but through all of that, I now look forward to just sharing the simple things in life with her and only her…household chores, trips to the coffee shop, going to Mass, and, most importantly, raising a family. I sincerely thank her for loving and supporting me in way which only she could…

Finally, I thank God for the many blessings He has bestowed upon me. It is through the strength He gives me and the love He shows me that I have found happiness.

TABLE OF CONTENTS

LIST OF TABLES

LIST OF FIGURES

LIST OF APPENDICES

GLOSSARY

ALP	alkaline phosphatase
BMP	bone morphogenetic protein
BSP	bone sialoprotein
Cbfa	core binding factor
COL	collagen
ECM	extracellular matrix
eGFP	enhanced green fluorescent protein
FBS	fetal bovine serum
FGF	fibroblast growth factor
FT-IR	fourier transform infrared
IGF	insulin-like growth factor
IRES	internal ribosomal entry site
NCS	newborn calf serum
OCN	osteocalcin
OPN	osteopontin
OSE	osteocalcin-specific element
PCL	poly(ε-caprolactone)
PCR	polymerase chain reaction
PDGF	platelet-derived growth factor
PLGA	polylactide-co-glycolide
RT	reverse transcriptase
Runx	runt-related gene
TGFβ	transforming growth factor-β

SUMMARY

Bone grafting is of significant clinical importance in orthopaedic, craniomaxillofacial, and dental reconstruction procedures. Bone tissue engineering strategies are currently being developed as alternative mechanisms to address the clinical demand for bioactive and biomechanical graft material. To date, these efforts have been largely restricted by inadequate supply of committed osteoprogenitor cells and loss of osteoblastic phenotype expression following *in vitro* culture and expansion.

The objective of this thesis research was to address the cell sourcing limitations of tissue-engineered bone grafts by combining the fundamental principles of osteoblast biology and genetic and tissue engineering. Specifically, the osteoblast-specific transcriptional activator Runx2/Cbfa1 was overexpressed in osteogenic target cells using retroviral gene delivery. It was hypothesized that sustained overexpression of Runx2 in marrow-derived primary stromal cells would augment osteoblastic differentiation, including osteoblast-specific gene and protein expression and matrix mineralization, both *in vitro* and *in vivo*. Following initial characterization of this Runx2 overexpression system in model non-osteoblastic and osteoblast-like cell lines, the global objective and hypothesis were tested through *in vitro* evaluation of Runx2-expressing marrow-derived stromal cells in monolayer culture and on three-dimensional (3-D) polymeric, biodegradable scaffolds, including both polylactide-co-glycolide (PLGA) foams and poly(ε-caprolactone) (PCL) fused deposition-modeled scaffolds. Additionally, the *in vivo* performance of Runx2-expressing stromal cells was evaluated in two systems, subcutaneous and craniotomy defect syngeneic animal models.

Runx2 overexpression in marrow-derived stromal cells enhanced expression of multiple osteoblastic genes, including osteocalcin and collagen type I, as well as alkaline phosphatase biochemical activity. More importantly, matrix mineralization was up-regulated nearly two-fold following 2 and 3 weeks of *in vitro* culture. To evaluate their performance in bone tissue engineering applications, Runx2-expressing cells were seeded onto PLGA and PCL polymeric scaffolds. These two 3-D matrices possessed substantially different physical characteristics including pore size, strut architecture, and physical integrity. Supporting flexibility of this genetic engineering system, Runx2-transduced cells demonstrated significantly higher levels of 3-D mineralization when cultured on either scaffold compared to control cell-seeded scaffolds.

To evaluate *in vivo* performance, Runx2-expressing cells were seeded onto PLGA scaffolds and subcutaneously implanted following various *in vitro* culture durations. Minimal quantifiable mineral was present on Runx2 or control constructs implanted following only 1 or 7 days of pre-culture, time points representing more immature scaffolds. Notably, Runx2-transduced cell-seeded constructs pre-cultured to a mineralizing state *in vitro* (21 days) prior to implantation demonstrated a 10-fold increase in total mineral deposition and a 5-fold increase in the average daily mineral deposition rate upon subsequent *in vivo* implantation compared to similarly pre-cultured control cells, demonstrating a synergistic effect of Runx2 overexpression and *in vitro* construct development.

Finally, Runx2 overexpression and *in vitro* construct maturation was examined in a critical size craniotomy defect model in syngeneic rats. In this study, Runx2 overexpressing and control cells were seeded on PCL fused deposition-modeled scaffolds

possessing a macroporous, fully interconnected architecture. Defects treated with cell-free PCL scaffolds demonstrated a significant healing response, suggesting that in this particular bone defect model, the open architecture and interconnected structural network of the fused deposition-modeled scaffolds provided a suitable osteoconductive scaffold capable of supporting significant new bone formation by infiltrating host cells. Further supporting these observations, immature cell-seeded scaffolds implanted 1 day after cell seeding demonstrated healing comparable to cell-free scaffolds independent of treatment. In contrast to observations from the subcutaneous animal model, *in vitro* construct development for 21 days demonstrated an inhibitory effect on subsequent *in vivo* bone formation in defects receiving control bone marrow stromal cell-seeded constructs. As observed in the subcutaneous model, however, defects receiving Runx2-modified cell-seeded PCL constructs pre-cultured for 21 days demonstrated significantly more new bone formation than similarly pre-cultured control constructs. The amount of new bone formation in Runx2-modified cell-seeded, 21 day pre-cultured constructs was comparable to cell-free scaffold and 1 day pre-culture construct groups, suggesting that Runx2 overexpression in pre-cultured bone marrow stromal cells enhanced subsequent *in vivo* implant performance capable of overcoming the inhibitory effects on new bone formation observed in response to extended *in vitro* pre-culture of control cells.

Collectively, these studies provided a thorough characterization regimen to observe the *in vitro* and *in vivo* performance of Runx2-expressing marrow-derived stromal cells and evaluated their potential as a candidate cell source for bone tissue engineering applications. Furthermore, this series of analyses provided a novel combination of tissue and genetic engineering techniques toward the development of a

Runx2-modified stromal cell/polymeric scaffold composite tissue-engineered bone graft substitute.

CHAPTER 1

INTRODUCTION

Bone grafting is of significant clinical importance in orthopaedic, craniomaxillofacial, spine, and dental reconstruction procedures. Although current clinical solutions, which include autologous and allogenic grafts, are successful in principle and function, these efforts are ultimately limited by the availability of donor bone, donor site morbidity, potential for immune rejection, processing-related reductions in biological activity, and risk of infection and disease transmission (Khan et al., 2000; Bucholz, 2002). Bone tissue engineering strategies, developed by dispersing an osteogenic cell source in a 3-D scaffold or carrier matrix, have emerged as promising alternatives to address the clinical demand for bone grafting material. To date, however, these efforts have been restricted by an inadequate supply of committed osteoprogenitor cells and loss of osteoblastic phenotype expression following *in vitro* expansion and culture (Bruder et al., 1997; Shi et al., 2002).

The objective of this thesis research was to address current cell sourcing limitations associated with bone tissue engineering strategies through exogenous overexpression of the osteoblast-specific transcriptional activator Runx2/Cbfa1 in an osteogenic cell population to enhance osteoblastic phenotype expression *in vitro* and *in vivo*. Specifically, this work focused on (i) the *in vitro* evaluation of primary bone marrow stromal cells genetically engineered to overexpress Runx2 in both monolayer and 3-D culture and (ii) the *in vivo* characterization of Runx2-expressing stromal cells in both subcutaneous and critical size craniotomy defect animal models. **It was hypothesized**

that sustained overexpression of Runx2 in osteogenic bone marrow stromal cells would augment osteoblastic differentiation, including osteoblast-specific gene and protein expression and matrix mineralization, both *in vitro* and *in vivo*, thereby providing an alternative cell source for the development of tissue-engineered bone graft substitutes. Functional Runx2 expression is essential to embryonic bone formation (Otto et al., 1997; Komori et al., 1997) and postnatal, physiologic bone turnover (Ducy et al., 1999). Additionally, forced expression of Runx2 in non-osteoblastic cells induces expression of other osteoblast-specific genes, including osteocalcin (Ducy et al., 1997; Xiao et al., 1999; Byers et al., 2002). More importantly, overexpression of Runx2 in the MC3T3-E1 immature osteoblast-like cell line resulted in acceleration and robust up-regulation of *in vitro* mineralized matrix production (Byers et al., 2002). The global objective was addressed by the following specific aims:

Aim 1: To genetically engineer primary bone marrow stromal cells to overexpress the osteoblast-specific transcription factor Runx2/Cbfa1 to augment *in vitro* osteoblastic differentiation and enhance synthesis of mineralized matrix production in monolayer culture. Transient overexpression (Ducy et al., 1997) and sustained, constitutive overexpression of Runx2 using a retroviral expression system (Byers et al., 2002) in non-osteoblastic and osteoblast-like cells induced or up-regulated osteoblast-specific gene expression, respectively. Additionally, exogenous Runx2 expression accelerated and up-regulated *in vitro* matrix mineralization in the MC3T3-E1 immature osteoblast-like cell line (Byers et al., 2002). Based on these initial studies, it was expected that the osteogenic subpopulation of the marrow stroma would be responsive to

Runx2 overexpression, resulting in robust up-regulation in osteoblast-specific gene expression and matrix mineralization *in vitro*.

Aim 2: To incorporate genetically engineered stromal cells into polymeric scaffolds to evaluate the effect of Runx2 overexpression on osteoblastic differentiation, specifically matrix maturation and mineralization, following 3-D *in vitro* culture. Runx2-expressing or unmodified stromal cells were seeded onto polymeric, biodegradable constructs for bone tissue engineering applications, namely polylactide-co-glycolide (PLGA) foams and poly(ε-caprolactone) (PCL) fused deposition-modeled scaffolds. It was hypothesized that *in vitro* cultured constructs containing Runx2-modified stromal cells would demonstrate enhanced osteoblastic phenotype expression and up-regulated mineralized matrix production compared to scaffolds seeded with unmodified cells.

Aim 3: To implement fundamental tissue engineering principles to evaluate the performance of Runx2-modified cells in a both an ectopic site and a critical size craniotomy bone defect model through integration of Runx2-transduced primary bone marrow stromal cells into 3-D polymeric, biodegradable scaffolds. Runx2-modified or unmodified control cells were seeded onto polymeric scaffolds, cultured *in vitro*, and evaluated in two syngeneic animal models, a subcutaneous implant study and a critical size craniotomy defect model. It was hypothesized that sustained Runx2 overexpression in the osteogenic stromal cells would result in significantly more mineralized tissue formation in an ectopic site and enhance new bone formation in the

craniotomy defect compared to unmodified stromal cells, thereby enhancing defect healing.

Collectively these analyses provided a broad-based characterization scheme to observe the *in vitro* and *in vivo* performance of Runx2-transduced bone marrow stromal cells and examined their potential as a cell source for bone tissue engineering therapies. Additionally, these results evaluated this combined tissue and genetic engineering strategy for the development of a Runx2-modified marrow stromal cell/polymeric scaffold composite for tissue-engineered bone graft substitutes. Finally, this research established the foundation for future work and optimization experiments necessary to achieve the long-term objective of developing mineralized templates for bone repair.

CHAPTER 2

SIGNFICANCE OF RESEARCH

A continuously increasing number of bone grafting procedures are performed to repair or treat damaged or diseased bone. It is estimated that each year more than 500,000 fracture non-unions require supplemental grafting to insight normal bone healing (Einhorn, 1999). Although clinically successful, autologous and allogenic grafts face limitations, including minimal available donor bone, donor site morbidity, processing-related reductions in biological activity and mechanical integrity, and risk of infection and disease transmission (Khan et al., 2000; Bucholz, 2002).

Tissue engineering approaches to generate bone graft substitutes offer a promising alternative to address the current limitations associated with conventional grafting procedures. The development of a successful tissue-engineered bone substitute requires the integration of three interrelated and significant components, including (i) an osteogenic cellular component capable of synthesizing a mature organic and mineralized extracellular matrix, (ii) biochemical factors, either soluble or matrix-associated, which direct and stimulate osteoblastic differentiation, and (iii) a synthetic scaffold with an interconnected pore structure that establishes the biomechanical characteristics of the construct and supports infiltration, proliferation, and differentiation of the cellular component (Reddi, 1994; Doll et al., 2001). Therefore, depending upon the chemical identity of the scaffold, i.e. polymeric as opposed to bioceramic, the cellular component may provide the only osteogenic, osteoinductive, osteoconductive, and osteointegrative identity of the construct. Notably, osteogenic cell sourcing remains the pivotal

component to the immediate and long term feasibility of bone tissue engineering endeavors, and, as a result, significant research has examined cell sourcing from osseous tissues, including marrow-derived and periosteal-derived cells as well as purified subpopulations of mesenchymal stem cells (Ishaug et al., 1997; Kadiyala et al., 1997; Vacanti and Bonassar, 1999). Bone marrow-derived stromal cells have emerged as a popular model system of a clinically relevant cell source for bone tissue engineering applications due to their relative frequency, ease of isolation, and propensity for osteoblastic differentiation (Ohgushi et al., 1993; Ishaug-Riley et al., 1997). The stroma is a heterogeneous cell population containing progenitors of several mesenchymal tissues, including bone, cartilage, fat, muscle, and tendon. Although stromal cells exist at low frequencies in the marrow, they can be selectively isolated from more prevalent hematopoeitic cells in bone marrow aspirates through adhesion-dependent *in vitro* culture (Maniatopoulos et al., 1988). *In vitro* and *in vivo* studies have clearly demonstrated the capacity of an osteogenic subpopulation of these adhesion-selected stromal cells to form bone-like mineralized nodules in response to osteoinductive stimulation (Maniatopoulos et al., 1988; Leboy et al., 1991; Aubin, 1999). While bone marrow-derived and purified mesenchymal stem cells exhibit adequate mineralization capacity in model systems (Ohgushi et al., 1989; Bruder et al., 1994; Breitbart et al., 1999; Quarto et al., 2001; Horwitz et al., 2002), the effectiveness of these cell-based therapies to generate mechanically robust grafts to repair large non-healing osseous defects is hampered by the low frequency and age-related decrease of committed osteoprogenitor cells, extensive precursor cell death resulting from bone trauma or disease, and extended *in vitro*

expansion time necessary to obtain sufficient cell numbers for scaffold population, often with a concomitant loss in differentiation potential (Bruder and Fox, 1999).

The objective of the proposed research was to address these cell sourcing limitations using genetic engineering principles to exogenously overexpress an osteoblast-specific transcription factor which is essential to normal bone formation and maintenance, thereby enhancing the osteogenic capacity of the target cells. To date, a variety of strategies have been examined to overcome the differentiation limitations associated with isolated primary cells, principally through the delivery of osteoinductive bone morphogenetic proteins (BMPs) or other soluble growth and differentiation factors. BMPs have been delivered into ectopic sites or craniotomy and orthotopic defects in their recombinant protein form (Kenley et al., 1994; Whang et al., 1998) and more recently using viral gene therapy techniques to exogenously express the morphogens in osteogenic (Lieberman et al., 1998; Lieberman et al., 1999; Partridge et al., 2002) and even non-osteogenic target cells, including skin fibroblasts (Krebsbach et al., 2000; Yang et al., 2003) and muscle-derived stem cells (Lee et al., 2002). Regardless of whether the genetically modified cells are themselves induced to form bone or serve as delivery vehicles to facilitate osteoblastic differentiation of infiltrating host cells, these strategies have shown success in healing of critical size defects in a variety of animal models. Nonetheless, inadequate delivery carriers, complex release kinetics, aphysiologic dosage and potency, insufficient expression duration and efficiency, immunogenicity, and long-term safety restrict the wide-spread efficacy of these treatments (Boden, 1999; Doll et al., 2001).

The research conducted herein addresses these issues by directly delivering and stably expressing Runx2/Cbfa1, a bone cell-specific transcription factor involved in the expression of multiple osteoblastic genes. Alternatively to strategies which deliver soluble factors that ultimately initiate secondary signaling cascades, exogenous overexpression of a tissue-specific transcription factor in a heterogeneous cell population, such as bone marrow stromal cells, is a more robust mechanism to direct and potentially synchronize the osteoblastic differentiation cascade of target cells. It is this direct nuclear manipulation of target cells which may provide more reproducible, consistent osteogenic differentiation than approaches which utilize soluble molecule delivery requiring secondary signaling molecules which may or not be simultaneously expressed within the target cell population.

Initial studies in model cell lines indicated that Runx2 overexpression enhances osteoblast-specific gene expression and up-regulates matrix mineralization in monolayer (Chapter 4). These results are significant in addressing cell sourcing limitations associated with bone tissue engineering, and the rigorous experimental scheme further examined in this research enabled more complete characterization of cellular phenotype as well as the organic and mineral components of the matrix deposited by these genetically modified stromal cells both *in vitro* and *in vivo*. Ultimately, it will be essential to optimize *in vitro* culture parameters and properties of the 3-D scaffolds in which Runx2-modified cells are incorporated to ensure the long term efficacy of this genetic and tissue engineering approach. Additionally, it was of significant importance to conduct the implantation studies presently detailed in order to evaluate the *in vivo* performance of Runx2-modified cells. The outcome of implantation in these animal

models was necessary to justify both extensive *in vitro* optimization experiments and higher order *in vivo* models.

The genetic engineering techniques involved in this approach are flexible and robust, promoting the examination of Runx2 overexpression in a broad array of cell types from a variety of species. Furthermore, the incorporation of Runx2-modified primary bone marrow stromal cells into candidate 3-D biodegradable, polymeric scaffolds and subsequent implantation in both subcutaneous and craniotomy defect animal models demonstrates the feasibility of this integrated genetic and tissue engineering approach and establishes a foundation for examination of additional bone defect models requiring auxiliary graft material to facilitate healing and repair.

CHAPTER 3

LITERATURE REVIEW

Bone and the Osteoblast

The varied and dynamic functions of bone include its role as the primary reservoir of calcium and other minerals, a storage facility and factory for hematopoeisis, the mechanical framework to support the soft tissues of the body as well as attachment for tendons and ligaments to facilitate locomotion (Yaszemski et al., 1996). As a structure, bone is composed of an organically synthesized matrix comprised primarily of type I collagen (95%) and multiple noncollagenous proteins, including osteopontin, bone sialoprotein, osteocalcin, and proteoglycans. This organic matrix is embedded with crystalline salts, primarily calcium and phosphate, in a lattice structure known as hydroxyapatite (Marks and Hermey, 1996). Four cell types execute the functional responsibilities required for normal bone physiology, including osteoblasts, bone lining cells, osteocytes, and osteoclasts. Osteoblasts, bone lining cells, and osteocytes primarily serve an anabolic activity to regulate synthesis and maintenance of mineralized bone matrix, although osteocytes are capable of localized resorption activity. These cell types arise from mesenchymal osteoprogenitor cells residing in the marrow cavity, periosteum, and endosteum. Osteoclasts, on the other hand, initiate from the fusion of circulating mononuclear cells of hematopoeitic origin to form multinucleated cells which serve as the primary resorptive cell type for bone remodeling (Marks and Hermey, 1996).

The bone marrow stroma is heterogeneous in nature, containing primitive, uncommitted stem cells as well as more developed progenitors committed to a variety of

mesenchymal tissue types, including osteoblastic, fibroblastic, adipogenic, myoblastic, and chondrogenic lineages (Bruder et al., 1994; Bianco et al., 2001). Identification of an osteoprogenitor subpopulation of stem cells present in the proliferative fibroblast component of the bone marrow stroma by Friedenstein (Friedenstein, 1976) and others elicited significant *in vitro* and *in vivo* studies to determine the origin and cues giving rise to fully differentiated osteoblasts. The progressive cascade of osteoblastic differentiation has been primarily characterized by *in vitro* systems to define a developmental sequence with three primary components, including (i) proliferation, (ii) organic matrix synthesis and maturation, and (iii) matrix mineralization (Stein et al., 1990).

A definitive pathway defining the interplay between stromal cell proliferation and differentiation, specifically for the osteoprogenitor subfraction, has yet to be completely elucidated; however, an extensive number of soluble growth factors and hormones have been shown to play a role in this complex and dynamic cascade. Mitogenic growth factors including platelet-derived growth factor (PDGF), epidermal growth factor (EGF), basic fibroblast growth factor (bFGF), and transforming growth factor β (TGFβ) have been shown to induce stem and progenitor cell proliferation in multiple studies (Gronthos and Simmons, 1995; Locklin et al., 1995). *In vitro* experiments have demonstrated that actively proliferating pre-osteoblastic cells express high levels of genes required for cell cycling, such as histone proteins, and regulatory factors responsible for cell growth and cell cycle progression, including c-*myc* and c-*fos* (Owen et al., 1990a; Choi et al., 1996).

Although osteoprogenitor cells of the stroma and bone surface regions, including the periosteum and endosteum, have a predisposition toward osteoblastic differentiation, this process is facilitated physiologically by local osteoinductive factors, systemic steroid

hormones, tissue-specific transcription factors, as well as cell-ECM and cell-cell interactions (Stein et al., 1990; Moursi et al., 1996; Robey and Boskey, 1996; Boyan et al., 1996; Lecanda et al., 1998; Xiao et al., 1998a). The induction of osteoblastic differentiation by soluble components isolated from demineralized bone matrix, later characterized as bone morphogenetic proteins (BMPs), was originally demonstrated by Urist (Urist, 1965). Related in structure and function, multiple homodimeric BMPs have been shown to be osteoinductive, including BMP-2, -4, -7, and -9, acting through a serine/threonine cell surface receptor signaling cascade to induce endochondral bone formation (Wozney, 2002). As stated, a variety of systemic and local proteins and steroids also have a pronounced impact on bone physiology, including parathyroid hormone, parathyroid hormone-related protein, vitamin D_3, estrogen, and glucocorticoids (Aubin and Liu, 1996).

Osteoblasts are postproliferative cells of mesenchymal origin responsible for the formation of the mineralized matrix composing both endochondral and intramembranous bone. Throughout the maturation process, osteoblasts express characteristic and identifiable, phenotype-specific markers including the components of the extracellular matrix, as well as growth factors, cytokines, and hormone receptors. Although differentiated osteoblasts may express only a subset of the complete repertoire of osteoblast-specific genes, the matrix-associated markers consist of alkaline phosphatase, type I collagen, osteocalcin, osteopontin, bone sialoprotein, proteoglycans, and fibronectin (Aubin and Liu, 1996). The time-dependent expression of osteoblastic genes has been largely elucidated by *in vitro* studies and corroborated by in situ hybridization

and immunohistochemical analyses of bone specimens (Stein et al., 1990; Weinreb et al., 1990; Owen et al., 1990b; Quarles et al., 1992).

While still in the first, proliferative phase of the maturation process, preosteoblasts initiate and actively synthesize elements comprising the structural components of the extracellular matrix (ECM), principally type I collagen (Stein et al., 1990). Type I collagen synthesis during this phase is consistent with the expression and role of TGFβ in regulating ECM biosynthesis (Bortell et al., 1990). At the conclusion of the proliferative phase, DNA synthesis and histone production decline. One of the earliest markers indicating the initiation of osteoblastic differentiation and concomitant cessation of proliferation is alkaline phosphatase (ALP), a membrane bound glycosyl-phosphatidylinositol protein. The onset of ALP expression has been shown in early pre-osteoblastic cells and an increase in transcript levels has been associated with progression to a more fully differentiated state (Stein et al., 1990). Two other bone-related proteins commonly examined during the progressive differentiation cascade are osteopontin and osteocalcin. Osteopontin expression is biphasic, appearing both at end of the first stage and toward the beginning of the final mineralization phase. Osteocalcin, on the other hand, is typically characterized as the latest functional osteoblast-specific marker, appearing only slightly before the onset of mineralization (Owen et al., 1990b). The culmination of this maturational process occurs through mineralization of the extracellular matrix. The crystalline structure found in bone, termed hydroxyapatite ($Ca_{10}(PO_4)_6(OH)_2$), contains a variety of ionic substitutions, most commonly carbonate, and is arranged in an oriented manner embedded within the fibrillar collagen matrix (Robey and Boskey, 1996).

Although significant work has led to the identification of numerous pathways that contribute to osteoblastic maturation, a great deal of uncertainty remains toward assimilating these signaling cascades, including those of biochemical and mechanical origins, in the complete elucidation of the developmental process beginning with a relatively immature multipotential stem cell and culminating in a quiescent, matrix embedded osteocyte. In particular, identifying the interactions of transcriptional pathways, whether linear or circular in nature that give rise to the natural progression of a developing osteoblast are currently receiving significant scientific research and exposure. A primary, if not the most central, transcription factor under investigation for its regulatory involvement in bone formation and skeletal maturity is Runx2, a transcriptional activator of osteoblastic differentiation.

Runx2 and Osteoblastic Differentiation

Runx2, also termed Cbfa1 (Banerjee et al., 1997; Ducy et al., 1997)/PEBP2αA (Ogawa et al., 1993)/AML3 (Levanon et al., 1994), has been characterized as an osteoblast-specific transcriptional activator (Ducy et al., 1997). Runx2 was identified as a trans-acting factor binding OSE2, a *cis*-acting element in the promoter of the osteocalcin (OCN) gene having the conserved sequence 5′-AACCACA-3′ (Ducy and Karsenty, 1995). Analysis of OSE2 (Geoffroy et al., 1995; Merriman et al., 1995) showed similarity to the DNA sequence targeted by Drosophila *runt* transcription factors (Gergen and Wieschaus, 1985; Daga et al., 1992). This transcription factor family is distinguished by a highly conserved 128 amino acid-long DNA-binding *runt* homology domain (Kagoshima et al., 1993) and contains three known isoforms, Runx1, Runx2, and

Runx3, expressed in a cell-type and tissue specific manner (Miyoshi et al., 1991; Wang and Speck, 1992; Bae et al., 1993; Bae et al., 1995; Meyers et al., 1995; Wijmenga et al., 1995; Meyers et al., 1996).

At least eight exons have been identified in the genomic code of the endogenous Runx2 gene (Geoffroy et al., 1998; Drissi et al., 2000), and the mature mRNA is highly conserved across multiple species, including human, rat, and mouse (Xiao et al., 1998b). The presence of two separate promoters and multiple splice donor and acceptor sequences primarily at the 5' end result in the utilization of two unique start codon translation sites that give rise to two Runx2 isoforms with different amino termini, spatiotemporal expression patterns, and physiologic functions (Drissi et al., 2000). The type I isoform begins with the MRIPVD amino terminus (Mundlos et al., 1997) and has been well characterized for its role in transcriptional activation of T-cell-specific gene expression (Ogawa et al., 1993). Furthermore, type I Runx2 appears ubiquitously in nonosseous mesenchymal tissues, including skin and muscle, and other nonmesenchymal sources, such as liver and lung (Sudhakar et al., 2001; Banerjee et al., 2001). Transcription from the P1 promoter encodes the second isoform, commonly referred to as the type II isoform (Thirunavukkarasu et al., 1998; Xiao et al., 1998b; Harada et al., 1999), which begins with the MASNSLF amino acid sequence. Transcripts of both isoforms have been detected in developing mesenchymal condensations, osteoblast progenitors, and mature osteoblasts (Ducy et al., 1997; Harada et al., 1999; Banerjee et al., 2001). Although *in vitro* exogenous transfection experiments have indicated the two isoforms have nearly equivalent transcriptional activation potential for the regulation of osteoblast-specific genes (Harada et al., 1999; Banerjee et al., 2001), analyses indicate

that only transcript mRNA splicing activity, protein levels, and DNA binding activity of the type II isoform are physiologically altered/up-regulated in response to osteoinductive stimulation and osteoblastic maturation (Banerjee et al., 2001). The type II Runx2 isoform was evaluated in the ensuing *in vitro* and *in vivo* analyses of this dissertation, therefore any generalized reference to Runx2 in subsequent reading refers specifically to the type II (MASNSLF) isoform unless otherwise stated.

To date, the mechanisms of tissue and cell-type-specific activity and modulation of Runx2 expression through transcriptional, post-transcriptional/translational, and post-translational regulation and/or modification have yet to be completely elucidated. However, each of these regulatory checkpoints is currently under examination. Current evidence indicates that each of these mechanism may play an integral and coordinated role in regulation and function of Runx2, including its participation in cell cycle progression and ultimately osteoblastic differentiation. For example, Banerjee et al. have demonstrated Runx2 transcript levels in rat osteoblasts were lower during the proliferative phase and increased to higher levels throughout later stages of differentiation. Furthermore, Runx2 protein levels dramatically increased between the proliferation (day 2) and differentiation (day 14) phases of primary rat calvarial osteoblasts *in vitro*, and expression levels remained at similar elevated levels even at late stages of differentiation (day 21). Interestingly, however, the DNA binding activity of Runx2 dramatically increased from day 14 to day 21, suggesting additional post-translational modifications facilitate transcriptional complex formation and enhance DNA binding (Banerjee et al., 2001). Contrary to these observations in rodent stromal cells and osteoblasts, temporal alterations in Runx2 mRNA expression were not observed in

immortalized human marrow stromal cell lines and osteoblasts (Satomura et al., 2000; Prince et al., 2001; Shui et al., 2003). Although Runx2 mRNA message levels were essentially constant, Runx2 protein levels increased with progressive osteoblastic differentiation (Prince et al., 2001), and activity was also up-regulated in a temporal manner, possibly due to interactions with other proteins and transcription factors and/or phosphorylation of the Runx2 protein, including tyrosine, threonine, and serine residues (Xiao et al., 2000; Prince et al., 2001; Shui et al., 2003).

Currently, the biological signals eliciting Runx2 transcription are not well understood. Several key developmental and regulatory transcription factors have been shown to regulate Runx2 expression, including MSX-2, AP-1, Bapx1, Hoxa-2, and Dlx-5 (Otto et al., 2003; Lee et al., 2003). The signaling pathways eliciting this regulatory control are only now being identified, and multiple growth factors and steroid hormones have been implicated in controlling Runx2 message and protein levels, such as BMP-2 (Banerjee et al., 2001) and BMP-4/7 (Tsuji et al., 1998) and the glucocorticoid family of steroid hormones (Prince et al., 2001). Furthermore, it has been demonstrated that Runx2 possesses autoregulatory capability. Specifically, the proximal "bone-related" P1 promoter that regulates expression of the type II Runx2 isoform contains at least five Runx2 binding domains, three of which are located within the 5' untranslated region of the mRNA (Xiao et al., 1998b; Fujiwara et al., 1999; Drissi et al., 2000). Co-transfection experiments of Runx2 and a reporter plasmid containing this promoter region revealed that Runx2 binding to only one of these three sites is sufficient to regulate autosuppression of Runx2 transcription (Drissi et al., 2000).

The potential for a post-transcriptional regulatory mechanism in Runx2 protein expression levels has also been detailed (Sudhakar et al., 2001; Xiao et al., 2001). In these studies, a basal level of splice variant Runx2 mRNA transcripts were detected by RNase protection analysis in a variety of osseous and non-osseous cell lines, including MC3T3-E1 osteoblast-like cells, ROS17/2.8 osteoblasts, C3H10T1/2 pluripotent fibroblasts, C2C12 myoblasts, and L929 skin fibroblasts. A common splice variant detected included an isoform containing a 'mini-intron' embedded within the 5' untranslated region (UTR) of exon 1. Present in C2C12 cells, this immature transcript underwent a micro-splicing event in response to BMP-2 treatment, and only the fully processed Runx2 mRNA was subsequently detected. The authors proposed that post-transcriptional processing may therefore be involved in tissue-specific expression of mature Runx2 protein. Specifically, basal levels of unprocessed Runx2 transcripts may exist in a variety of tissues, including those nonosseous in nature, but only following osteoblast-specific signaling or induction is the post-transcriptional processing necessary for production of mature Runx2 mRNA and protein initiated.

The involvement of Runx2 in skeletal development has been extensively investigated (Ducy et al., 1997; Otto et al., 1997; Komori et al., 1997; Mundlos et al., 1997; Kim et al., 1999; Inada et al., 1999; Enomoto et al., 2000; Takeda et al., 2001; Ueta et al., 2001). OSE2 sequences have been discovered in the promoters of genes expressed only (OCN (Ducy and Karsenty, 1995)) or highly (α1(I) and α2(I) collagen (Kern et al., 2001), bone sialoprotein (BSP) (Benson et al., 1999), osteopontin (OPN) (Sato et al., 1998), and CCAAT/enhancer–binding protein δ (C/EBPδ) (McCarthy et al., 2000)) in osteoblasts. Additional genes involved in bone development and turnover have also been

shown to be positively regulated by Runx2 expression, including vascular endothelial growth factor (VEGF) (Zelzer et al., 2001), collagenase III (Jimenez et al., 2001), and osteoprotegerin (Thirunavukkarasu et al., 2000). Transient forced expression of Runx2 in non-osteoblastic cells induces expression of several osteoblast-specific genes, including OCN and BSP (Ducy et al., 1997). In addition to its role as regulatory factor in osteoblastic differentiation, Runx2 is expressed in high levels in proliferating osteoblasts and mediates cell cycle progression toward a more differentiated state (Pratap et al., 2003).

Runx2 transactivational and repressor functions are mediated through complexes involving numerous cofactors existing both ubiquitously and temporally throughout the osteoblastic differentiation cascade. Cbfβ, is a non-DNA binding, runt homology domain-associating co-factor similarly essential to normal bone formation (Miller et al., 2002; Kundu et al., 2002). CCAAT/enhancer–binding protein (C/EBP) family members, specifically β and δ, have been implicated in osteoblastic differentiation and synergistically interact with Runx2 to enhance expression of osteoblast-specific genes, including osteocalcin (Gutierrez et al., 2002). Additionally, autophosphorylation of cytoplasmic components of the TGFβ or BMP receptors in response to morphogen binding elicits a signaling cascade which propagates to the nucleus via Smads, small accessory transcription factors which among other targets, co-localize with Runx2 to regulate gene transcription both positively and negatively (Li et al., 1998; Zaidi et al., 2002). Runx2 also functions as a repressor of gene expression largely in combination with members of the Groucho/TLE/R-esp transcription factor family (Javed et al., 2000).

Functional expression of Runx2 is essential to normal bone formation. Specifically, Runx2-deficient mice have normally patterned cartilaginous skeletons but display a complete lack of endochondral and intramembranous bone formation, while heterozygous mutants ($Runx2^{+/-}$) have hypoplastic clavicles among other deformations arising from delayed development of intramembranous bones (Otto et al., 1997; Komori et al., 1997). The human autosomally dominant disorder cleidocranial dysplasia (CCD) demonstrates a phenotype consistent with $Runx2^{+/-}$ mutant mice (Mundlos et al., 1997; Lee et al., 1997). Nearly 75% of all CCD cases are attributable to haploinsufficiency resulting from genomic alteration of the Runx2 sequence (Mundlos, 1999). Additionally, transgenic mice engineered to postnatally overexpress a nontransactivating Runx2 DNA-binding domain competitor protein have normal skeletons at birth but develop an osteopenic phenotype thereafter (Ducy et al., 1999), indicating that expression of functional Runx2 protein is essential to normal physiologic bone turnover. Runx2 expression is also involved in chondrocyte maturation, specifically in hypertrophic chondrocytes participating in calcification of the growth plate (Kim et al., 1999; Inada et al., 1999; Enomoto et al., 2000; Ueta et al., 2001).

Collectively, these findings demonstrate the essential role of functional Runx2 expression in embryonic bone formation as well as regulation of bone matrix deposition by differentiated osteoblasts throughout adult life.

Bone Graft Technology Overview

In excess of 500,000 clinical procedures are performed annually (Einhorn, 1999) in which bone grafting plays an integral role in native tissue repair, including diseases,

such as osteoimperfecta, malignant or benign tumors, and osteoporosis, and in fracture nonunions occurring in orthopaedic, craniomaxillofacial, spinal, and dental areas (Boden, 1999; Einhorn, 1999). Even though many bone injuries are self-healing, there exists a high frequency of clinical applications which require healing enhancement/engraftment due to terminal compromise of native tissue. Currently, there is a lack of effective bone repair and regeneration solutions, especially for large segmental defects. As a result, alternative healing mechanisms are being investigated, most notably bone tissue engineering strategies. In accordance with innate regenerative capacity of bone, the requirements of a clinically successful bone graft substitute are defined by its capacity to be: (i) osteointegrative, supporting chemical bonding with the surface of bone; (ii) osteoconductive, promoting the growth of bone over its surface; (iii) osteoinductive, inducing the differentiation of cells adjacent to the implantation site down the osteoblastic lineage; (iv) osteogenic, forming new bone within the graft through a cellular component present within the graft (Yaszemski et al., 1996; Moore et al., 2001); (v) mechanically accommodative, providing sufficient localized mechanical integrity essential for immediate and permanent restitution of mechano-continuity in load bearing applications while minimizing detrimental stress-shielding of native tissue (Athanasiou et al., 2000).

Biological Bone Grafts

Currently, the clinical gold standard of bone grafting is the autogenous cancellous bone graft (Yaszemski et al., 1996), which is the only solution capable of satisfying all of the biological requirements of a graft material, provided sufficient precursors cells

survive the implantation procedure. These efforts are, however, limited by the supply of autograft tissue, donor site morbidity, chronic pain (Crane et al., 1995; Perry, 1999; Moore et al., 2001), as well as insufficient biomechanical properties. Although lacking a cellular component to provide osteogenic characteristics, allograft material from cadaveric bone is more abundant, addressing the supply and donor site morbidity complications associated with autografts. However, graft resorption, risk of pathogen transfer, as well as minor immuno-acceptance issues complicate these efforts (Crane et al., 1995). Furthermore, excessive donor variability (Heiple et al., 1987) and processing-related reduction of bioactivity and mechanical properties result in significant variability in osteoinductivity and heightened risk of fracture, complications which limit the overall effectiveness of these techniques.

Synthetic Materials

In addition to biocompatibility, the physical attributes essential to synthetic materials include a similar level of strength, modulus of elasicity, and fracture toughness to minimize stress shielding of native tissue and fatigue under cyclic loading (Moore et al., 2001). A variety of synthetic materials have been investigated in bone grafting or implant applications including ceramics, polymers, metals, and hybrid composites. These biomaterials pose a variety of limitations including an obvious lack of osteogenic or osteoinductive component and elicitation of detrimental inflammatory responses and adverse host tissue necrosis or resorption due to relatively poor biomechanical compatibility, e.g. stress-shielding of native tissue, or generation of wear debris (Yaszemski et al., 1996; Bauer and Muschler, 2000). Calcium phosphate ceramics,

including bioactive glasses (el Ghannam et al., 1997), β-tricalcium phosphates (TCP) (Dong et al., 2002), and synthetic or coralline hydroxyapatites (Ohgushi et al., 1993; Shors, 1999), have been extensively investigated for their osteoconductive properties. Unfortunately, bioactive glasses and ceramics possess poor fracture toughness and are incapable of adequately filling cyclically loaded bone defects. Hydroxyapatites and β-TCP are also brittle under tension and shear, which compromises their *in vivo* functionality and complicates manufacturing and processing techniques. Additionally, these ceramics have variable bioresorptive properties in which either complete or minimal resorption occurs, thereby restricting timely integration and remodeling.

Bone Tissue Engineering Strategies

Overview

Tissue engineering has been described as an interdisciplinary field in which the principles of engineering and the life sciences are applied toward the generation of biologic substitutes aimed at the creation, preservation, or restoration of lost organ function (Vacanti and Bonassar, 1999; Laurencin et al., 1999; Goldstein, 2002). The well-established regenerative capacity of bone, whether from injury or normal biological turnover, can be advantageously utilized in bone tissue engineering strategies through the isolation and incorporation of committed osteogenic cells into biocompatible three-dimensional (3-D) matrices. The maturation of these osteoprogenitor cells within the construct, namely through migration and proliferation and ultimately guided differentiation toward the osteoblastic lineage, recapitulates the intramembranous bone formation cascade. Introduction of this biological component promotes the critical

osteogenic and even osteoinductive characteristics required for successful grafting, providing a viable alternative to address the clinical demand for bioactive bone graft material.

Ultimately, three principle components essential to the development of successful tissue-engineered constructs include (i) an osteogenic cells source, (ii) a 3-D matrix or scaffold designed to promote cellular growth and differentiation, and (iii) regulatory/inductive/stimulatory signals to direct osteoblastic differentiation (Reddi, 1994; Bruder and Fox, 1999).

Cell Sourcing Strategies for Bone Tissue Engineering

The principle of cell-based bone tissue engineering focuses on the isolation of cells, commonly osteogenic in nature, from a relatively small tissue specimen, expansion typically under adhesion-dependent *in vitro* culture, and delivery to a defect site within a carrier material or configuration that will generate a new functional tissue (Vacanti and Bonassar, 1999). To address this principle, multiple cell sources from osseous and nonosseous tissues in a variety of animal models have been examined for their osteogenic differentiation capacity either endogenously or following osteoinductive stimulation, including bone marrow stroma (Maniatopoulos et al., 1988; Ishaug-Riley et al., 1997), purified marrow-derived, mesenchymal stem cells (Bruder et al., 1997), osteoprogenitors from fetal calvaria (Ishaug-Riley et al., 1998; Malaval et al., 1999), periosteal cells (Breitbart et al., 1999; Vacanti and Bonassar, 1999), vascular-derived pericytes (Doherty et al., 1998), muscle-derived stem cells (Deasy et al., 2001; Jankowski et al., 2002), and

even adipose-derived cells and human marrow-derived adipocytes (Park et al., 1999; Halvorsen et al., 2001).

Based on their relative ease of harvest and traditionally simplistic *in vitro* isolation and expansion techniques, bone marrow-derived stromal cells provide one of the most accessible and viable sources of multipotent cells available for therapeutic applications (Bianco et al., 2001). The endogenous *in vitro* osteogenic capacity of marrow-derived stromal cells has been extensively investigated (Maniatopoulos et al., 1988; Leboy et al., 1991; Aubin, 1999; Calvert et al., 2000), and their candidacy as an osteogenic cell source for bone tissue engineering applications has been demonstrated in both *in vitro* and *in vivo* model systems (Ohgushi et al., 1989; Ohgushi et al., 1993; Bruder et al., 1994; Ishaug et al., 1997; Kadiyala et al., 1997; Breitbart et al., 1999; Quarto et al., 2001; Horwitz et al., 2002; Holy et al., 2003). However, the effectiveness of these stromal cell-based therapies is hampered by the low frequency of committed osteoprogenitor cells (0.001% of total viable nucleated marrow cells) (Bruder et al., 1997) and further complicated by the observed decrease in osteoprogenitor frequency in the marrow of aged patients, who find themselves at the greatest risk of catastrophic bone fracture (Quarto et al., 1995; Glowacki, 1995). Additionally, extensive precursor cell death resulting from bone trauma or disease and extended *in vitro* expansion time necessary to obtain sufficient cell numbers for scaffold population (Bruder and Fox, 1999) limit these approaches. Furthermore, adhesion-dependent *in vitro* expansion of bone marrow stromal cells results in a loss of osteoblastic differentiation capacity (Ter Brugge and Jansen, 2002; Shi et al., 2002; Simonsen et al., 2002).

Scaffold Technology in Bone Tissue Engineering

Primary qualifications of synthetic scaffolds for bone tissue engineering applications include biocompatibility, osteoconductivity, sterilizability, and biodegradability over a reasonable and appropriate time-scale (Crane et al., 1995). Furthermore, secondary parameters which will ultimately enhance bone tissue engineering successes consist of high porosity for cell loading and surface characteristics which support protein adsorption and cell attachment, growth, and differentiation (Crane et al., 1995; Boyan et al., 1996).

Osteogenic cells, primarily bone marrow stromal cells, have been used in conjunction with osteoconductive hydroxyapatites and other calcium phosphate ceramics (Ohgushi et al., 1993; Yoshikawa et al., 1998; Bareille et al., 2000) (Livingston et al., 2002; Dong et al., 2002) to demonstrate ectopic bone formation in a subcutaneous site and healing in bone defect models. However, suboptimal *in vivo* degradation properties, poor fracture toughness, and lack of a complete interconnected pore structure complicate efforts to identify a suitable bioceramic for bone tissue engineering applications. Incorporation of osteogenic cells into polymer-based scaffolds, including poly (α-hydroxy) esters, including copolymers of polylactide and polyglycolide (PLGA) (Hollinger, 1983; Athanasiou et al., 1996; Ishaug et al., 1997; Ishaug-Riley et al., 1998; Calvert et al., 2000; Holy et al., 2000; Lin et al., 2003) and polycaprolactones (Hutmacher et al., 2001; Zein et al., 2002), have also received significant attention because of their biodegradability and status as FDA-approved biomaterials. These osteogenic cell-polymeric composite scaffolds have been evaluated through *in vitro* characterization and subcutaneous implantation or non-load bearing bone defect repair

models. Importantly, these solutions are often incapable of providing long term success in large critical size defects due to poor mechanical properties, discontinuity of degradation rates, and minimal osteoconductive and osteointegrative properties.

Osteoinductive Bioactive Factors in Bone Tissue Engineering

Examination of soluble molecules which initiate signaling cascades that promote osteogenesis have primarily focused on bone morphogenetic proteins (BMPs) (Hollinger et al., 1998), since the early discovery of an osteoinductive component present in demineralized bone matrix (Urist, 1965) and subsequent isolation and cloning of specific osteoinductive isoforms including BMP-2, 4, and 7 (Ebara and Nakayama, 2002). Additional growth factors have also been examined in the healing of bone defects, including PDGF (Park et al., 2000), TGFβ (Mehrara et al., 1999), FGF (Nakamura et al., 1997), and IGF (Busch et al., 1996).

Although successful in principle, delivery of soluble purified or recombinant BMPs or growth factors to a wound site often proves ineffective for several reasons (Doll et al., 2001), including insufficient dosing and temporal inconsistencies largely due to ineffective delivery vehicles (Marshall, 1995), asynchrony between growth factor availability and the kinetics of signaling receptor expression (Howell et al., 1997), transient active half-life of growth factors (Centrella et al., 1994), inappropriate target cell populations, and excessive diffusion, sequestering by plasma membranes, and proteolytic degradation in the wound healing environment (Bonadio et al., 1999).

These limitations have resulted in the implementation of genetic engineering strategies, including both *in vivo* and *ex vivo* gene transfer to appropriate target cells in

order to elicit a more stable and constant delivery or expression of a therapeutic gene to enhance bone tissue engineering initiatives.

Genetic Engineering in Bone Tissue Engineering

Gene delivery techniques are gaining popularity and significance in the treatment of diseased or damaged tissue because of the functionality and flexibility associated with the varied genetic engineering strategies currently available. These consist of non-viral transient transfection methods as well as techniques which utilize viral machinery and cell surface adhesion mechanisms to introduce therapeutic genetic information into target cell populations. Although delivery of naked or liposome-complexed osteogenic plasmid DNA has been investigated (Fang et al., 1996), transfection efficiencies are often quite low and transgene expression duration typically lasts for a very limited timeframe. The most common gene therapy strategies for the stringent bone tissue engineering applications involve either adeno- or retroviral-mediated transgene delivery. Briefly, adenoviruses (Ad) enter a cell via a capsid protein ligand-cell surface receptor interaction, introduce genetic information as temporary episomal elements, and infect either dividing or non-dividing target cells. Adenoviruses can be used for either *ex vivo* or *in vivo* gene therapy as they possess a relatively high multiplicity of infection. However, adenoviruses also elicit an undesirable and perhaps antagonsitic immunogenic response *in vivo*. Alternatively, retroviruses are more suited to *ex vivo* gene delivery applications due to their lower titers and inability to transduce non-dividing cells. These enveloped viruses, which enter the cell through receptor-ligand and membrane fusion events, deliver viral RNA which is reverse transcribed and ultimately stably integrated

into the genome of a proliferating target cell population by companion viral polymerases and other enzymes. This stable integration promotes sustained and theoretically permanent transgene expression, as the therapeutic message is maintained in daughter cells.

To date, the primary strategies of genetic engineering in bone regeneration applications have been the incorporation of AdBMP(-2 and -7)-transduced target cells into carrier matrices for implantation into a defect (Lieberman et al., 1999) or through direct injection of AdBMP supernatant to demonstrate heterotopic bone formation (Musgrave et al., 1999; Okubo et al., 2000). The target cells are either osteogenic in nature, such as primary stromal cells (Lieberman et al., 1999; Partridge et al., 2002), or nonosseous cells (Krebsbach et al., 2000), which are themselves induced to form bone or function as a delivery vehicle for the osteoinductive soluble factor in order to stimulate native osteogenic cells surrounding or infiltrating into the defect site. These techniques have been investigated in subcutaneous implantation models (Musgrave et al., 1999) as well as cranial (Krebsbach et al., 2000) and segmental (Lieberman et al., 1999) critical size defects. Although less prevalent than adenoviral vectors, *ex vivo* retroviral expression systems for BMP-2 (Laurencin et al., 2001), -4 (Gysin et al., 2002), and -7 (Breitbart et al., 1999) have also been investigated. These analyses demonstrated sustained BMP expression as well as healing of critical size cranial defects.

SUMMARY

Although genetic modification of cells to overexpress BMPs and other soluble growth factors have successfully repaired critical size defects in model systems,

diffusional limitations, safety concerns involving the inadvertent targeting and morphogenesis of neighboring nonosseous tissues, requisite accessory receptors and cofactors which functionalize the signal into a transcriptional message, and the adverse tissue environment present in large critical size and segmental defects may ultimately reduce the effectiveness of these techniques. An alternative approach to the delivery of a soluble osteoinductive factor that elicits directed differentiation through secondary signaling mechanisms is to genetically engineer isolated osteoprogenitor cells to overexpress an osteogenic transcription factor, such as Runx2. In principle, this approach serves to directly overexpress a primary transcriptional activator which is a prominent and characteristic downstream target of many osteoinductive BMPs. Additionally, Runx2 is a robust selection for exogenous overexpression in osteoprogenitor cells due to its regulatory involvement in the expression of numerous osteoblastic genes/proteins that comprise a significant portion of the organic matrix of bone and essentiality for normal bone development and turnover.

CHAPTER 4

RUNX2 OVEREXPRESSION IN MODEL CELL LINES*

INTRODUCTION

Functional expression of the transcriptional activator Runx2/Cbfa1 is essential for osteoblastic differentiation and bone formation and maintenance (Ducy et al., 1997; Otto et al., 1997; Komori et al., 1997; Ducy et al., 1999). Forced expression of Runx2 in non-osteoblastic cells induces expression of osteoblast-specific genes (Ducy et al., 1997; Xiao et al., 1999), but the effects of Runx2 overexpression on *in vitro* matrix mineralization had not previously been examined. In order to determine whether exogenous Runx2 expression was sufficient to direct *in vitro* mineralization, sustained expression of Runx2 expression was investigated in non-osteoblastic and osteoblast-like cell lines using retroviral gene delivery. As expected, forced expression of Runx2 induced several osteoblast-specific genes in NIH3T3 and C3H10T1/2 fibroblasts and up-regulated expression in MC3T3-E1 immature osteoblast-like cells. However, Runx2 expression enhanced matrix mineralization in a cell-type dependent manner. NIH3T3 and IMR-90 fibroblasts transduced with Runx2 did not produce a mineralized matrix, indicating that forced expression of Runx2 in these non-osteogenic cell lines was not sufficient to direct

* Modified from Byers BA, Pavlath GK, Murphy TJ, Karsenty G and Garcia AJ (2002) Cell-type-dependent up-regulation of in vitro mineralization after overexpression of the osteoblast-specific transcription factor Runx2/Cbfal. J Bone Miner Res 17: 1931-1944.

in vitro mineralization. Consistent with the pluripotent nature of the cell line, a fraction (25%) of Runx2-expressing C3H10T1/2 fibroblast cultures produced mineralized nodules in a viral supernatant-dependent manner. Notably, bone sialoprotein gene expression was detected at significantly higher levels in mineralizing Runx2-modified C3H10T1/2 cells compared to Runx2-expressing cultures which did not mineralize. Treatment of Runx2-transduced C3H10T1/2 cultures with dexamethasone enhanced osteoblastic phenotype expression, inducing low levels of mineralization independent of viral supernatant. Finally, Runx2 overexpression in immature osteoblast-like MC3T3-E1 cells resulted in acceleration and robust up-regulation of matrix mineralization compared to controls. These results suggested that, although functional Runx2 is essential to multiple osteoblast-specific activities, *in vitro* matrix mineralization requires additional tissue-specific cofactors which supplement Runx2 activity.

MATERIALS AND METHODS

Cells and Reagents

Characterization of forced Runx2 expression was investigated in well-established model cell lines. NIH3T3 murine fibroblasts (CRL-1658) obtained from American Type Culture Collection (Manassas, VA) served as model non-osteoblastic cells, as this cell line does not express osteoblast-specific genes nor mineralize the ECM *in vitro*. C3H10T1/2 murine pluripotent fibroblasts (ATCC, CCL-226) were chosen as a potentially more responsive fibroblastic cell line. This multipotential cell line does not endogenously express osteoblast-specific markers, but Runx2 and other markers of osteoblastic differentiation are induced following exposure to BMP-2 (Katagiri et al.,

1990) and BMP-7 (Ducy et al., 1997). MC3T3-E1 murine immature osteoblast-like cells (RCB1126) were purchased from the Riken Cell Bank (Hirosawa, Japan) and used as a model for osteoblastic differentiation. Under specific *in vitro* culture conditions, this established cell line expresses osteoblast-specific genes and produces mineralized nodules, undergoing the developmental stages associated with differentiating osteogenic cells (Sudo et al., 1983).

Fetal bovine serum (FBS) and newborn calf serum (NCS) were obtained from Hyclone Laboratories (Logan, UT) and Mediatech (Herndon, VA), respectively. Recombinant human BMP-2 was purchased from Kamiya Biomedical Co. (Seattle, WA). Remaining cell culture supplies were obtained from Invitrogen (Carlsbad, CA), while chemical reagents were purchased from Sigma Chemical Co. (St. Louis, MO). RNA isolation and DNA purification reagents were acquired from Qiagen (Valencia, CA). Molecular biology reagents for reverse transcription (RT) and conventional polymerase chain reaction (PCR) were purchased from Invitrogen, reagents for real-time PCR were acquired from Applied Biosystems (Foster City, CA), and PCR oligos were obtained from Integrated DNA Technologies (Coralville, IA).

Cell Culture

NIH3T3 fibroblasts were grown in Dulbecco's modified Eagle's medium (DMEM), 10% NCS, and 1% penicillin-streptomycin. C3H10T1/2 fibroblasts were cultured in Basal Medium Eagle, 10% FBS, and 1% pen-strep. The MC3T3-E1 cell line was maintained in α-minimum essential medium (α-MEM), 10% FBS, and 1% pen-strep. All cell lines were subcultured using standard techniques. Primary skin fibroblasts were

isolated from murine skin explants digested in collagenase/trypsin and maintained in DMEM, 10% FBS, and 1% pen-strep.

Runx2 Retroviral Vector and Retroviral Transductions

Murine cDNA for the MASNSLF Runx2 isoform was amplified from the originally reported pCMV-Osf2/Cbfa1 expression plasmid (Ducy et al., 1997) using the Advantage®-GC 2 high fidelity PCR system (Clontech Laboratories, Palo Alto, CA) and primers: 5'-CGAGGGCGTTTAAATGGTTAA-3' and 5'-GCCATGGTTGACGAATTTCAA-3'. Following fragment purification and blunt-ending, SfiI adapters (formed with oligonucleotides 5'-CTAGGCCTACA-3' and 5'-AGGCCTAG-3') were ligated onto the PCR fragment. The gel-purified fragment was then ligated into the SfiI universal cloning site of the pTJ66 retroviral expression vector (Abbott et al., 2000) (See Appendix A for detailed description of vector cloning). The Runx2 isoform investigated in this study contains the N-terminal 19 residue transcriptional activation domain (AD1) (Thirunavukkarasu et al., 1998). The pTJ66 vector utilizes a retroviral long terminal repeat promoter to express a single, bicistronic mRNA that produces a therapeutic protein through cap-dependent translation and a zeocin resistance-eGFP fusion protein by internal ribosomal entry site (IRES) translation. The resulting Runx2 retroviral expression plasmid (Figure 4-1) was confirmed by DNA sequencing (Emory University DNA Sequencing Core Facility, Atlanta, GA).

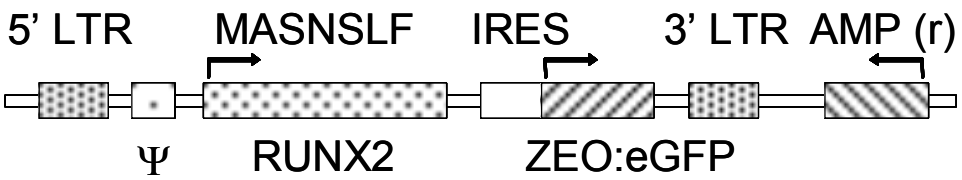

Figure 4-1. Linear representation of the Runx2 retroviral expression plasmid. (8544 bp) Constitutive transcription of the MASNSLF Runx2 isoform is regulated by the viral promoter in the long terminal repeat (LTR), a Zeo:eGFP selectable marker is translated from an IRES, and ampicillin resistance (Amp) is present for selection in bacteria. Ψ: viral packaging sequence.

Retroviruses were packaged by transient transfection of helper-virus free ΦNX amphotropic producer cells (Pear et al., 1993) with plasmid DNA as previously described (Abbott et al., 1998). Briefly, ΦNX producer cells were plated at 9×10^4 cells/cm^2 the day prior to transfection and maintained in DMEM supplemented with 10% FBS and 1% pen-strep in a humidified 5% CO_2 atmosphere at 37°C. Cultured cells at 50-80% confluence were transfected with plasmid DNA, either Runx2 or control vector (no Runx2 insert), by calcium phosphate coprecipitation (Pear et al., 1993) and 25 μM chloroquine for 8-12 hours prior to refeeding with fresh growth media. Twenty-four hours after the start of the transfection, media was replaced and dishes were transferred to a humidified 5% CO_2 atmosphere at 32°C to enhance retroviral titer (Kotani et al., 1994). Retrovirus-containing supernatants were collected at 48, 60, and 72 hours after transfection, filtered through a 0.45 μm cellulose acetate filter, aliquoted, snap frozen, and stored at -80°C until use.

Prior to retroviral transduction, target mammalian cells were plated on 0.1% type I collagen-coated (Vitrogen-100; Cohesion, Palo Alto, CA) 6 well plates at a density of 1×10^4 cells/cm^2 and incubated in growth media overnight at 37°C. Cells at 50-80%

confluence were transduced by adding 0.2 ml/cm^2 of retroviral supernatant supplemented with 4 μg/ml hexadimethrine bromide (Polybrene) and spinning at 2500 rpm (1200 g) for 30 minutes at 32°C in a Beckman model GS-6R centrifuge with swinging bucket rotor (Springer and Blau, 1997). Transductions and endpoint assays were performed in parallel on all target cell types, and empty vector served as a control for all transductions. After transduction, growth media was reapplied, and the cells were returned to incubation at 37°C. To increase transduction efficiency, an additional transduction was performed 10-12 hours later. After this final transduction, media was supplemented with 50 μg/ml L-ascorbic acid and 3 mM sodium β-glycerophosphate to support osteoblastic differentiation and mineralization. In addition to their respective supplemented growth media, NIH3T3 and C3H10T1/2 fibroblasts were also cultured in α-MEM supplemented with 10% FBS, the same differentiation media shown to support endogenous mineralization in the MC3T3-E1 cells. Media was replaced every 48 hours. The combined effect of forced Runx2 expression and additional osteoinductive factors in C3H10T1/2 cells was also examined. These factors, including rhBMP-2 (300 ng/ml) (Katagiri et al., 1990; Lee et al., 1999) and the synthetic glucocorticoid dexamethasone (10 nM) (Bellows et al., 1987), were added to the culture medium following the final transduction and maintained with fresh media changes for the duration of the experiments.

No significant differences in viral titer or gene transduction efficiency were observed among independent viral supernatant stocks. Retroviral titer, determined similarly to Galipeau et al. (Galipeau et al., 1999), of Runx2 viral supernatants were in the range of 1-2×10^5 cfu/ml. During experimental transductions, retrovirally transduced

cells were noninvasively analyzed for eGFP expression by fluorescence microscopy (Figure 4-2A) and flow cytometry (Figure 4-2C), using a Becton-Dickinson FACS Vantage SE Cell Sorter. After two rounds of retroviral transduction, cytometric analyses indicated a transduction efficiency >95% in NIH3T3 cells (Figure 4-1D), >90% in C3H10T1/2 cells, and >85% in MC3T3-E1 cells.

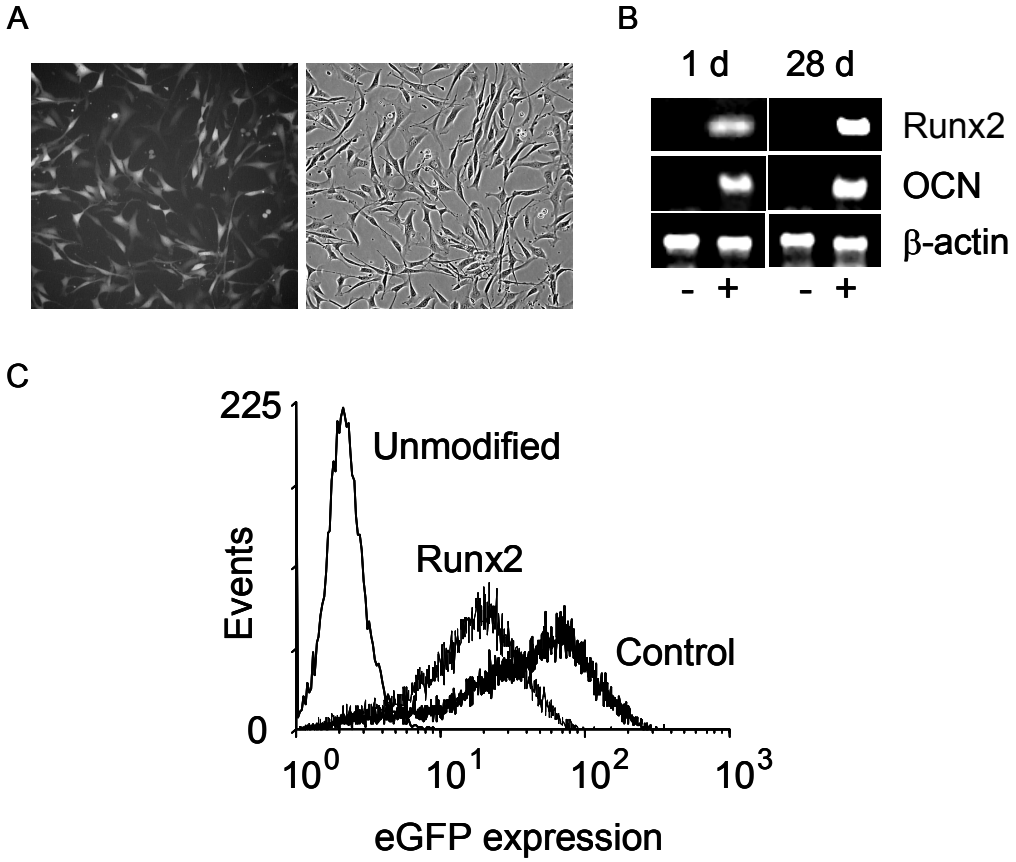

Figure 4-2. Observation of transduction efficiency and Runx2 gene expression in Runx2-transduced and control NIH3T3 fibroblasts. (A) Noninvasive detection of eGFP expression by fluorescence (left) and phase contrast (right) micrographs of Runx2-expressing NIH3T3 fibroblasts, indicating high and uniform transduction efficiency. (B) Runx2 and OCN transcripts detected by PCR at 1 and 28 days post transduction in NIH3T3 Runx2-expressing (+) and control cultures (-), demonstrating immediate and sustained gene expression and functional protein expression of Runx2. (C) Flow cytometry histograms of Runx2-transduced and control NIH3T3 fibroblasts 3 days post transduction.

Osteoblast-Specific Gene Expression

Total RNA was isolated at 1, 3, and 7 days post transduction using the RNeasy RNA isolation kit. cDNA synthesis was performed on DNaseI-treated (27 Kunitz units/sample) total RNA (1 μg) by oligo(dT) priming using the Superscript II™ Preamplification System. Conventional PCR was performed using recombinant Taq DNA polymerase and the Perkin Elmer GeneAmp® System 9700 thermal cycler (35 cycles, melting: 30 sec at 94ºC, annealing: 60 sec at 57ºC, extension: 90 sec at 72ºC). Conventional PCR oligonucleotide primers (Table 4-1) for Runx2 were designed using Primer Premier (Premier Biosoft International, Palo Alto, CA), those for BSP and OCN were previously reported (Tintut et al., 1999), and β-actin was obtained from Clontech. Gene expression was normalized to cytoskeletal β-actin using agarose gel electrophoresis and the Kodak Digital Science 1D image analysis software (Eastman Kodak Co., Rochester NY). Real-time PCR oligonucleotide primers (Table 4-1) were designed using Primer Express software (Applied Biosystems). Real-time products were analyzed on 2.2% agarose gels to confirm primer specificity. Real-time PCR using Sybr Green intercalating dye was performed with the ABI Prism 7700 Sequence Detection System (Applied Biosystems) (40 cycles, melting: 15 sec at 95ºC, annealing and extension: 60 sec at 60ºC). Gene transcript concentration in template cDNA solutions was quantified by generating a linear standard curve from a decade-dilution of an absolute standard for each gene and plotting the log of concentration vs. the C_T value, which is the cycle number at which the observed fluorescence reaches a threshold level. Standards for each gene were amplified from template cDNA using real-time oligonucleotides, purified

using a Qiagen agarose gel extraction kit, and diluted over a functional range of concentrations.

Table 4-1. PCR oligonucleotides for murine osteoblastic genes

Gene	Type	Forward Primer	Reverse Primer	Size (bp)
Runx2	C	mRunx2-490.F 5'-GCAGTGCCCCGATTGAGG-3'	mRunx2-976.R 5'-CATACTGGGATGAGGAATGCG-3'	487
AF010284¥	R-T	mRunx2-217.F RT 5'-AGCCTCTTCAGCGCAGTGAC-3'	mRunx2-275.R RT 5'-CTGGTGCTCGGATCCCAA-3'	59
BSP	C	mBSP-402.F 5'-CTCGGGTGTAACAGCTAGCTAC-3'	mBSP-785.R 5'-CGTTCAGAAGGACAGCTGTCTG-3'	384
L20232	R-T	mBSP-219.F RT 5'-TCCTCCTCTGAAACGGTTTCC-3'	mBSP-291.R RT 5'-GGAACTATCGCCGTCTCCATT-3'	73
OCN	C	mOCN-91.F 5'-CTCTGTCTCTCTGACCTCACAG-3'	mOCN-450.R 5'-GGAGCTGCTGTGACATCCATAC-3'	360
X04142	R-T	mOCN-126.F RT 5'-CGGCCCTGAGTCTGACAAA-3'	mOCN-193.R RT 5'-GCCGGAGTCTGTTCACTACCTT-3'	68
COLα1(I)	R-T	mCOLα1(I)-3963.F RT 5'-TGG ATT CCC GTT CGA GTA CG -3'	mCOLα1(I)-4024.R RT 5'-TCA GCT GGA TAG CGA CAT CG-3'	62
U08020				
β-actin	C	β-actin-25.F 5'-GTGGGCCGCTCTAGGCACCAA-3'	β-actin-564.R 5'-CTCTTTGATGTCACGCACGATTTC-3'	540
X03672	R-T	mβ-actin-459.F RT 5'-TTCAACACCCCAGCCATGT-3'	mβ-actin-527.R RT 5'-TGTGGTACGACCAGAGGCATAC-3'	69

¥: GenBank accession number; m, murine; C, conventional PCR; R-T, real-time PCR.

Alkaline Phosphatase Biochemical Activity

As an early marker of osteoblastic differentiation (Aubin and Liu, 1996), alkaline phosphatase (ALP) activity was quantified at 3, 7, and 14 days post transduction using a modification of the method of Sodek and Berkman (Sodek and Berkman, 1987). Briefly, cells were rinsed and scraped in ice-cold 50 mM Tris·HCl. Following sonication and centrifugation, total soluble protein concentration was quantified using the MicroBCA Protein Assay Kit (Pierce, Rockford, IL). Equal amounts of protein (2.5 μg) were added to 60 μg/mL 4-methyl-umbelliferyl-phosphate fluorescent substrate in diethanolamine buffer (pH 9.5). Following incubation for 60 minutes at room temperature, the fluorescence was read at 365 nm excitation/450 nm emission on an HTS 7000 Plus

BioAssay Reader (Perkin Elmer, Norwalk, CT). Enzymatic activity was standardized using purified calf intestinal alkaline phosphatase (Sigma) and normalized to total protein concentration.

Matrix Mineralization

Cultures were fixed in 70% ethanol at 14 and 21 days and examined histochemically for mineralized matrix formation by von Kossa staining. Following addition of 5% $AgNO_3$, plates were incubated under uniform light exposure for 30 minutes. The stain was then fixed in 5% Na_2SO_3 for 2 min and cultures were air-dried. Mineralized surface area was quantified by capturing and averaging sixteen representative 1.8× images using Image Pro image analysis software (Media Cybernetics, Silver Springs, MD). For further characterization of the mineral phase, chemical composition analyses were performed on acetone-fixed cultures by Fourier Transform Infrared (FT-IR) microscopy (Nicolet Magna 550, ThermoNicolet, Madison, WI) (Boskey et al., 1996).

A calcium dissolution assay was performed to determine the onset of matrix mineralization in Runx2-modified and control MC3T3-E1 cultures. Beginning at 6 and continuing to 12 days post transduction, cultures were rinsed twice in calcium-free PBS, lysed and homogenized in equal volumes of 0.5 N HCl, and shaken for 4 hrs at 4ºC. Cell lysates were sonicated and centrifuged (8000 g) for 10 minutes, and total soluble calcium was quantified using a colorimetric assay kit and calcium/phosphorous standards (Sigma) according to the manufacturer's instructions. NIH3T3 cells, which do not mineralize, were harvested at each time point to determine baseline cellular calcium levels.

Data Analysis

All analyses were performed on assays conducted at least three times, each with unique Runx2 retroviral supernatant preparations. Data are reported as mean ± SEM, and statistical comparisons using SYSTAT 8.0 were based on an analysis of variance (ANOVA) and Tukey's test for pairwise comparisons with a p-value < 0.05 considered significant. In order to make the variance independent of the mean, statistical analysis of real-time PCR data was performed following logarithmic transformation (Sokal and Rohlf, 1980).

RESULTS

Runx2 induces/up-regulates osteoblast-specific gene expression

Osteoblast-specific gene expression, including Runx2, OCN, BSP, and COLα1(I), was investigated at multiple time points after Runx2 transduction by conventional (Figure 4-3A) and real-time PCR (Figure 4-3B). Runx2 expression was detected in Runx2-expressing target cells as early as 24 hours and remained at an up-regulated level at 28 days (Figures 4-2B and 4-3). Runx2 transcripts in Runx2-transduced NIH3T3 cultures were 4-fold higher than in C3H10T1/2 cells and 6-fold higher than in MC3T3-E1 cultures as determined by real-time PCR at 1 day. Runx2 transcripts were absent from NIH3T3 and C3H10T1/2 fibroblasts with control vector at all time points as shown by conventional PCR (Figure 4-3A), and real-time data indicated that signal was 2 to 3 orders of magnitude lower than Runx2-expressing cultures (Figure 4-3B). In comparison to endogenous expression in MC3T3-E1 controls, Runx2 expression in Runx2-treated

MC3T3-E1 cultures was nearly 10-fold greater at 1 day, 5-fold higher at 3 days, and 2-fold greater at 7 days.

OCN provides a primary marker for Runx2 overexpression, as it is expressed only in mature osteoblasts (Hauschka et al., 1989; Weinreb et al., 1990) and is transcriptionally regulated by a Runx2-binding cis-acting element (Ducy and Karsenty, 1995). In non-osteoblastic cells, Runx2 induced OCN expression at all time points examined, whereas control cultures lacked detectable OCN expression (Figure 4-3). Sustained expression of OCN in Runx2-treated non-osteoblastic cells at 28 days (Figure 4-2B) indicated stable integration of the Runx2 sequence into the host genome and constitutively active translation of a functional Runx2 protein. Additionally, OCN expression was accelerated and enhanced in Runx2-expressing MC3T3-E1 cells. OCN transcripts were detected as early as 1 day post Runx2-treatment, whereas endogenous expression was not detected in control cultures until day 7 by conventional PCR. Real-time PCR displayed 5 to 8-fold up-regulated OCN expression at various time points (Figure 4-3B).

BSP transcripts were not detected in Runx2-expressing NIH3T3 fibroblasts in four separate retroviral transductions (Figures 4-3A and 4-3B). Runx2-expressing C3H10T1/2 fibroblasts typically did not produce BSP levels detectable by conventional PCR (Figure 4-3A). Using the enhanced sensitivity of real-time PCR, BSP transcripts were detected at 3 and 7 days in Runx2-treated cultures, yet the relative expression was more than 50-fold less than that detected in parallel MC3T3-E1 cultures (Figure 4-3B). In one C3H10T1/2 transduction, which is further detailed later, BSP transcripts were detected at levels comparable to Runx2-treated MC3T3-E1 cultures. Finally, BSP

expression was up-regulated nearly 10-fold in Runx2-expressing MC3T3-E1 cultures at later time points. As with OCN, endogenous BSP expression in control MC3T3-E1 increased over time, in accordance with the progressive differentiation program of this immature osteoblast-like cell line.

Runx2 overexpression resulted in no differences in COLα1(I) gene expression when examined by conventional PCR in any of the three cell types (data not shown). Corroborating these results, no significant differences in COLα1(I) transcript levels were detected by real-time PCR (Figure 4-3B).

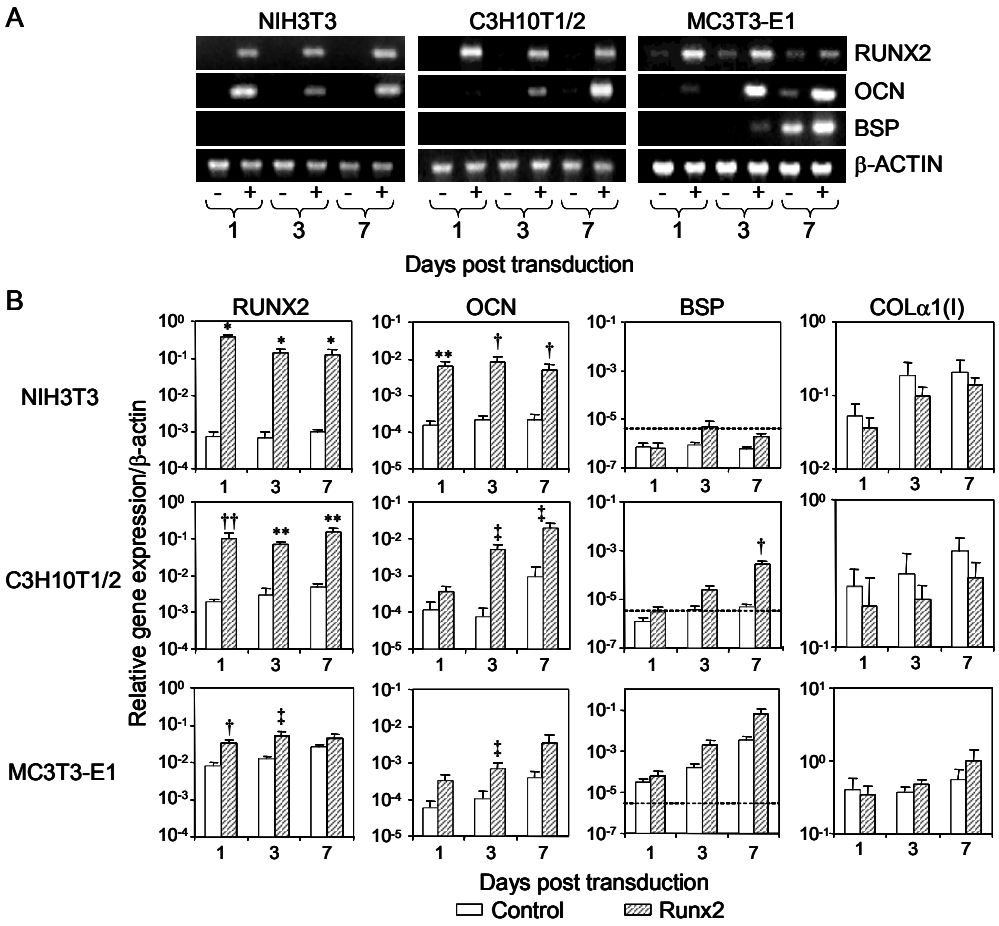

Figure 4-3. Osteoblast-specific gene expression in Runx2-modified and control fibroblastic and osteoblast-like cell lines. (A) Conventional RT-PCR for osteoblast-specific gene expression in NIH3T3, C3H10T1/2, and MC3T3-E1 cells transduced with Runx2 (+) and control (-) at various time points. Runx2 and OCN transcripts were detected in all Runx2-infected cell types, indicating induction of osteoblast-specific gene expression in the fibroblasts and accelerated up-regulation in the immature osteoblast-like cells. As detected by conventional PCR, BSP expression was only up-regulated in MC3T3-E1 cells overexpressing Runx2. Samples were normalized to endogenous cytoskeletal β-actin expression. (B) Relative gene expression (mean, SEM) for Runx2, OCN, BSP, and COLα1(I) generated from real-time PCR of NIH3T3 (n=4), C3H10T1/2 (n=3), and MC3T3-E1 (n=4) cells transduced with Runx2 and control virus. Tabulated concentrations were normalized to β-actin expression and plotted on a log scale. ANOVA showed significant differences between Runx2-modified and controls: NIH3T3, Runx2 ($p<0.000001$) and OCN ($p<0.000001$); C3H10T1/2, Runx2 ($p<0.000001$), OCN ($p<0.0005$), and BSP ($p<0.0001$); MC3T3-E1, Runx2 ($p<0.0002$) and OCN ($p<0.03$). Pairwise comparisons: * different from control ($p<0.00001$); ** different from control ($p<0.001$); † different from control ($p<0.005$); †† different from control ($p<0.0001$); ‡ different from control ($p<0.05$). Dotted line represents the assay detection limit (6.0E-06).

Runx2 expression enhances alkaline phosphatase activity

ALP activity was examined at 3, 7, and 14 days post transduction (Figure 4-4). NIH3T3 cells expressing Runx2 demonstrated only moderate ALP activity at 7 and 14 days. However, Runx2-expressing C3H10T1/2 pluripotent fibroblasts demonstrated up-regulated and sustained activity nearly equivalent to that seen in the immature osteoblast-like cells, an observation consistent with previous work (Harada et al., 1999). Forced expression of Runx2 in MC3T3-E1 cells resulted in a 4-fold higher activity at 3 and 7 days and a 2-fold increase at 14 days compared to endogenous levels in control cultures. Consistent with osteoblast-specific gene expression results, ALP activity in Runx2-treated and control cultures progressively increased over time up to 14 days.

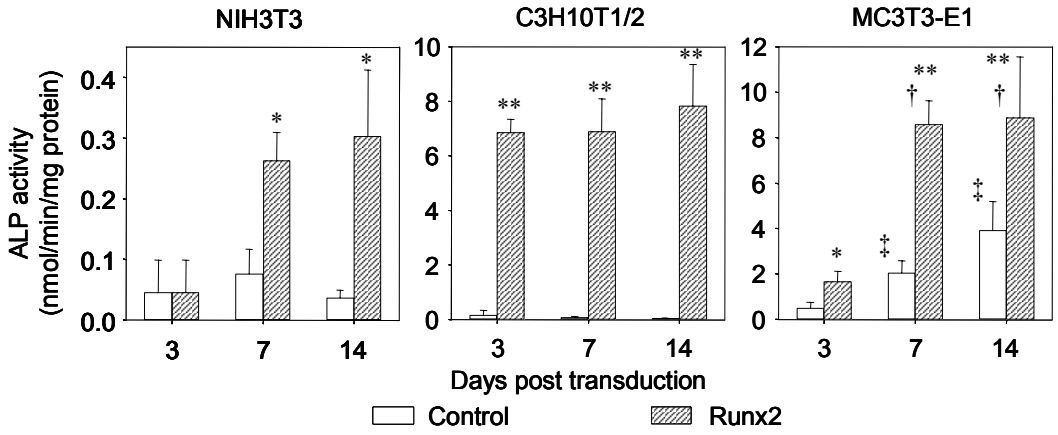

Figure 4-4. Alkaline phosphatase activity of model fibroblastic and osteoblast-like cell lines transduced with Runx2 or control virus. Data are reported as [(mean, SEM), n=3]. ANOVA demonstrated significant differences between Runx2-transduced and controls ($p<0.0001$) and among time points ($p<0.01$). Pairwise comparisons: * different from control ($p<0.05$); ** different from control ($p<0.01$); † different from 3 day Runx2-infected ($p<0.01$); ‡ different from 3 day control ($p<0.05$).

Effects of forced expression of Runx2 on matrix mineralization

NIH3T3 fibroblasts. Matrix mineralization was examined by von Kossa staining at 14 and 21 days. Even though Runx2-transduced NIH3T3 fibroblasts expressed multiple osteoblast-specific genes, mineralization was completely absent in cultures maintained even to 28 days. In order to ensure that this response was not specific to this established fibroblastic cell line, IMR-90 human lung fibroblasts (ATCC, CCL-186) were also examined for matrix mineralization following Runx2 overexpression. eGFP expression was detected by fluorescence microscopy, indicating this human cell line was transduced by the amphotropic retrovirus (data not shown). Although murine Runx2 was overexpressed in a human cell line, the MASNSLF Runx2-isoform contains high sequence homology in both exonic and intronic regions across mouse, rat, and human species (Xiao et al., 1998b). Functionality was confirmed by detection of human OCN gene expression by conventional RT-PCR in Runx2-modified IMR-90 cultures (data not shown), yet Runx2-expressing IMR-90 fibroblasts also failed to mineralize in all experiments.

C3H10T1/2 fibroblasts. This pluripotent cell line displayed induction of several osteoblast-specific genes as well as dramatically enhanced ALP activity in response to Runx2 overexpression. Interestingly, the capacity of C3H10T1/2 fibroblasts to mineralize *in vitro* revealed two responses. In six of eight (75%) mineralization experiments, each conducted with independent Runx2 retroviral supernatants, the Runx2-expressing C3H10T1/2 cells did not produce a mineralized matrix (data not shown). However, two of these eight supernatants resulted in mineralization (Figure 4-5A),

although significantly less than matched MC3T3-E1 control cultures. In all cases, cells transduced with control virus did not mineralize. Osteoblast-specific gene expression and ALP activity were examined in one of the two mineralizing cultures. Conventional PCR revealed ubiquitous OCN gene expression in both mineralizing and non-mineralizing Runx2-modified C3H10T1/2 cultures at 7 days. However, BSP transcripts were only detected in the mineralizing Runx2-expressing C3H10T1/2 culture (Figure 4-5B). Furthermore, quantification of Runx2 and OCN transcript levels in the mineralizing Runx2-transduced C3H10T1/2 culture at 1, 3, and 7 days indicated nearly equivalent expression levels of these two genes when compared to non-mineralizing Runx2-expressing cultures at all time points (data not shown). Additionally, 7 day ALP activity of the mineralizing Runx2-modified culture (4.9 nmol/min/mg protein) was approximately equal to that of non-mineralizing Runx2-expressing C3H10T1/2 cultures (6.9 nmol/min/mg protein). In contrast, BSP gene expression in this mineralizing Runx2-treated culture exhibited large differences when compared to those Runx2-expressing cultures which did not mineralize. At 1 day, BSP expression levels in both cases were approximately equal to the assay detection limit. However, the mineralizing Runx2-modified C3H10T1/2 culture displayed 100-fold higher BSP transcript levels at 3 days and nearly 60-fold higher levels at 7 days compared to non-mineralizing Runx2-transduced cultures (data not shown). This expression level in the mineralizing Runx2-expressing culture was nearly equivalent to Runx2-expressing MC3T3-E1 cells. Following these observations, parallel transductions were performed simultaneously on all target cells with retroviral supernatants which both had and had not previously resulted in C3H10T1/2 mineralization. Viral supernatant-dependent expression of BSP

and mineralization in C3H10T1/2 cultures was again observed, i.e. the same two Runx2 viral stocks resulted in high levels of BSP expression and mineralization in C3H10T1/2 cultures, while remaining lots did not induce mineralization. Matched NIH3T3 and IMR-90 fibroblast cultures failed to mineralize in all cases, and Runx2-modified MC3T3-E1 cells demonstrated indistinguishable up-regulated mineralization independent of the particular Runx2 viral stock. These parallel analyses indicated that no significant differences in viral titer or transduction efficiency existed among various viral supernatants and showed that the stochastic response to different Runx2 viral supernatant stocks was unique to the C3H10T1/2 cell line and most likely attributable to secondary factors in the retroviral supernatant.

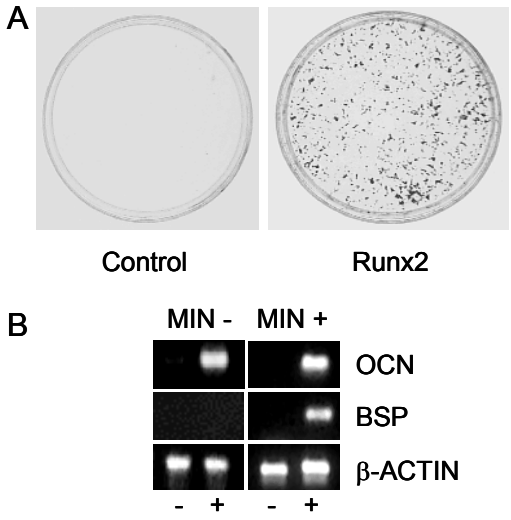

Figure 4-5. Mineralization staining and gene expression of mineralizing and non-mineralizing Runx2-expressing C3H10T1/2 cells. (A) Matrix mineralization (21 days) in Runx2-expressing C3H10T1/2 pluripotent fibroblasts. Overexpression of Runx2 in two of eight independent experiments each with unique retroviral supernatant lots resulted in mineralization, although much less than matched MC3T3-E1 controls. (B) Conventional PCR for osteoblast-specific gene expression (7 days) from non-mineralizing (MIN-) and mineralizing (MIN+) Runx2-modified (+) and control (-) C3H10T1/2 fibroblasts. OCN transcripts were detected in both cases; however, BSP expression was only detected in the culture which ultimately mineralized.

Subsequent experiments were performed to further examine this stochastic mineralization response in C3H10T1/2 fibroblasts. Three independent, non-mineralizing Runx2 viral supernatants were used in combination with the osteoinductive factors rhBMP-2 and dexamethasone. It was hypothesized that BMP-2 would complement the effects of Runx2 overexpression in C3H10T1/2 cells to direct osteoblastic differentiation and induce mineralization independent of Runx2 viral stock. BMP-2 is a potent stimulator of osteoblastic differentiation both *in vitro* and *in vivo* and induces osteoblast-specific gene expression in non-osteoblastic C3H10T1/2 cells (Katagiri et al., 1990) and the myoblastic C2C12 cell line (Lee et al., 1999). Additionally, BMP-2 enhances expression of the Id (inhibitor of differentiation) family of transcription factors, which act to inhibit function of helix-loop-helix transcription factors of alternative differentiation pathways, such as MyoD (Ogata et al., 1993; Locklin et al., 2001). Dexamethasone stimulates *in vitro* nodule formation in rat calvarial osteoblasts (Bellows et al., 1987) and osteoblastic gene expression in rat bone marrow stromal cells (Leboy et al., 1991). The complete mechanism of action of dexamethasone in osteoblastic differentiation has not been elucidated; however, as in the case of BMP-2, it was hypothesized that these pathways may act synergistically with Runx2 to enhance osteoblastic differentiation and mineralization of C3H10T1/2 cells.

Matrix mineralization was examined at 14 days by von Kossa staining (Figure 4-6A). As previously seen with the non-mineralizing Runx2 viral stocks, all Runx2-expressing C3H10T1/2 cultures without BMP-2 or dexamethasone did not mineralize, and all control cultures failed to mineralize in the presence or absence of either BMP-2 or dexamethasone. Small, sparsely stained regions, only detectable at high magnification,

were present in Runx2-expressing cultures supplemented with BMP-2 (Figure 4-6A3). Notably, dexamethasone-treated, Runx2-modified cultures mineralized to a greater extent (Figure 4-6A5). Osteoblast-specific gene expression was also examined in these cultures at 7 days by real-time PCR. Gene expression levels of the previously described mineralizing Runx2-expressing C3H10T1/2 culture (Min +) are presented for reference (Fig 4-6B). Runx2 gene expression levels were approximately equal in all Runx2-treated cultures, independent of treatment with BMP-2 or dexamethasone. OCN levels were significantly increased in all Runx2-expressing cultures, and these expression levels were comparable to the mineralizing Runx2-modified C3H10T1/2 culture. BMP-2 treated, control C3H10T1/2 cultures showed significantly higher OCN expression compared to untreated control cultures, indicating bioactivity of the BMP-2 stock used in these experiments. Interestingly, BSP transcript levels increased slightly (4-fold) in Runx2-expressing cells supplemented with BMP-2 and significantly higher (25-fold) with exposure to dexamethasone. Control Runx2-expressing NIH3T3 fibroblasts failed to mineralize in the absence or presence of BMP-2 or dexamethasone, and no distinguishable differences in mineralized surface area were detected between control Runx2-transduced MC3T3-E1 cultures and those supplemented with these osteoinductive agents (data not shown).

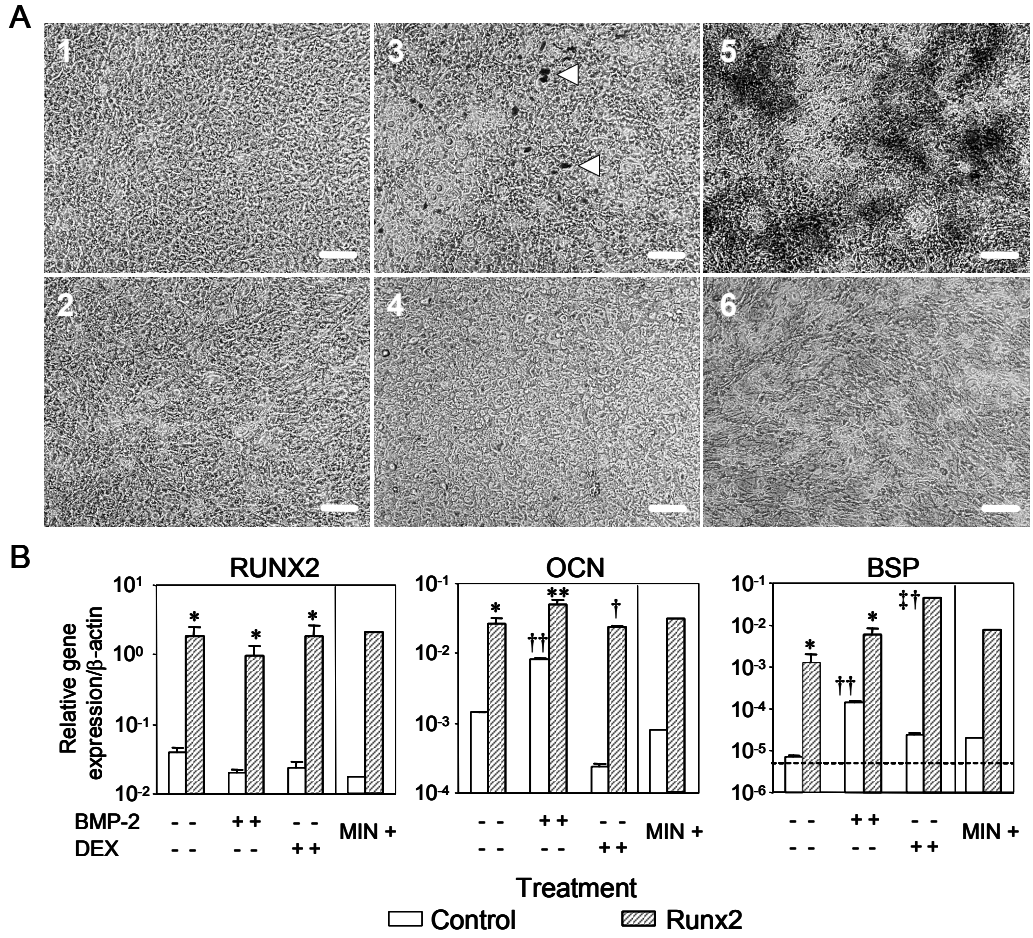

Figure 4-6. Mineralization and gene expression in Runx2-transduced and control C3H10T1/2 cultures co-treated with either BMP-2 or dexamethasone. (A) von Kossa stained (1) Runx2-transduced, (2) control, (3) Runx2 + BMP-2 (small nodules indicated by arrows), (4) control + BMP-2, (5) Runx2 + dexamethasone, and (6) control + dexamethasone cultures at 14 days. Bar represents 100 microns. (B) Real-time PCR data [(mean, SEM), n=3] at 7 days for Runx2, OCN, and BSP. For reference, expression levels from the 7 day mineralizing Runx2-expressing culture (MIN+) are included. ANOVA showed significant differences ($p<0.000001$) between Runx2-modified and controls for all genes. Pairwise comparisons: * different from same treatment control ($p<0.001$); ** different from same treatment control ($p<0.01$); † different from same treatment control ($p<0.00001$); †† different from control ($p<0.01$); ‡ different from Runx2-transduced, no treatment ($p<0.002$). Dotted line represents the assay detection limit (6.0E-06).

Primary skin fibroblasts. In order to further characterize the effects of exogenous Runx2 expression in fibroblasts, primary mouse skin fibroblasts were harvested, expanded in culture, and transduced with Runx2. Real-time PCR analysis at 7 days demonstrated significant up-regulation in OCN and BSP gene expression in Runx2-expressing primary cells compared to controls (Figure 4-7). Mineralization studies in Runx2-expressing primary skin fibroblasts at 14 days revealed minute, sparse nodule-like regions independent of Runx2 retroviral supernatant lot. However, these areas covered less than 5% of the culture surface area and were only distinguishable at high magnification (data not shown). The authors note that selection was not performed to establish a homogenous population of primary skin fibroblasts. As a result, cell types of the dermal region which may be responsive to Runx2 overexpression, including adipogenic or vascular lineages, were potentially present in the cultures examined. Therefore, further studies are necessary to completely elucidate the Runx2-responsiveness of primary skin fibroblasts.

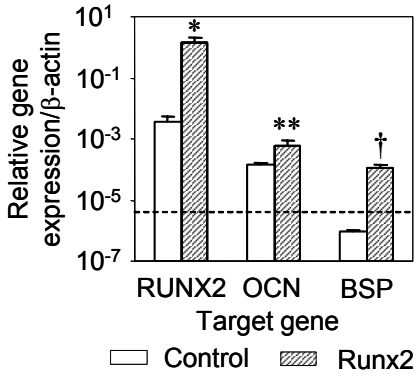

Figure 4-7. Osteoblast-specific gene expression at 7 days in Runx2-expressing and control murine primary skin fibroblasts. Data are reported as [(mean, SEM), n=3]. ANOVA showed significant differences between Runx2-transduced and controls for all genes: * different from control ($p<0.001$); ** different from control ($p<0.05$); † significant over assay detection limit ($p<0.002$). Line represents the assay detection limit (6.0E-06).

MC3T3-E1 immature osteoblast-like cells. This cell line was selected as a model of osteoblastic differentiation as it produces a mineralized matrix *in vitro* (Sudo et al., 1983), indicating endogenous expression of all essential factors necessary for mineralization. As expected, overexpression of Runx2 in MC3T3-E1 cells significantly up-regulated *in vitro* matrix mineralization at 14 and 21 days compared to controls (Figure 4-8A and B). Quantification of mineralized surface area revealed a 4-fold increase at 14 days and a 2-fold increase at 21 days (Figure 4-8C). This indicated that *in vitro* mineralization was up-regulated in Runx2-modified cultures, yet mineralized surface area, which was ultimately restricted by the culture dish surface area, eventually saturated as control cultures approached similar levels of total mineralized area at later time points. Comparison of Runx2-treated cultures to controls revealed an increase in the number of mineralized foci, suggesting that forced-Runx2 expression in these osteogenic cells increased the number of clones capable of differentiating and ultimately producing a mineralized matrix. No detectable differences in mineralized surface area existed between cultures transduced with control retrovirus and cultures undergoing no retroviral transduction, indicating that retroviruses did not adversely impact mineralization capacity.

The detection of high OCN expression at one day and up-regulated ALP activity at early time points in Runx2-expressing MC3T3-E1 cells indicated the acceleration of osteoblast-specific gene and protein expression. A calcium dissolution assay was performed to determine the extent to which Runx2 overexpression accelerated the onset of matrix mineralization. Beginning 6 and continuing to 8 days post transduction, incorporated calcium levels in both Runx2-expressing and control cultures were

indistinguishable from background levels (Figure 4-8D). At day 9, a significant increase in incorporated calcium was observed in Runx2-expressing MC3T3-E1 cultures compared to both control cultures at day 9 and Runx2-transduced cultures at day 8. However, an increase in calcium incorporation was not detected in control cultures until day 10, indicating that in addition to accelerating osteoblast-specific gene expression, Runx2 overexpression accelerated matrix mineralization in the MC3T3-E1 osteoblast-like cell line. In agreement with mineralized surface area quantification data, calcium incorporation in Runx2-expressing cultures was higher than controls over the time course of the study.

Mineralized areas were examined by FT-IR spectroscopy to determine the chemical composition of the mineral phase, ensuring biological hydroxyapatite formation rather than ectopic precipitation of calcium phosphate potentially resulting from increased alkaline phosphatase activity. Mineral phase from MC3T3-E1 and C3H10T1/2 cultures transduced with Runx2 were compared to cadaveric bone as a positive control (Figure 4-8E). Peaks of interest include the phosphate stretching peak at 1100 cm^{-1} and the doublet split at 560 cm^{-1} and 605 cm^{-1}, which are representative of a bending mode of crystallized phosphate. Finally, the presence of a carbonate peak at approximately 870 cm^{-1} is characteristic of the biological substitution of carbonate for hydroxide (type I) and/or carbonate for phosphate (type II) in the hydroxyapatite crystalline structure (Mendelsohn et al., 1989; Boskey et al., 1996).

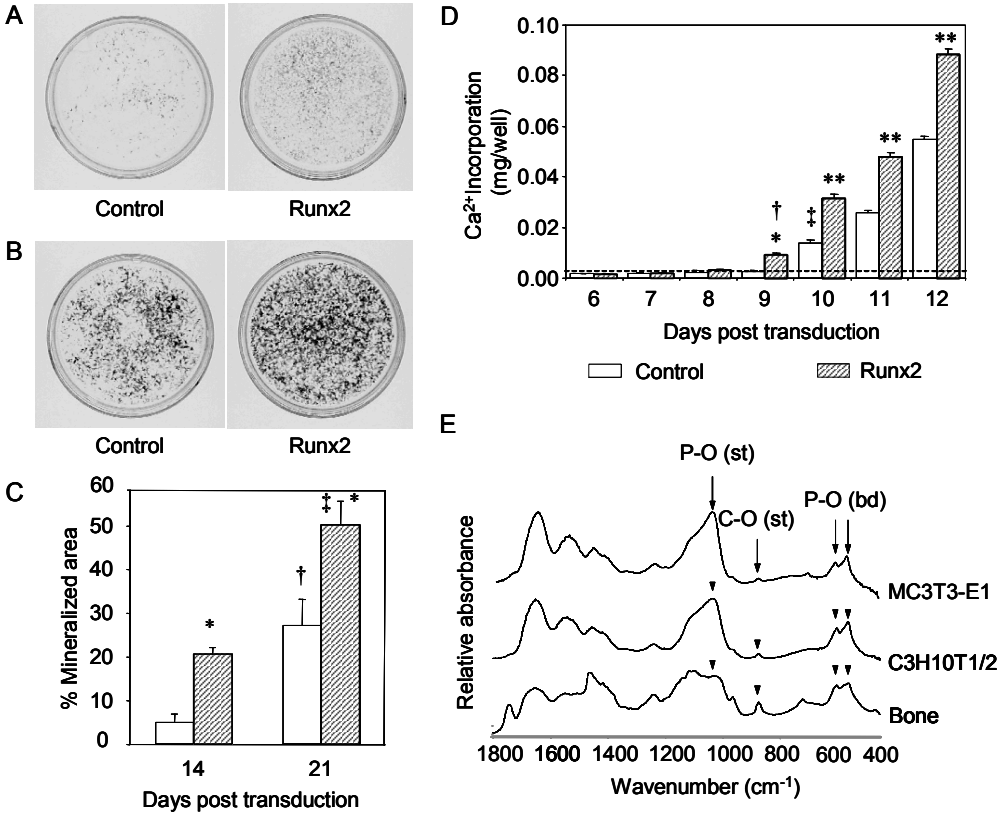

Figure 4-8. Mineralization of Runx2-transduced and control MC3T3-E1 immature osteoblast-like cells. Forced expression of Runx2 in MC3T3-E1 immature osteoblast-like cells significantly enhanced matrix mineralization at (A) 14 and (B) 21 days. (C) Mineralized surface area of cultures transduced with Runx2 and control virus quantified by image analysis [(mean, SEM), n=3]. ANOVA demonstrated significant differences between Runx2-modified and control cultures ($p<0.002$) and among time points ($p<0.001$). Pairwise comparisons: * different from control ($p<0.03$); † different from 14 day control ($p<0.05$); ‡ different from 14 day Runx2-transduced ($p<0.05$). (D) Onset of mineralization as detected by Ca^{2+} incorporation in Runx2-expressing and control MC3T3-E1 cultures [(mean, SEM), 3 independent experiments each in duplicate]. ANOVA for days 8-12 showed significant differences between Runx2-transduced and controls ($p<0.000001$). Pairwise comparisons: * different from control ($p<0.0001$); † different from 8 day Runx2-modified ($p<0.0001$); ** different from control ($p<0.00001$); ‡ different from 9 day control ($p<0.001$). Dotted line represents the mean background cellular Ca^{2+} levels (0.003 mg/well) of NIH3T3 cells. (E) FT-IR spectra of mineralized nodules from 21 day Runx2-expressing MC3T3-E1 and mineralizing C3H10T1/2 cultures and a cadaveric bone positive control. Spectra showed bands characteristic of biological hydroxyapatite formation, including phosphate- and carbonate-related vibrations. st: stretching vibrations, bd: bending vibrations.

DISCUSSION

The requirement of Runx2 for osteoblastic differentiation and *in vivo* bone formation and maintenance has been clearly shown (Otto et al., 1997; Komori et al., 1997; Mundlos et al., 1997; Ducy et al., 1999). Furthermore, Runx2 forced expression induced osteoblast-specific gene and protein expression *in vitro* as detailed here and elsewhere (Ducy et al., 1997; Xiao et al., 1998b; Xiao et al., 1999), yet the effects of Runx2 overexpression on *in vitro* matrix mineralization had not been demonstrated. Mineralized matrix formation is time-intensive, requiring nearly one to two weeks of *in vitro* culture prior to initial nodule formation in the MC3T3-E1 cell line (Marsh et al., 1995; Choi et al., 1996). Therefore, conventional *in vitro* transfection techniques provide insufficient efficiency and expression duration to examine the long term effect of Runx2 overexpression on this complex differentiation cascade. To address this complication, this study focused on exogenous expression of Runx2 in target cells using retroviral gene delivery, which provided highly efficient, constitutively active, and sustained gene expression.

Runx2-expressing NIH3T3 fibroblasts did not form mineralized nodules *in vitro*, even though the presence of OCN transcripts in Runx2-expressing cultures demonstrated that the cell line was responsive to exogenous Runx2 expression (Figure 4-3). The IMR-90 fibroblastic cell line also failed to mineralize following Runx2 overexpression. These results indicated that forced expression of Runx2 in these non-osteogenic cell lines was not sufficient for *in vitro* matrix mineralization, suggesting that additional cofactors which spatiotemporally interact either directly with Runx2 or its gene targets are required. Lack of mineralization was consistent with the absence of BSP gene expression

and potentially insufficient ALP activity in these cell lines. BSP has been shown to be an enhancer of *in vitro* hydroxyapatite nucleation even at low concentrations, suggesting it plays a critical role in the initiation of bone mineralization (Hunter et al., 1996). Furthermore, ALP activity in Runx2-expressing NIH3T3 fibroblasts was more than 30 times less than in mineralizing MC3T3-E1 cultures, and it has been shown that isolated calvarial cells from ALP knockout mice fail to produce mineralized matrix *in vitro* (Wennberg et al., 2000).

C3H10T1/2 fibroblasts overexpressing Runx2, although not ubiquitously, were capable of producing a biologically equivalent mineralized matrix (Figs. 4-5 and 4-8E), consistent with the pluripotent nature of this cell line. However, this was a low-frequency, stochastic response which occurred in a retroviral supernatant lot-dependent manner and was independent of viral titer and Runx2 transduction efficiency. Additionally, OCN gene expression and alkaline phosphatase activity were approximately equal in both non-mineralizing and mineralizing Runx2-modified C3H10T1/2 cultures. Detection of 50 to 100-fold higher levels of BSP transcripts in mineralizing Runx2-expressing C3H10T1/2 cultures compared to Runx2-treated cultures which failed to mineralize, suggested that the variable response in matrix mineralization arises from the activation of additional pathways by secondary factors in the retroviral supernatant, possibly serum growth factors. This stochastic behavior was cell type-dependent, however, as simultaneously transduced Runx2-expressing NIH3T3 and IMR-90 cultures failed to produce mineralized nodules, and MC3T3-E1 cells demonstrated equivalent up-regulated mineralization independent of viral supernatant. Further substantiating the requirement of additional factors for mineralization in the C3H10T1/2

cell line, a synergistic induction of mineralization was observed in Runx2-treated cultures treated with dexamethasone, whereas control Runx2-modified and dexamethasone-treated control cultures failed to mineralize in all cases (Figure 4-6A).

When cultured under appropriate conditions, immature osteoblast-like MC3T3-E1 cells endogenously express all factors necessary for *in vitro* mineralization, and it was expected that this cell line would therefore be highly responsive to Runx2 overexpression. In accordance with the observed up-regulation in osteoblast-specific gene and protein expression, enhanced mineralization capacity was observed in this osteogenic cell line following forced Runx2 expression (Figure 4-8). Appearance of OCN transcripts in Runx2-transduced MC3T3-E1 cultures as early as one day post transduction indicated accelerated expression of this late marker of osteoblastic maturation, and examination of calcium incorporation revealed the onset of mineralization was also accelerated in Runx2-expressing cultures (Figure 4-8D). Furthermore, overexpression of Runx2 in this immature osteoblast-like cell line increased the population of fully differentiated, mineralized matrix-producing clones as a greater number of mineralizing foci were observed in Runx2-expressing cultures when compared to controls. Interestingly, Liu et al. reported *in vivo* overexpression of Runx2 under control of the tissue-specific pro-α1(I) collagen promoter arrests osteoblast maturation and results in osteopenia and multiple fractures in transgenic mice (Liu et al., 2001). These results underscored the dynamic complexity of *in vivo* osteoblastic differentiation and emphasized the requirement of regulated, spatiotemporal expression of Runx2 for normal *in vivo* bone formation.

Transient transfection of Runx2 has been shown by other groups to enhance osteoblast-specific gene expression and increase osteoblast-specific promoter construct activities in NIH3T3, C3H10T1/2, and MC3T3-E1 cells (Ducy et al., 1997; Harada et al., 1999; Xiao et al., 1999). In agreement with these observations, this study demonstrated that forced expression of Runx2 induced or up-regulated OCN in non-osteoblastic and osteoblastic cell lines, respectively. Temporal observation of osteoblast-specific gene expression showed BSP up-regulation in Runx2-treated MC3T3-E1 cells (Figure 4-3), although transcripts were not detected as early as OCN. Additionally, BSP expression was not detected in Runx2-expressing NIH3T3 fibroblasts and at substantial levels in only a fraction of C3H10T1/2 cultures examined. These results suggest that Runx2 regulation of BSP is indirect and cell type-dependent, requiring additional factors. For example, Enomoto *et al.* examined the forced expression of Runx2 in chick immature chondrocytes and showed an up-regulation of collagen type X and collagenase-3 protein expression, but did not detect OCN gene transcripts (Enomoto et al., 2000). Benson *et al.* reported two putative Runx2 binding sites within a 2.5-kb fragment of the murine BSP promoter. Neither exhibited significant enhancer activity, suggesting that other factors may bind to cis-acting elements in the BSP promoter and thereby induce transcription (Benson et al., 1999). No significant differences were detected in COLα1(I) gene expression in any of the cell lines examined. Kern et al. (Kern et al., 2001) reported that the Runx2 cis-acting element in the COLα1(I) promoter is only active in osteoblasts and not in cell lines of non-osteoblastic origin. However, they demonstrated activation of a luciferase reporter construct containing four copies of the α1(I) OSE2 cis-acting elements fused to a minimal α1(I) collagen promoter that was co-transfected with Runx2 in COS-7

cells. While these results confirm that an exogenous murine collagen promoter construct is responsive to Runx2 overexpression, the up-regulation of endogenous COLα1(I) gene expression following forced expression of Runx2 may not be observed in non-osteoblastic cells, such as the NIH3T3 and C3H10T1/2 fibroblasts examined here, due to cell type-specific promoter inactivation. Although COLα1(I) transcript levels trended higher at later time points in Runx2-expressing MC3T3-E1 cultures, a significant increase in expression was not observed. Notably, endogenous COLα1(I) expression levels were orders of magnitude higher than other osteoblast-specific genes investigated (Figure 4-3B). As a result, Runx2 overexpression may not have provided a detectable effect on COLα1(I) expression in this osteogenic cell line.

Cell type-dependent induction/enhancement in expression of certain osteoblast-specific genes, such as BSP, supported the hypothesis that Runx2 interacts with additional factors or other osteoblast-specific transcriptional pathways throughout the differentiation cascade. For example, McLarren et al. suggested that TLE corepressors and HES-1 modulate Runx2 transcriptional activation (McLarren et al., 2000), and physical association of Runx2 with cofactors such as c-fos and c-jun of the AP-1 complex (Hess et al., 2001) or the CCAAT/enhancer binding proteins (Gutierrez et al., 2002) may be a mechanism for regulating tissue-specific gene expression. Finally, the identification of Osterix (Osx) as an essential osteoblast-specific transcription factor acting downstream of Runx2 provides even more insight into the complexity of osteoblast differentiation (Nakashima et al., 2002). Similar to Runx2 knockouts, Osx null mice lacked osteocalcin and BSP expression as well as differentiated osteoblasts. Osterix expression was ablated in Runx2 knockouts, yet it has not been determined if Runx2 directly or cooperatively

regulates Osx expression. These or other currently undefined transcriptional pathways support the cell-type dependent activity of Runx2 observed in the present study.

In summary, this study demonstrated that forced expression of Runx2 via retroviral gene delivery induced or up-regulated several osteoblast-specific genes and proteins ubiquitously in non-osteoblastic and osteoblast-like cells, respectively, while expression of other osteoblast-specific genes (notably BSP) was enhanced in cell type-dependent manner. Furthermore, results indicated that sustained overexpression of Runx2 enhanced *in vitro* osteoblastic differentiation by up-regulating and accelerating mineralized matrix formation in an immature osteoblast-like cell line. These results suggest that Runx2 is an essential but insufficient transactivating factor for complete *in vitro* osteoblastic lineage differentiation and matrix mineralization.

CHAPTER 5

RUNX2-EXPRESSING PRIMARY BONE MARROW STROMAL CELLS

INTRODUCTION

Bone marrow stromal cells have been extensively examined as a candidate cell source for bone tissue engineering applications in both *in vitro* and *in vivo* model systems (Ohgushi et al., 1989; Ohgushi et al., 1993; Bruder et al., 1994; Ishaug et al., 1997; Kadiyala et al., 1997; Breitbart et al., 1999; Quarto et al., 2001; Horwitz et al., 2002; Holy et al., 2003), yet the effectiveness of these stromal/osteoprogenitor cell-based therapies is hampered by their initially low frequency in healthy marrow (0.001% of nucleated cells) (Bruder et al., 1997) and propensity for dedifferentiation in response to adhesion-dependent *in vitro* expansion (Ter Brugge and Jansen, 2002; Shi et al., 2002; Simonsen et al., 2002).

Based on the Runx2-responsiveness of MC3T3-E1 osteoblast-like cells (Chapter 4) (Byers et al., 2002), it was of particular interest to examine exogenous Runx2 expression in bone marrow stromal cells. Marrow-derived stromal cells, isolated from the marrow young adult rats, were subjected to Runx2 retroviral transduction and maintained under *in vitro* osteogenic culture conditions. Runx2-modified stromal cells demonstrated increased osteoblastic gene and protein expression and produced significantly higher quantities of mineralized matrix compared to control cultures. Furthermore, subcultured stromal cells undergoing considerable *in vitro* expansion retained the ability to produce a mineralized matrix in response to Runx2 overexpression.

MATERIALS AND METHODS

Reagents

Fetal bovine serum (FBS) was obtained from Hyclone Laboratories (Logan, UT). Remaining cell culture supplies were purchased from Invitrogen (Carlsbad, CA), while chemical reagents were acquired from Sigma Chemical Co. (St. Louis, MO). RNA isolation reagents were purchased from Qiagen (Valencia, CA). Molecular biology reagents for reverse transcription (RT) were obtained from Invitrogen, reagents for real-time PCR were acquired from Applied Biosystems (Foster City, CA), and PCR oligonucleotides were purchased from Integrated DNA Technologies (Coralville, IA).

Cell Isolation and Culture

Primary bone marrow stromal cells were harvested from the femora of young adult male Wistar rats as previously described (Maniatopoulos et al., 1988) in accordance to an IACUC-approved protocol. Briefly, following excision, hindleg femora and tibia were cleared of soft tissue and processed through three consecutive 15 minute rinses in growth media (α-minimum essential medium supplemented with 10% FBS, 1% penicillin-streptomycin, 50 μg/ml gentamicin sulfate, and 0.3 μg/ml fungizone). The ends of the long bones were then removed, and the marrow space was flushed with excess culture media (3 to 5 ml) using a syringe with an 18 gauge needle. Marrow isolates were pooled (typically 6 to 8 rats per harvest), centrifuged, resuspended in growth media, and seeded for adhesion-dependent selection on tissue culture polystyrene dishes. Nonadherent hematopoeitic cells were removed during subsequent media exchanges that occurred every other day. Following 7 days of *in vitro* expansion,

adherent stromal cells were trypsinized, counted, plated on 0.1% type I collagen-coated (Vitrogen-100; Cohesion, Palo Alto, CA) 6-well dishes at a density of 1×10^4 cells/cm^2, and incubated in growth media overnight at 37°C. After two rounds of retroviral transduction, cultures were maintained in osteogenic media consisting of growth media supplemented with 50 μg/ml L-ascorbic acid, 3 mM sodium β-glycerophosphate, and 10 nM dexamethasone (+Dex) (Bellows et al., 1987; Leboy et al., 1991). To isolate the effect of Runx2 overexpression from the osteogenic influence of dexamethasone, some cultures were also maintained in the absence of dexamethasone (-Dex). In all experiments, media was changed every second day. Additional experiments were performed to examine the effect of Runx2 overexpression on serially passaged stromal cells. At confluence, subcultured cells were trypsinized, counted, and reseeded for continued subculture at 5×10^3 cells/cm^2 (Bruder et al., 1997) or seeded for retroviral transduction following passages 2, 4, and 8 as described. During subculture, cells were maintained in growth media with exchanges every other day.

Runx2 Retroviral Vector and Retroviral Transductions

Cloning of the Runx2 retroviral expression vector containing the type II (MASNSLF) Runx2 isoform, packaging of Runx2 and control (no Runx2 insert) retroviruses, and retroviral transduction procedures were performed as described in Chapter 4 and Appendix A (Byers et al., 2002). Retrovirally transduced cells were noninvasively analyzed for transduction efficiency by flow cytometric detection of eGFP expression (Figure 5-1A) using a Becton-Dickinson FACS Vantage SE Cell Sorter.

Osteoblast-Specific Gene Expression

Total RNA was isolated at 1, 3, and 7 days post transduction using the RNeasy RNA isolation kit and quantified by spectroscopy. cDNA synthesis was performed on DNaseI-treated (27 Kunitz units/sample) total RNA (1 μg) by oligo(dT) priming using the Superscript II™ Preamplification System. Real-time PCR was performed with the ABI Prism 7700 Sequence Detection System and Sybr Green intercalating dye (Applied Biosystems). Generation of standard templates and quantification techniques were performed as previously described in Chapter 4 (Byers et al., 2002). Real-time PCR oligonucleotide primers for rat osteoblast-specific genes (Table 5-1) were designed using Primer Express software (Applied Biosystems).

Table 5-1. Real-time PCR oligonucleotides for rat osteoblastic genes

Gene	Forward Primer	Reverse Primer	Size (bp)
Runx2 AF010284¥	5'-AGCCTCTTCAGCGCAGTGAC-3'	5'-CTGGTGCTCGGATCCCAA-3'	59
OCN X04141	5'-ACGAGCTAGCGGACCACATT-3'	5'-CCCTAAACGGTGGTGCCATA-3'	67
COL α1(I) Z78279	5'-TCGATTCACCTACAGCACGC-3'	5'-GACTGTCTTGCCCCAAGTTCC-3'	67
BSP J04215	5'-TGACGCTGGAAAGTTGGAGTT-3'	5'-GCCTTGCCCTCTGCATGTC-3'	69
ALP 7106245	5'-CGTGGCCAAGAACATCATCA-3'	5'-GCGGGCAGCTGTCACTGT-3'	67
OPN AB001382	5'-TGAGACTGGCAGTGGTTTGC-3'	5'-CCACTTTCACCGGGAGACA-3'	63

¥: GenBank accession number

NOTE: Runx2 primer sequences reported were designed to detect murine type II isoform cloned into retroviral expression vector, but the sequences will detect endogenous rat Runx2 as they are conserved across both species.

Alkaline Phosphatase Biochemical Activity

Alkaline phosphatase (ALP) activity was quantified at 7 days post transduction using 4-methyl-umbelliferyl-phosphate fluorescent substrate as detailed in Chapter 4 (Byers et al., 2002) and normalized to total DNA, which was quantified with PicoGreen reagent according to the manufacturer's instructions (Molecular Probes, Eugene, OR).

Matrix Mineralization Quantification and Fourier-Transform Infrared Spectroscopy

Following 7, 14, and 21 days, cultures were fixed in 70% ethanol and examined histochemically for mineralized matrix by von Kossa staining as detailed in Chapter 4 (Byers et al., 2002). Image Pro image analysis software (Media Cybernetics, Silver Springs, MD) was used to quantify low magnification light micrographs of von Kossa-stained cultures. FT-IR analyses were performed as described (Bonewald et al., 2003) on bulk ethanol-fixed cultures prepared in potassium bromide (KBr) pellets. Spectra, 64 scans acquired at 4 cm^{-1}, were obtained on a Nexus 470 FT-IR spectrometer (ThermoNicolet, Madison, WI) under N_2 purge. A spectral range from 400-2000 cm^{-1} was analyzed for mineral and matrix peaks characteristic of the mineral phase of bone. Rat calvarial bone, lyophilized, pulverized, and similarly prepared in KBr pellets, served as a positive control.

Data Analysis

All analyses were performed on assays conducted at least three times, each with unique Runx2 retroviral supernatant preparations. Data are reported as mean ± SEM, and statistical comparisons using SYSTAT 8.0 were based on an analysis of variance

(ANOVA) and Tukey's test for pairwise comparisons with a p-value < 0.05 considered significant. In order to make the variance independent of the mean, statistical analysis of real-time PCR data was performed following logarithmic transformation (Sokal and Rohlf, 1980).

RESULTS

Transduction efficiency in marrow stromal cells

Flow cytometry analyses indicated transduction efficiencies of approximately 50% in both Runx2-transduced and control cells (Figure 5-1). Similar transduction efficiencies in rat bone marrow stromal cells have been reported for HA-LB MLV amphotropic retrovirus (Peng et al., 2001). Cell selection procedures (e.g., eGFP/Runx2-positive) were not performed to avoid removal of accessory cells which may support osteoblastic differentiation. Aubin proposed a stimulatory heterotypic cell-cell interaction between non-adherent hematopoeitic cells and adherent cells (Aubin, 1999), and a similar complementary interaction may exist across heterogeneous adherent cell populations. DAPI cell-cycle analyses revealed no significant differences in cell proliferation between Runx2-transduced and control cells (data not shown). Finally, no differences were observed between unmodified stromal cells and those transduced with control retrovirus in any osteoblastic assay (data not shown).

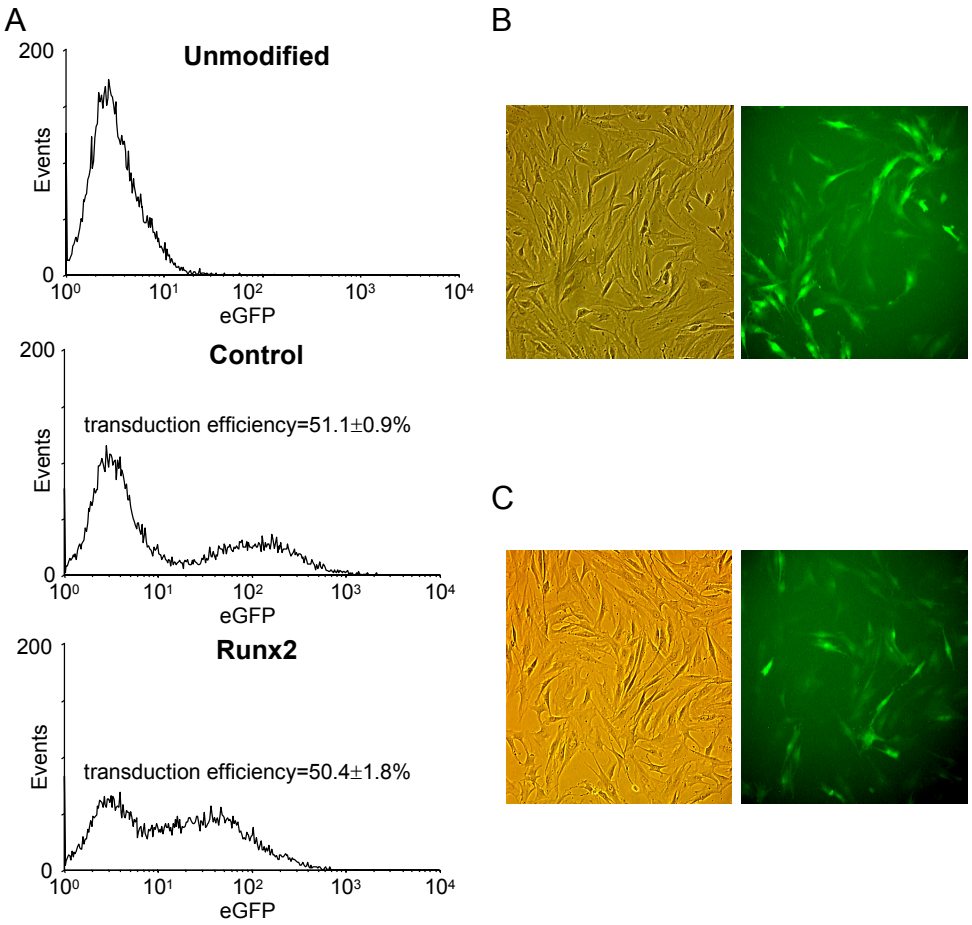

Figure 5-1. Retroviral transduction efficiency of marrow stromal cells examined by flow cytometry and fluorescence microscopy. (A) Flow cytometry histograms depicting eGFP co-selectable marker expression at 3 days in retrovirally transduced bone marrow stromal cells, including unmodified cell autofluorescence (top), control retrovirus (middle), and Runx2 retrovirus (bottom). Transduction efficiencies are reported as an average of the independent experiments each conducted with unique lots of retroviral supernatant [(mean, SEM), n=3]. (B) Phase contrast (left) and fluorescence (right) micrographs of control virus-transduced bone marrow stromal cells. (C) Phase contrast (left) and fluorescence (right) micrographs of Runx2-expressing bone marrow stromal cells.

Runx2 enhances expression of osteoblastic genes

Under standard osteogenic culture conditions (including 10 nM dexamethasone) for bone marrow stromal cells, Runx2-transduced cells demonstrated more than 10-fold higher Runx2 gene expression compared to endogenous levels in control cultures at each of the time points examined (Figure 5-2). Up-regulated transcript levels were also observed for osteocalcin (OCN) and collagen α1 (I) (COLα1(I)) throughout culture time. In contrast, apart from the day 3 time point, bone sialoprotein (BSP) and osteopontin (OPN) gene expression levels were not different between Runx2-modified and control cultures. ALP mRNA levels were higher in Runx2-engineered cells at 1 and 3 days, but equivalent expression levels were attained by day 7. ALP biochemical activity, however, was nearly two-fold higher in Runx2-expressing stromal cells compared to control cultures at the same time point (Figure 5-3).

Because dexamethasone is a potent stimulator of osteoblastic differentiation in bone marrow stromal cells (Bellows et al., 1987; Leboy et al., 1991), additional experiments were performed in the absence of dexamethasone. No differences in Runx2 transcript levels were observed between dexamethasone-treated and dexamethasone-free cultures for both Runx2-modified and control cells (Figure 5-2), indicating that dexamethasone does not alter Runx2 mRNA expression. On the other hand, significantly higher expression levels were observed for all osteoblastic genes examined in Runx2-transduced cultures compared to controls at 7 days in the absence of dexamethasone. The increases were most significant in OCN (>50-fold) and BSP (>30-fold) and still pronounced for COLα1(I), OPN, and ALP (3 to 9-fold). As expected, expression of all osteoblastic markers in dexamethasone-free control (no Runx2) cultures was lower than

that corresponding to dexamethasone-treated control cultures at 7 days. These results demonstrate that exogenous Runx2 expression enhances osteoblastic gene expression in stromal cells, particularly in the absence of dexamethasone.

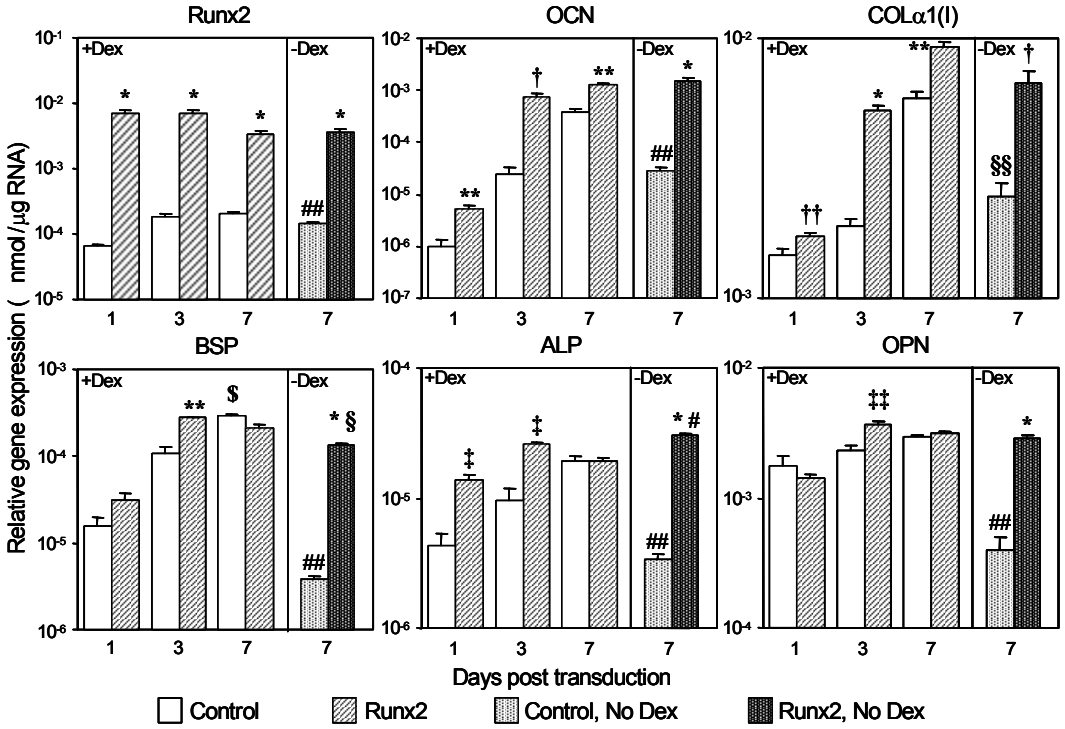

Figure 5-2. Relative gene expression in Runx2-transduced and control bone marrow stromal cells in the presence and absence of dexamethasone. Data are reported as [(mean, SEM, n=6] at 1, 3, and 7 days. ANOVA showed a significant effect of genetic modification (control versus Runx2 overexpression) and time: Runx2, OCN, COLα1(I), BSP, and ALP ($p<0.000001$ for both) and OPN ($p<0.025$ for treatment and $p<0.000001$ for time). Pairwise comparisons for same time point: * ($p<0.000001$); ** ($p<0.0005$); † ($p<0.00005$); †† ($p<0.04$); ‡ ($p<0.005$); ‡‡ ($p<0.01$); $ ($p<0.03$). Gene expression was also quantified at 7 days for control and Runx2-modified cultures which had dexamethasone excluded from the culture media. ANOVA for all 7 day cultures showed differences in genetic modification (control versus Runx2 overexpression) for Runx2 ($p<0.000001$) and genetic modification and culture media supplementation (+/- dexamethasone) for OCN, COLα1(I), BSP, ALP, and OPN ($p<0.000001$ for both). Pairwise comparisons: Runx2-modified (-Dex) versus control (-Dex): * ($p<0.000001$); † ($p<0.00005$), Runx2-modified (-Dex) versus Runx2-modified (+Dex): § ($p<0.01$); # ($p<0.005$), and control (-Dex) versus control (+Dex): §§ ($p<0.0001$); ## ($p<0.00001$).

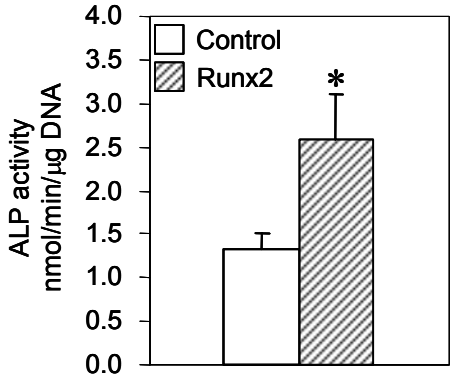

Figure 5-3. Alkaline phosphatase biochemical activity following 7 days of *in vitro* culture for control and Runx2-modified cells maintained in the presence of dexamethasone. Data are reported as [(mean, SEM), n=6]. Single factor ANOVA showed differences in treatment * ($p<0.05$).

Runx2 up-regulates mineralization by marrow stromal cells

Runx2 overexpression enhanced matrix mineralization in stromal cell cultures (Figure 5-4). Mineralized areas were present at 7 days in Runx2-transduced cultures maintained either in the presence or absence of dexamethasone, whereas controls cultures lacked appreciable von Kossa-positive regions. At 14 days, Runx2-engineered cultures supplemented with dexamethasone exhibited nearly 2-fold more mineralization than either Runx2-modified or dexamethasone-treated samples, whereas as dexamethasone-free controls displayed minimal mineralization. The additive effects of Runx2 expression and dexamethasone treatment on the mineralization capacity of stromal cells were also evident at 21 days. Dexamethasone-free control cultures displayed punctate nodules at 21 days, in agreement with the observation that a subpopulation of stromal cells is predisposed to osteoblastic differentiation even in the absence of dexamethasone (Aubin, 1999).

FT-IR spectroscopy was used to examine the chemical composition of the mineral phase deposited by Runx2-transduced and control cultures (Figure 5-5). This analysis is important because *in vitro* osteogenic culture conditions can lead to von Kossa-positive deposits that do not correspond to biological mineralization (Bonewald et al., 2003). Similar to the mature bone positive control, Runx2-modified and control stromal cell cultures displayed the amide I and II peaks indicative of protein, a broad phosphate stretching peak near 1100 cm^{-1}, a phosphate bending doublet split at 560 cm^{-1} and 605 cm^{-1}, and a carbonate peak near 870 cm^{-1} which is characteristic of the biological substitution of carbonate for hydroxide (type I) and/or carbonate for phosphate (type II) in the hydroxyapatite crystalline structure (Mendelsohn et al., 1989; Boskey et al., 1996). These chemical moieties characteristic of the mineral phase are representative of a poorly crystalline apatite (Bonewald et al., 2003). Taken together, these results demonstrate that exogenous Runx2 expression up-regulates formation of a biological mineralized matrix in primary bone marrow stromal cell cultures.

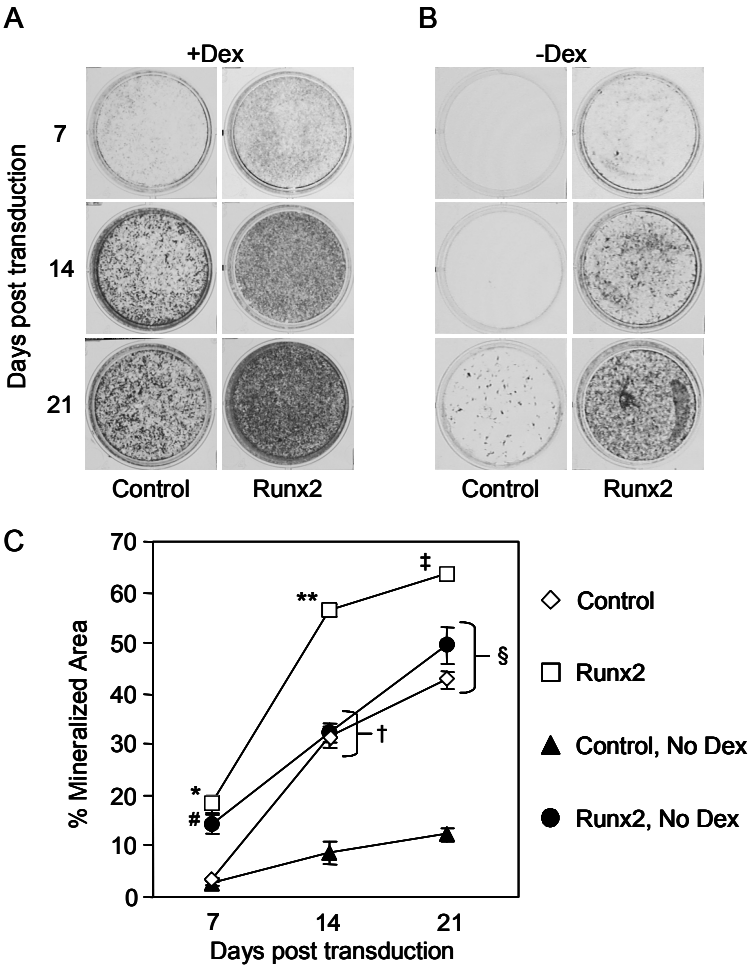

Figure 5-4. Mineralized surface area for Runx2-transduced and unmodified stromal cells with and without dexamethasone treatment. (A) von Kossa-stained control and Runx2-expressing cultures co-treated with dexamethasone at multiple time points. (B) von Kossa-stained control and Runx2-modified cultures maintained in the absence of dexamethasone at multiple time points. (C) Mineralized surface area quantification of control and Runx2-transduced marrow stromal cells in both the presence and absence of dexamethasone [(mean, SEM), n=6)]. ANOVA showed differences in genetic modification (control versus Runx2 overexpression), culture media supplementation (+/- dexamethasone), and time ($p<0.000001$ for all). Pairwise comparisons for same time point: * greater than control (+Dex) ($p<0.00005$) and control (-Dex) ($p<0.00001$); # greater than control (+Dex) ($p<0.005$) and control (-Dex) ($p<0.001$); ** greater than Runx2 (-Dex), control (+Dex), and control (-Dex) ($p<0.000005$); † both greater than control (+Dex) and control (-Dex) ($p<0.000005$); ‡ greater than Runx2 (-Dex) ($p<0.00005$) and control (+Dex) and control (-Dex) ($p<0.000005$); § both greater than control (+Dex) and control (-Dex) ($p<0.000005$).

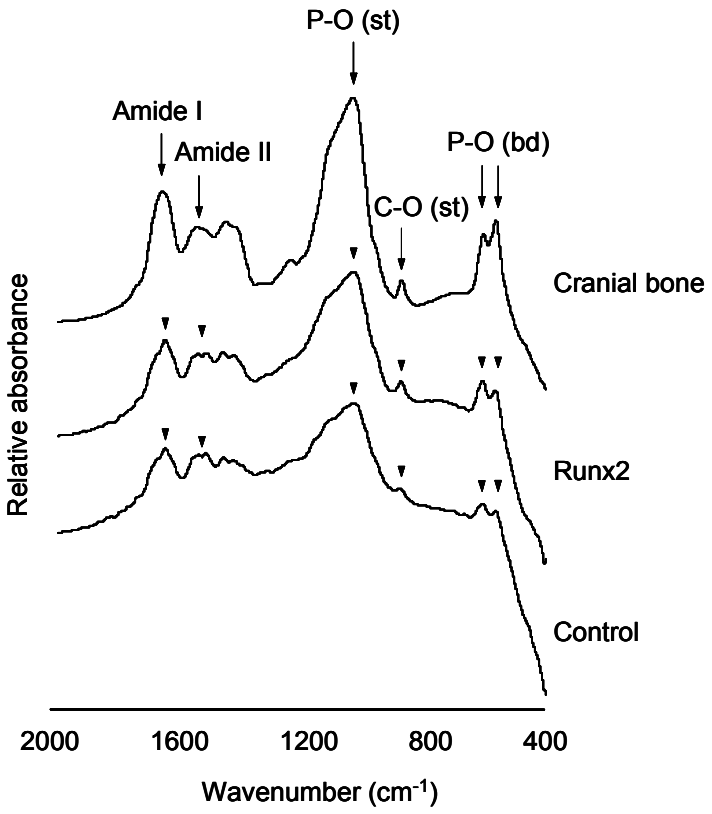

Figure 5-5. Comparative FT-IR spectra of Runx2-modifed and control bone marrow stromal cells. Adult rat cranial bone was included as a positive control. Transmission spectra, generated from bulk phase, ethanol fixed cultures in KBr pellets, showed bands characteristic of biological hydroxyapatite formation, including phosphate- and carbonate-related vibrations. st: stretching vibrations, bd: bending vibrations.

Runx2 overexpression maintains mineralization capacity of subcultured stromal cells

The effect of Runx2 overexpression on mineralization of bone marrow stromal cells expanded in culture was also examined. Therapeutic applications involving marrow-derived cells require large numbers of phenotypically stable cells, but stromal cells often lose the ability to differentiate when expanded *in vitro* (Ter Brugge and Jansen, 2002; Shi et al., 2002; Simonsen et al., 2002). Stromal cells expanded to passages 2, 4, and 8 without osteogenic stimulation were transduced with Runx2 or control retrovirus and subsequently cultured with or without dexamethasone (Figure 5-6). These passage numbers correspond to 2.5, 7, and 13 cumulative population doublings beyond passage 1 (Figure 5-6D). Consistent with the response of passage 1 cultures, Runx2 overexpression and dexamethasone treatment enhanced matrix mineralization compared to Runx2 modification or dexamethasone stimulation alone (Figure 5-6C). More importantly, forced Runx2 expression in high-passage cells retained the capacity to mineralize, although at lower levels than earlier passages, while the endogenous mineralization capacity of subcultured control stromal cells ceased prior to passage 8 even in the presence of dexamethasone.

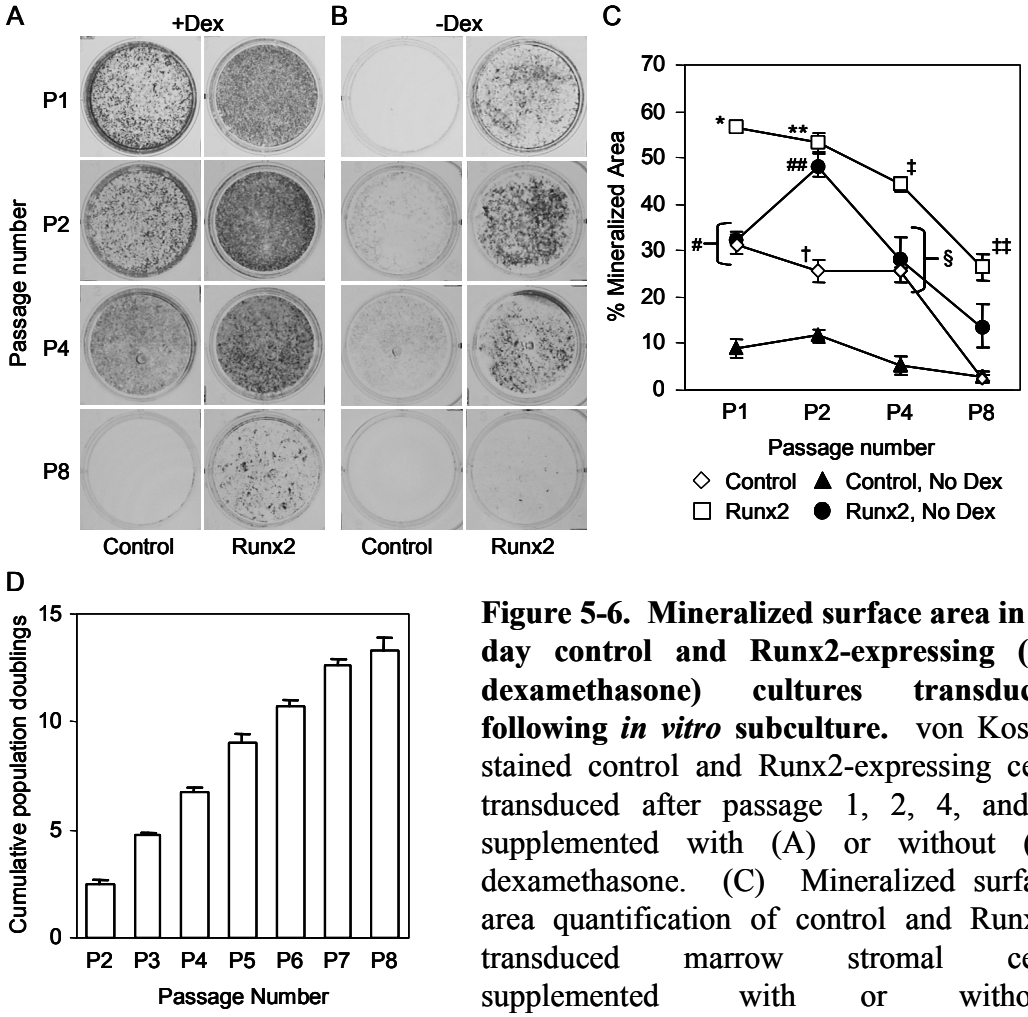

Figure 5-6. Mineralized surface area in 14 day control and Runx2-expressing (+/- dexamethasone) cultures transduced following *in vitro* subculture. von Kossa-stained control and Runx2-expressing cells transduced after passage 1, 2, 4, and 8 supplemented with (A) or without (B) dexamethasone. (C) Mineralized surface area quantification of control and Runx2-transduced marrow stromal cells supplemented with or without dexamethasone and transduced following passages 1, 2, 4, and 8 [(mean, SEM), n=6]. ANOVA demonstrated differences in genetic modification (control versus Runx2 overexpression), culture media supplementation (+/- dexamethasone), and time ($p<0.000001$ for all). Pairwise comparisons between same passage treatments: * greater than Runx2 (-Dex), control (+Dex), and control (-Dex) ($p<0.000005$); # both greater than control (-Dex) ($p<0.000005$); ** greater than control (+Dex), and control (-Dex) ($p<0.000005$); ## greater than control (+Dex) ($p<0.00001$) and control (-Dex) ($p<0.000005$); † greater than control (-Dex) ($p<0.01$); ‡ greater than Runx2 (-Dex) ($p<0.001$), control (+Dex) ($p<0.0001$), and control (-Dex) ($p<0.000005$); § both greater than control (-Dex) ($p<0.00005$); ‡‡ greater than control (+Dex) and control (-Dex) ($p<0.005$). (D) Cumulative population doubling data for stromal cells subcultured up to 8 passages prior to transduction with Runx2 retrovirus.

DISCUSSION

These results demonstrated that sustained and elevated Runx2 expression up-regulates osteoblast-specific gene and protein expression as well as biological matrix mineralization in primary bone marrow stromal cells. Consistent with observations that Runx2 overexpression accelerates and up-regulates the differentiation and mineralization capacity of immature MC3T3-E1 osteoblast-like cells (Chapter 4) (Byers et al., 2002). The up-regulated expression of osteoblastic markers in stromal cells in response to exogenous Runx2 most likely resulted from enhanced differentiation of osteoprogenitor cells present in the stromal compartment. Additionally, forced Runx2 expression in the non-osteoblastic progenitor cell fraction of the stroma, such as adipocytes, myoblasts, and chondroblasts, could result in additional cells differentiating down the osteoblastic lineage.

The effect of Runx2 overexpression on osteoblastic differentiation in the presence or absence of dexamethasone was also analyzed. This synthetic glucocorticoid is a potent stimulator of ALP and OPN gene expression but only modestly affects OCN mRNA levels in rat marrow stromal cells (Leboy et al., 1991). In the presence of dexamethasone, exogenous Runx2 expression up-regulated COLα1(I) and OCN mRNA transcripts, indicating induction of early and late osteoblastic markers. These genes contain consensus Runx2 DNA binding elements which are positively regulated by Runx2 (Frendo et al., 1998; Kern et al., 2001). Although ALP transcript levels were higher in Runx2-modified cells at early time points, they were equivalent to control levels at 7 days. On the other hand, ALP activity at 7 days was 2-fold higher in Runx2-modified cultures compared to controls. This difference between ALP mRNA levels and

enzyme activity could arise from accumulation of ALP protein throughout the time course of the study. Alternatively, Runx2 or a downstream target of Runx2 may exert post-transcriptional regulation on ALP, thereby enhancing production or activity of ALP protein from equivalent amounts of mRNA message. No differences were observed in OPN or BSP gene expression between Runx2-treated and control cells, suggesting either lack of Runx2 involvement in the regulation of these genes or saturation of transcriptional activity in response to dexamethasone. To separate the effects of Runx2 overexpression from dexamethasone stimulation, additional experiments were performed in the absence of dexamethasone. All genes, including BSP and OPN, exhibited significantly higher expression levels for Runx2-transduced cells compared to dexamethasone-free controls. In fact, Runx2 overexpression alone was sufficient to attain gene expression levels similar to those observed in Runx2-modified cultures treated with dexamethasone. Interestingly, the observation of elevated BSP transcript levels in Runx2-expressing cultures was unexpected. Previous groups reported that the BSP promoter lacks Runx2 responsiveness and Runx2 expression suppressed BSP transcripts (Benson et al., 1999; Javed et al., 2001). This inconsistency may be explained by cell type-dependent effects or differences in exogenous Runx2 expression levels or duration. The mechanism by which this enhancement in BSP expression occurred in stromal cells, whether by direct Runx2 transactivation or secondary transcription pathways, remains unknown.

Consistent with increased osteoblastic gene expression, Runx2 overexpression in combination with dexamethasone increased matrix mineralization compared to forced Runx2 expression or dexamethasone treatment alone, while dexamethasone-free control

cultures displayed minimal mineralization. These results are in agreement with the combined effects of forced Runx2 expression and dexamethasone on the osteoblastic differentiation of C3H10T1/2 pluripotent cells (Chapter 4) (Byers et al., 2002). The additive effects of Runx2 overexpression and dexamethasone supplementation on mineralization can be explained by (i) contributions from distinct subpopulations (i.e. Runx2-responsive and dexamethasone-responsive cells) in the heterogeneous stromal cell population or (ii) dexamethasone-mediated enhancement of Runx2 activity. However, the results with expanded cell cultures (Figure 5-6) do not support a model with separate contributions to mineralization from distinct cell populations. Dexamethasone-treated control cultures did not mineralize at passage 8, while both dexamethasone-free Runx2-transduced and dexamethasone-treated, Runx2-engineered cells produced significant mineralization. Moreover, dexamethasone-treated Runx2-modified cells still deposited higher levels of mineralized matrix than Runx2 overexpression alone, suggesting that dexamethasone enhances Runx2 activity. Because it did not alter Runx2 gene expression, dexamethasone most likely enhances the effects of Runx2 by directly altering Runx2 functional activity or activating pathways complementary to Runx2. Indeed, Prince et al. demonstrated higher Runx2 protein levels and DNA-binding activity in response to dexamethasone, even though dexamethasone supplementation did not alter Runx2 mRNA levels (Prince et al., 2001). Interactions between Runx2 and dexamethasone may involve the CCAAT/enhancer-binding protein (C/EBP) transcription factor family. C/EBPβ mRNA expression and DNA binding affinity are enhanced by dexamethasone (Gotoh et al., 1997). Furthermore, Gutierrez et al. demonstrated C/EBPβ-mediated activation of the OCN promoter and direct interaction between Runx2

and C/EBPβ in the synergistic enhancement of OCN gene expression (Gutierrez et al., 2002). C/EBP factors have also been implicated in COLα1(I) expression (Attard et al., 2000), which, in addition to OCN, was up-regulated by Runx2 overexpression in the present study. These results suggest that complementary interactions between dexamethasone-responsive regulatory factors, such as C/EBP, and Runx2 may be responsible for the additive effects of Runx2 overexpression and dexamethasone on mineralization.

Runx2 overexpression, but not dexamethasone treatment, maintained the mineralization capacity of expanded stromal cells. *In vitro* serial expansion of bone marrow stromal cells results in a complete loss of osteoblastic differentiation and mineralization capacity as demonstrated in this and other studies (Ter Brugge and Jansen, 2002; Shi et al., 2002; Simonsen et al., 2002). In a heterogeneous cell population, such as bone marrow stromal cell cultures, several mechanisms could be responsible for the loss of osteoblastic differentiation capacity. For instance, mitotically active cells lacking inherent osteoprogenitor characteristics (e.g., fibroblasts) may overtake osteoprogenitor cells, thereby reducing the frequency of osteogenic cells. Alternatively, the osteoprogenitor subpopulation could become restricted in its differentiation capacity either due to lack of requisite external signals and/or cessation of internal pathways critical to the osteoblastic differentiation cascade. Regardless of the underlying mechanism, these results demonstrate that serially expanded stromal cells lose their ability to produce a mineralized matrix, even in the presence of dexamethasone, but a fraction of this population remains responsive to Runx2 overexpression even after 13 population doublings (>8000-fold expansion) beyond initial passage. These findings are

particularly significant to cell-based strategies for therapeutic applications requiring large numbers of osteogenic cells to synthesize mineralized constructs for the treatment of large bone defects.

CHAPTER 6

IN VITRO AND SUBCUTANEOUS *IN VIVO* EVALUATION OF RUNX2-MODIFIED CELLS IN 3-D PLGA SCAFFOLDS

INTRODUCTION

Tissue engineering to develop bone graft substitutes offers a promising alternative to address the clinical demand and limitations associated with conventional autologous and allogenic bone grafting substrates (Crane et al., 1995; Baum and Mooney, 2000). After demonstrating that Runx2 overexpression enhanced osteoblast phenotype expression of primary bone marrow stromal cells in monolayer culture (Chapter 5), specifically osteoblast-specific gene expression and mineralization, Runx2-modified cells were integrated into 3-D polymeric scaffolds to create tissue-engineered constructs. Compared to unmodified cells, Runx2 overexpression significantly up-regulated osteoblastic differentiation and mineralization of 3-D scaffolds *in vitro* and *in vivo* in an ectopic, nonosseous site. Additionally, *in vitro* construct development to create a mineralized template prior to implantation dramatically enhanced *in vivo* mineralized tissue formation, suggesting a novel templating tissue engineering strategy to improve *in vivo* mineralization. Finally, Runx2 overexpression and *in vitro* construct development synergistically enhanced *in vivo* mineralization compared to *in vitro* construct development or genetic engineering with Runx2 alone.

MATERIALS AND METHODS

Stromal cell isolation and retroviral transductions

Primary bone marrow stromal cells were isolated from the femora of 6-week-old young adult male Wistar rats (Maniatopoulos et al., 1988) and expanded in culture for 7 days prior to retroviral transduction as described (Chapter 5). Runx2-transducing and control (no Runx2 insert) retroviruses were produced using standard techniques and sub-confluent cultures of target cells were transduced with retroviruses (1-2 x 10^5 cfu/ml viral titer) as described (Chapter 4).

Cell culture and construct preparation

Following transduction, cells were seeded 2 days post transduction into Innopol® 75/25 PLGA scaffolds (Innotech Medical, Korea; 8 mm diameter × 5 mm thick, 100-200 micron pore size, 85% porosity) (Nam et al., 2000) at 10^6 cells/scaffold, a seeding density consistent with previously published work (Ishaug et al., 1997; Holy et al., 2000). To enhance initial cell adhesion, constructs were pre-coated in a solution of rat plasma fibronectin in PBS (20 μg/mL). During *in vitro* culture, constructs were maintained statically in osteogenic media (α-minimum essential medium, 10% fetal bovine serum, 1% penicillin-streptomycin, 50 μg/ml gentamicin sulfate, and 0.3 μg/ml fungizone, 50 μg/ml L-ascorbic acid, 3 mM sodium β-glycerophosphate, and 10 nM dexamethasone), and media was exchanged every other day.

Subcutaneous implantation surgeries

Cell-seeded constructs were implanted into subcutaneous pockets made by blunt dissection in the backs of 7-week-old syngeneic rats in accordance to an IACUC-approved protocol. Each animal received two implants (one Runx2 and one unmodified

cell-seeded scaffold) (Figure 6-1) on opposite sides of a midline incision (n=5). Some animals received cell-free scaffolds for comparative analysis to observe any abnormal inflammatory responses to the scaffold material or implanted cells. Constructs were explanted after 4 weeks of implantation following euthanasia.

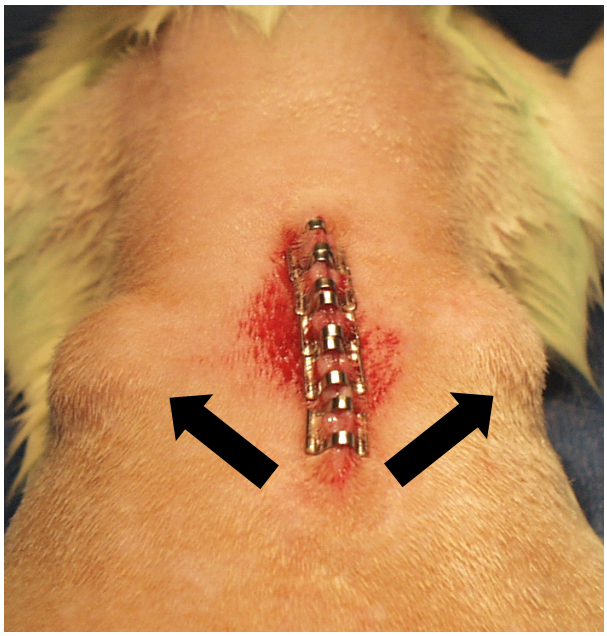

Figure 6-1. Image depicting the location of the subcutaneous site (arrows point to implanted constructs).

Microcomputed tomography

In vitro and *in vivo* mineralization of 3-D scaffolds was quantified by high resolution X-ray microcomputed tomography (micro-CT) using a Scanco Medical μCT 40 imaging system (Bassersdorf, Switzerland). Formalin-fixed specimens were scanned in 70% ethanol at 16 μm voxel resolution and evaluated at a threshold corresponding to a linear attenuation of 0.96 cm^{-1}, filter width of 1.2, and filter support of 2.0. The reconstructed and thresholded 3-D images were evaluated using direct distance

transformation methods to calculate mineralized matrix volume within each construct or explant (Hildebrand et al., 1999).

Histology

Histological sections (5 μm) were prepared using the paraffin tape-transfer system (Instrumedics, Hackensack, NJ) to enhance adhesion and retention of the scaffold to the slide during deparaffinization and staining. Sections were stained with hematoxylin-eosin or von Kossa-nuclear fast red to observe cellular distribution and mineralization of the 3-D polymeric scaffolds.

Data Analysis

In vitro analyses were conducted at least three times, each with unique Runx2 retroviral supernatant preparations and donor cell harvests. Data are reported as mean ± SEM, and statistical comparisons were based on ANOVA and Tukey's test for pair-wise comparisons with a p-value < 0.05 considered significant.

RESULTS

Runx2 expression increases 3-D construct in vitro mineralization

Cells were cultured within porous PLGA scaffolds to examine the kinetics of *in vitro* construct mineralization. This formulation of biodegradable scaffold is extensively used in bone tissue engineering applications and supports *in vitro* mineralization by stromal cells (Ishaug et al., 1997; Holy et al., 2000; Murphy et al., 2000). DNA measurements verified equivalent cell seeding between Runx2-modified and control

constructs (data not shown). Micro-CT revealed significantly higher levels of mineralization at 21 (8-fold), 28 (3-fold), 42 (2-fold), and 56 (2-fold) days in culture on scaffolds seeded with Runx2-expressing cells compared to unmodified cells (Figure 6-2).

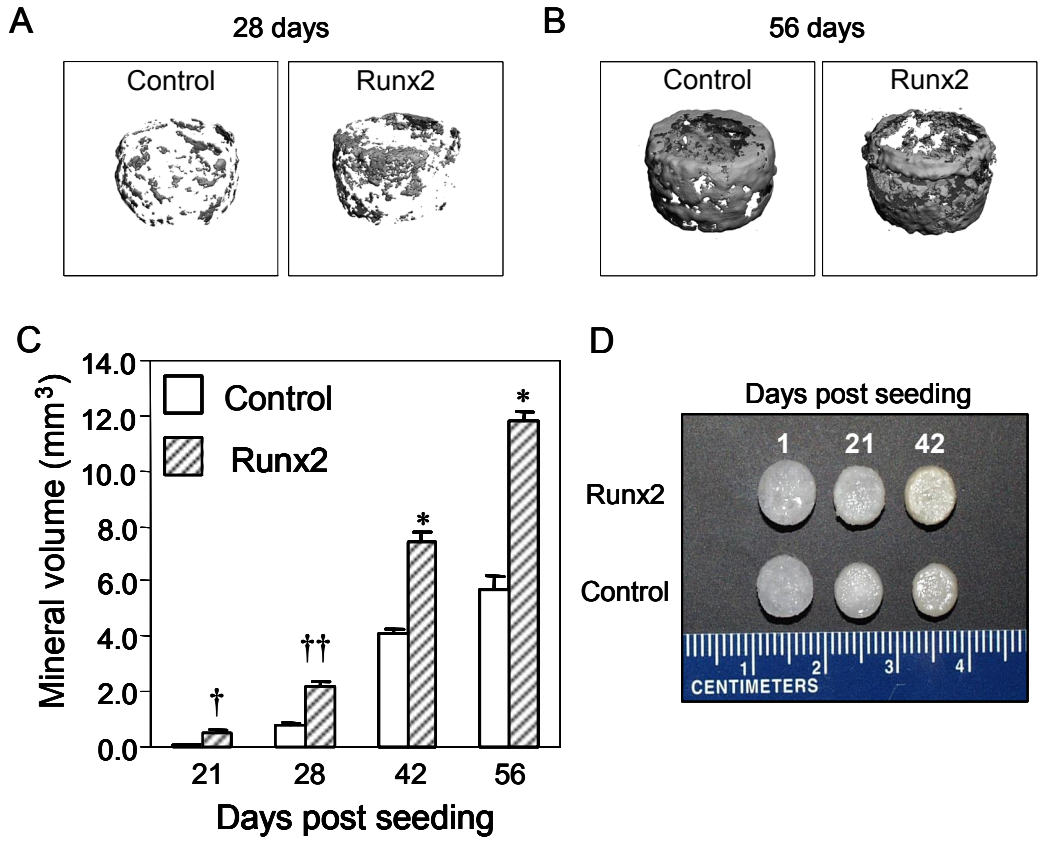

Figure 6-2. Mineralization of 3-D PLGA scaffolds seeded with Runx2-transduced or control cells following various *in vitro* culture times. (A) micro-CT images of control and Runx2-expressing cell-seeded PLGA constructs at 28 days (A) and 56 days (B) of *in vitro* culture. (C) Quantification of total mineral volume following static *in vitro* culture for various time periods [(mean, SEM), n=9]. ANOVA showed differences in treatment ($p<0.000001$). Pairwise comparisons: † ($p<0.05$); †† ($p<0.005$); * ($p<0.00001$). (D) Photograph of Runx2-expressing and control cell-seeded PLGA scaffolds following various durations of *in vitro* culture.

Interestingly, a definitive macroscopic difference existed between scaffolds seeded with Runx2-modified and control cells. Specifically, a time-dependent, cell-mediated contraction was consistently observed, and this artifact appeared to be more prevalent in control cell than Runx2-transduced cell-seeded scaffolds (Figure 6-2D). Although the precise origin of this difference was not determined, it suggests that in the absence of Runx2 overexpression, a greater number of stromal cells retained a more fibroblastic, contractile phenotype even in the presence of osteogenic differentiation medium.

Histological analyses confirmed the presence of mineralized regions in pore spaces adjacent to the polymer scaffold (Figure 6-3A). Although cells were present throughout the constructs, metabolically active cells, those producing significant quantities of mineralized matrix, were primarily confined to the outer 100-250 μm of the scaffold periphery (Figure 6-3B), an artifact commonly observed for statically-cultured 3-D constructs (Ishaug et al., 1997). This phenomenon was consistent for both Runx2-transduced and control cell-seeded scaffolds and confirmed by cross-sectional analysis of micro-CT micrographs (Figure 6-3C).

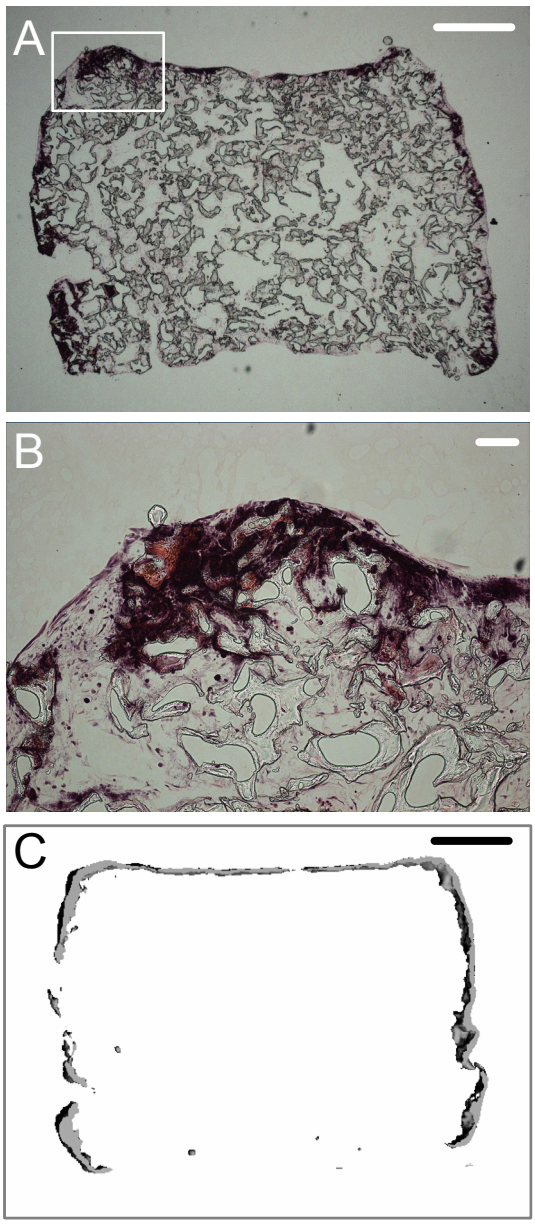

Figure 6-3. Histological sections of an *in vitro* cultured Runx2-transduced cell-seeded PLGA scaffold at 56 days. (A) Full cross-section of a hematoxylin-eosin-stained Runx2-modified stromal cell-seeded scaffold at 56 days (bar = 1 mm). (B) High magnification histological micrograph of region shown in A (bar = 100 μm). (C) Cross-section of a reconstructed micro-CT image of a Runx2 cell-seeded scaffold following 56 days of static *in vitro* culture demonstrating peripherally located mineralized tissue (bar = 1 mm).

In vitro construct development and Runx2 expression synergistically enhance in vivo mineralized tissue formation

The ability of these tissue-engineered constructs to promote *in vivo* mineralization was evaluated in a heterotopic, subcutaneous site. This is a stringent implantation model to examine the *in vivo* mineralization capacity of an osteogenic cell source due to the absence of regenerative and osteoinductive cues typically present in orthotopic defects. In addition to investigating the effects of Runx2 overexpression, the contributions of *in vitro* construct development to *in vivo* mineralization were analyzed. The rationale for these studies was that *in vitro* mineralization prior to implantation may provide a template for subsequent *in vivo* mineralization. Three stages of *in vitro* construct maturity were examined: (i) cell-scaffold constructs with minimal cell-mediated matrix (1 day post-seeding, cultured in growth media lacking osteogenic supplements), (ii) constructs containing more significant quantities of organic matrix prior to mineralization (7 days of pre-culture in osteogenic media), and (iii) constructs having significant amounts of mineralized matrix (21 days of *in vitro* culture in osteogenic media).

Following 28 days of subcutaneous implantation, relatively insignificant amounts of *in vivo* mineral formation (<0.1 mm^3 mineral volume, Figure 6-4A) were observed by micro-CT for both Runx2-expressing and control cell-seeded constructs cultured for either 1 or 7 days prior to implantation. In contrast, constructs pre-cultured for 21 days prior to implantation exhibited a dramatic increase in mineral volume (Fig. 6-4A-C), indicating that *in vitro* construct development enhances *in vivo* mineralization in this subcutaneous model. More importantly, following 21 days of pre-culture, constructs containing Runx2-modified cells displayed 10-fold more mineral volume than control

scaffolds after 28 days of subcutaneous implantation (Figure 6-4A-C). This 10-fold enhancement of *in vivo* mineralization was significantly higher than the 2.5-fold increase observed between parallel Runx2-modified cell-seeded constructs maintained for similar durations *in vitro* (Figure 6-2B). *In vivo* mineralization enhancement was not a simple consequence of the presence of more *in vitro* mineral prior to implantation, but instead, was synergistically up-regulated by Runx2 overexpression in the implanted cells. Specifically, comparative analysis between total mineral volume present on *in vitro* constructs following 21 days of pre-culture (Figure 6-4C, left bars) and 28 day *in vivo* explant constructs (Figure 6-4C, right bars) revealed a greater than 5-fold faster average daily mineral deposition rate for Runx2-modified constructs (0.32 mm^3/day) compared to controls (0.06 mm^3/day). Collectively, these results indicate an interaction between *in vitro* culture duration and Runx2 overexpression which acted synergistically to up-regulate the *in vivo* mineralization of tissue-engineered constructs.

A

In vitro development time (days)	Treatment	Mineral volume (mm^3)
1	Control	0.003 ± 0.002
	Runx2	0.004 ± 0.002
7	Control	0.010 ± 0.008
	Runx2	0.022 ± 0.009
21	Control	0.98 ± 0.22
	Runx2	9.72 ± 0.81 **

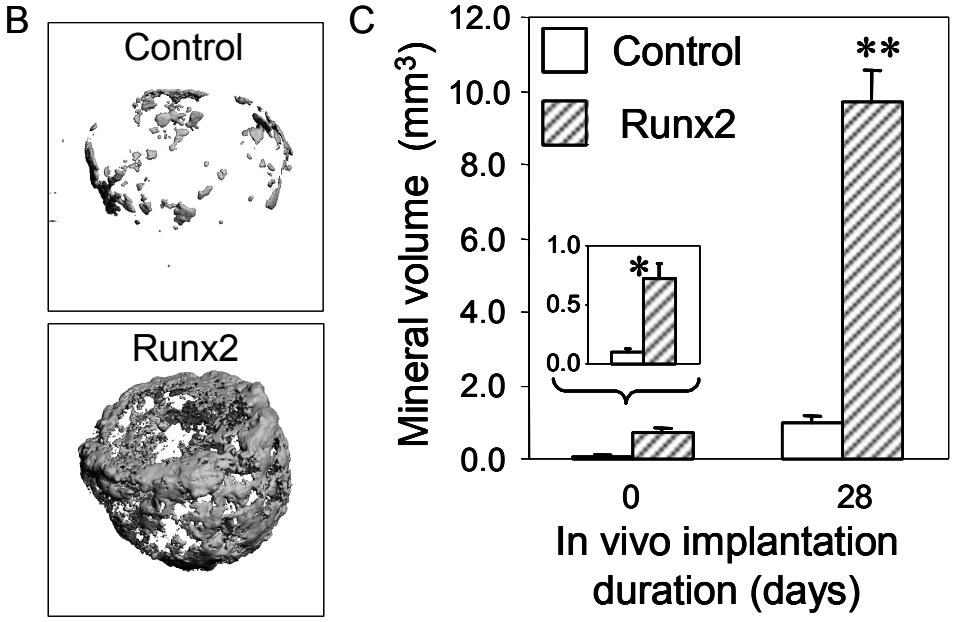

Figure 6-4. Mineralization of 3-D PLGA scaffolds seeded with Runx2-expressing or control cells and implanted subcutaneously for 28 days following various *in vitro* pre-culture conditions. (A) Total mineralized matrix volume quantified by micro-CT following various *in vitro* pre-culture durations and subsequent 28 day subcutaneous implantation [(mean,SEM), n=5]. ANOVA showed significance in treatment and *in vitro* culture time ($p<0.000001$). Pairwise comparison: ** greater than 21 day control and 1 and 7 day pre-cultured, both treatments ($p<0.00001$). (B) micro-CT images of control (top) and Runx2-transduced (bottom) cell-seeded scaffolds subcutaneously implanted for 4 weeks following 21 days of *in vitro* development. (C) Total mineral volume quantified by micro-CT for (i) 21 day *in vitro* pre-cultured constructs (0 days *in vivo*) (n=3) and (ii) 28 day explant constructs pre-cultured for 21 days (28 days *in vivo*) (n=5) for Runx2-modified and control cell-seeded constructs. One-way ANOVA was performed on each group, i.e. input constructs (0 days) and explant constructs (28 days) and showed significance in treatment: * ($p<0.01$); ** ($p<0.00001$).

Histological analyses showed equivalent host tissue responses among cell-free scaffolds and cell-seeded constructs, indicating minimal inflammatory/immune response to Runx2-modified and control cells (data not shown). Uniform distribution of infiltrating host cells was characteristically observed throughout construct explants which had been pre-cultured for either 1, 7, or 21 days prior to implantation (Figure 6-5). In agreement with micro-CT analyses, mineralized regions were not observed in histological micrographs (Figure 6-5A and B). However, significant mineralized regions were observed in close association with the scaffold periphery for those constructs pre-cultured for 21 days prior to implantation (Figures 6-5C and 6-6). Furthermore, much higher levels of mineralized tissue were observed for constructs containing Runx2-modified cells compared to controls. The peripheral localization of these mineralized areas is likely explained by the observation that at the time of implant, matrix and cellular distribution were already primarily confined to the outer 100-200 μm of the scaffold following only 21 days of *in vitro* pre-culture (data not shown). As a result, subsequent *in vivo* mineralization was also confirmed to be peripherally located at the interface of the construct and the encapsulating subcutaneous tissue (Figure 6-5C and 6-6).

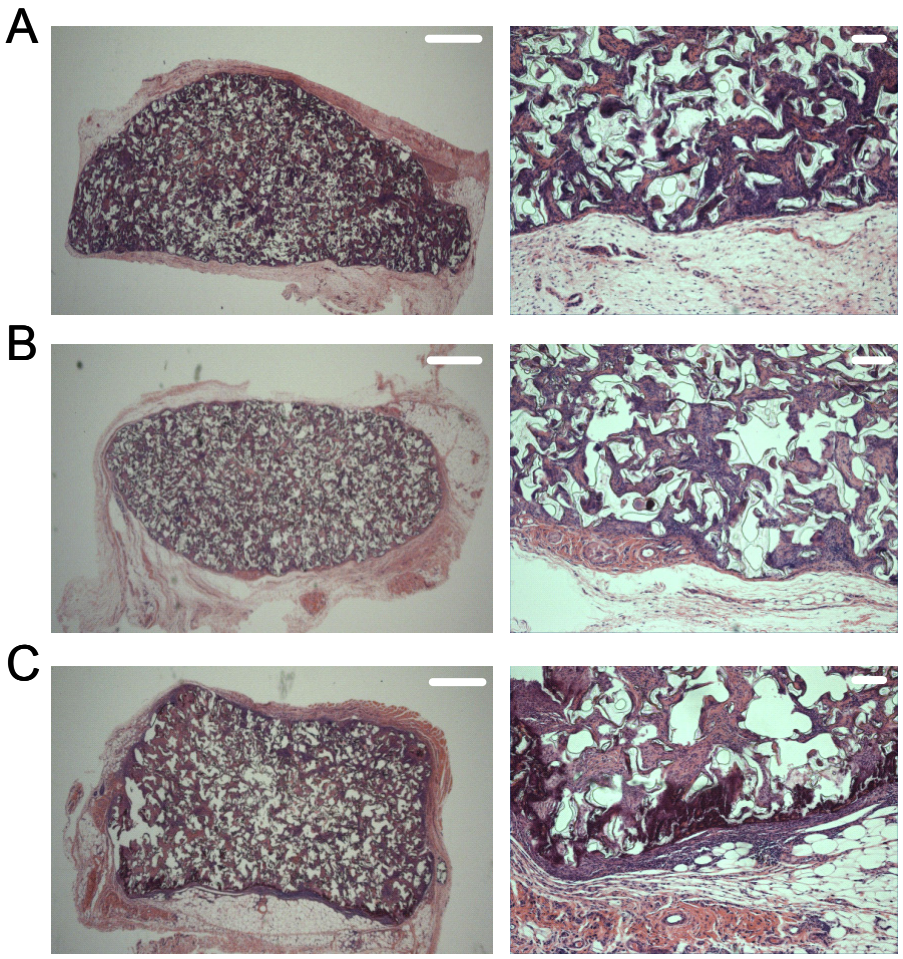

Figure 6-5. Histological micrographs of Runx2-modified cell-seeded scaffolds implanted subcutaneously for 28 days following 1, 7, and 21 days of *in vitro* pre-culture. (A) Hematoxylin-eosin stained Runx2-modified cell-seeded scaffolds following 1 day of *in vitro* maturation and 28 days of subcutaneous implantation. (B) Hematoxylin-eosin stained Runx2-modified cell-seeded scaffolds following 7 days of *in vitro* maturation and 28 days of subcutaneous implantation. (C) Hematoxylin-eosin stained Runx2-modified cell-seeded scaffolds following 21 days of *in vitro* maturation and 28 days of subcutaneous implantation. (right column, bar = 1 mm, left column, bar = 100 μm).

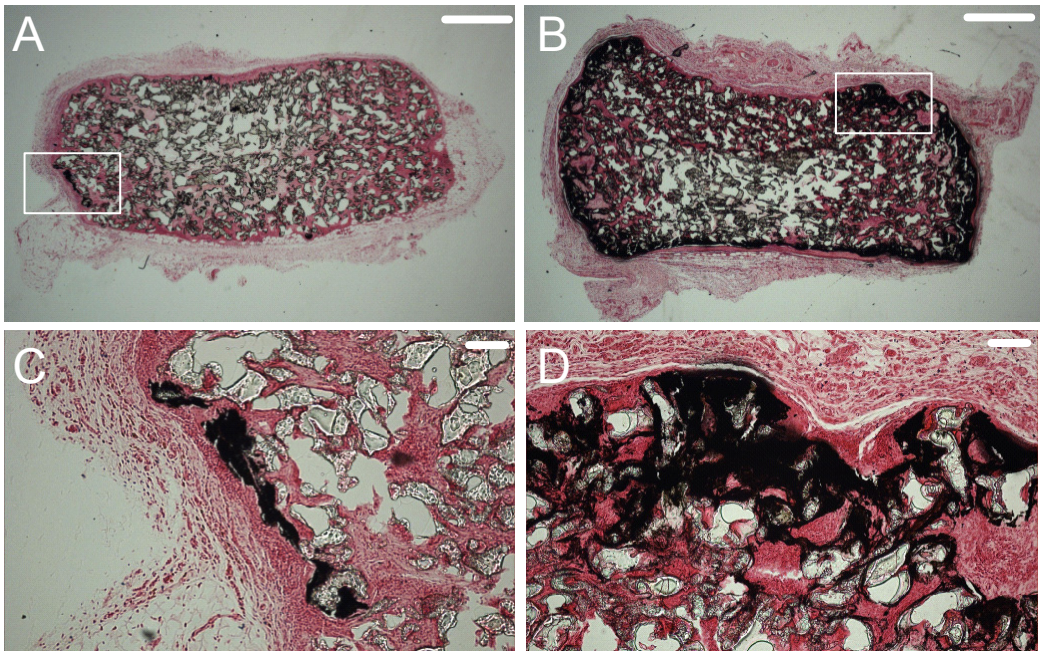

Figure 6-6. Histological micrographs of control and Runx2-modified cell-seeded scaffolds implanted subcutaneously for 28 days following 21 days of *in vitro* pre-culture. von Kossa-nuclear fast red stained (A) Control and (B) Runx2-modified cell-seeded scaffolds following 21 days of *in vitro* maturation and 28 days of subcutaneous implantation (bar = 1 mm). (C) High magnification micrograph of inset in A (bar = 100 μm). (D) High magnification micrograph of inset in B (bar = 100 microns).

DISCUSSION

Isolation, expansion, and controlled phenotypic maturation of cells capable of robust osteoblastic differentiation and matrix deposition represent critical steps in the successful clinical application of bone tissue engineering approaches. To date, several groups have demonstrated the potential of bone marrow-derived progenitors as candidate osteogenic cells in model systems (Ohgushi et al., 1993; Ishaug-Riley et al., 1997; Kadiyala et al., 1997), yet the ultimate application of this cell type to tissue engineering is limited by the ability to harvest sufficient cell numbers and maintain their osteogenic differentiation capacity in *ex vivo* culture environments. To address these cell sourcing limitations, retroviral gene delivery to constitutively overexpress the osteoblast-specific transcriptional activator Runx2 was examined in this study. The evaluation of Runx2-modifed stromal cells incorporated into 3-D scaffolds builds upon the rigorous *in vitro* analyses of monolayer cultures as described in Chapter 5, in which it was demonstrated that Runx2 overexpression in stromal cells significantly increased osteoblast-specific gene and protein expression and matrix mineralization. Notably, Runx2-transduced stromal cells produced a robust mineralized matrix compared to controls following 3-D *in vitro* culture (Figure 6-2A-C), indicating their responsiveness to Runx2 overexpression throughout the duration of the complex, time-dependent osteoblastic differentiation cascade.

Runx2-expressing bone marrow stromal cells also up-regulated *in vivo* mineralization compared to control cells (Figure 6-4 and 6-5). These results contrast recent reports of Runx2 overexpression in other cell types using adenoviral gene delivery. Yang et al. implanted Runx2-expressing pluripotent C3H10T1/2 cells subcutaneously and

showed sparse bone and cartilage-like tissue formation at levels considerably lower than BMP-2-expressing cells (Yang et al., 2003). Hirata and colleagues implanted scaffolds seeded with primary skin fibroblasts overexpressing Runx2 into craniotomy defects and observed negligible bone-like tissue formation by Runx2-modified cells *in vivo* (Hirata et al., 2003). Several factors, such as cell type, transgene expression duration, and *in vitro* construct development, could be responsible for these contradictory observations. For instance, as observed in Chapter 4, exogenous Runx2 expression was not sufficient to promote significant *in vitro* mineralization in either primary fibroblasts or C3H10T1/2 cells (Byers et al., 2002). Furthermore, dexamethasone supplementation up-regulated *in vitro* mineralization by Runx2-modified stromal cells (Chapter 5). Taken together, these results suggest the existence of additional pathways or factors which act either in series to complement Runx2 activity or in parallel cascades to supplement the physiologic role of Runx2 in directing terminal differentiation of osteoblasts. Currently, the complex interactions of these pathways and factors in the complete osteoblastic differentiation process and specifically in Runx2 transactivation/repression are not well understood. As a result, significant attention must be directed toward target cell selection and gene delivery approaches for bone tissue engineering applications.

It was demonstrated that *in vitro* construct development to create mineralized templates, especially when combined with Runx2 overexpression, enhances *in vivo* mineralization in an ectopic implantation site (Fig. 6-4A-C). These results provide a promising templating tissue engineering strategy to develop bone grafting substrates, in which osteogenic cell-scaffold constructs are matured under osteogenic culture conditions to create mineralized templates, and then implanted into a defect site to

facilitate healing. This approach is fundamentally different from typical *in vivo* models for tissue-engineered bone substitutes, which focus on direct implantation of scaffolds immediately following cell seeding and/or *ex vivo* genetic modification of target cells (Ishaug-Riley et al., 1997; Kadiyala et al., 1997; Lieberman et al., 1999; Krebsbach et al., 2000). These techniques, while successful in model systems, result in the implantation of a relatively undeveloped construct. Consequently, the active contribution of the implanted cells to the healing process may actually be limited due to the infiltration of high quantities of host cells into the defect site. This scenario provides a likely explanation for the current results, in which immature, non-mineralized constructs (1 or 7 days of *in vitro* pre-culture) failed to produce significant quantities of mineralized tissue *in vivo* compared to more mature, mineralized constructs which had been pre-cultured *in vitro* for 21 days prior to implantation.

Finally, Runx2 overexpression and *in vitro* construct development synergistically enhanced *in vivo* mineralization compared to *in vitro* construct development or genetic engineering alone. This interaction presents further evidence that construct mineralization prior to implantation enhances subsequent *in vivo* mineralization and construct performance in this subcutaneous model by providing a mature, mineralized template prior to implantation. These results suggest this novel integrated genetic and tissue engineering strategy to create mineralized bone grafting templates may overcome limitations associated with conventional genetic and tissue engineering approaches, especially for creating mechanically robust grafts for repairing large, non-healing bone defects.

CHAPTER 7

EVALUATION OF RUNX2-TRANSDUCED CELLS SEEDED IN FUSED DEPOSITION-MODELED POLYCAPROLACTONE SCAFFOLDS BOTH *IN VITRO* AND IN A CRANIOTOMOY DEFECT MODEL

INTRODUCTION

Runx2 overexpression in bone marrow-derived stromal cells significantly enhanced 2-D and 3-D *in vitro* osteoblastic phenotype expression (Chapters 5 and 6), specifically through increases in osteoblastic gene expression, alkaline phosphatase activity, and matrix mineralization. Additionally, Runx2-expressing stromal cells and *in vitro* pre-culture synergistically enhanced *in vivo* mineralization of 3-D polymeric scaffolds in a subcutaneous implantation model. These initial studies were of significant scientific interest toward validating this genetic and tissue engineering methodology; however, the ultimate effectiveness and potential of this strategy will be validated through examination of the ability of Runx2-modified stromal cells to facilitate healing of critical size bone defects.

Craniotomy defect studies are a common, non-loaded critical size defect (CSD) model, in which an osseous defect of sufficient size is created to prohibit spontaneous healing during the lifetime of the animal (Schmitz and Hollinger, 1986). The rat CSD model has been commonly used in characterizing a broad range of therapeutic healing mechanisms including recombinant BMP delivery and gene delivery techniques to deliver a variety of soluble osteoinductive and mitogenic agents which facilitate defect healing (Kenley et al., 1994; Hollinger et al., 1998; Krebsbach et al., 2000; Gysin et al., 2002; Hirata et al., 2003). The accepted defect size in rat craniotomy studies is 8 mm in diameter, which has been characterized as non-healing beyond three months (Schmitz

and Hollinger, 1986; Schmitz et al., 1990). Additionally, the healing response demonstrated in these models has been largely attributed to progenitor cells in the dura as opposed to ingrowth of cranial bone from the periphery of the defect (Wang and Glimcher, 1999). Although sensitive in nature due to the proximity of the defect to the brain, the craniotomy defect model was in principle a logical selection for an initial characterization of Runx2-modified cells. Other bone defect models, such as the femoral segmental defect model, require accessory fixation devices which definitively complicate surgical techniques and may potentially introduce even greater variability amongst subjects. Furthermore, the current work involved genetic manipulation of rat primary bone marrow stromal cells; however, an autologous implantation model was impractical based on the study parameters. Therefore, a rat syngeneic implantation study was selected as an alternative strategy in order to minimize experimental complications arising from immuno-rejection of the implanted cells.

The evaluation of Runx2-modified stromal cells in any bone defect model requires the identification of a suitable scaffold carrier for cellular delivery and implantation. Based on the outcomes of the subcutaneous implantation model (Chapter 6), it was of particular interest to further examine the role the interactive role of Runx2 overexpression and *in vitro* construct maturation on subsequent healing in a bone defect model. Based on the previous study, the pre-culture conditions selected for the craniotomy model would play a significant role toward identifying characteristic requirements, specifically the mechanical integrity, of a candidate carrier matrix/scaffold for the delivery of Runx2-modified cells. Although a modest increase in *in vivo* mineralization occurred by extending *in vitro* pre-culture time from 1 to 7 days, the most

significant enhancement in subsequent *in vivo* performance was observed in constructs matured for 21 days prior to implantation. Therefore, two construct development conditions were selected for the craniotomy defect model: (i) 1 day of *in vitro* culture following cell seeding, a condition which reflects the typical protocol for implantation of genetically modified osteogenic/osteoinductive cells and further represents a relatively immature construct and (ii) constructs pre-cultured for 21 days, a time point beyond the onset of *in vitro* mineralization which therefore provides a more mature, mineralized template in the defect site. Previous 3-D *in vitro* culture studies involving Runx2-modified and especially control cell-seeded PLGA scaffolds demonstrated a pronounced cell-mediated scaffold contraction following extended *in vitro* culture, even in as little as 21 days (Figure 6-2D). Therefore, to ensure the implantation of constructs of similar size and pore architecture independent of *in vitro* culture parameters, it was necessary to identify a scaffold material possessing sufficient mechanical integrity to resist cell-mediated contraction. Furthermore, similar to previous subcutaneous studies, it was of interest to evaluate the performance of Runx2-modified cells on a polymeric scaffold which was deficient in osteoconductive properties characteristic of bioceramics. Poly(ε-caprolactone) (PCL) fused deposition-modeled scaffolds (Hutmacher et al., 2001; Zein et al., 2002) were selected as an appropriate biodegradable, polymeric scaffold. PCL is an FDA-approved bioresorbable polymer which provided suitable mechanical integrity to resist previously observed cell-mediated contraction artifacts. Additionally, the fused deposition manufacturing technique provided a completely interconnected honeycomb-like architecture at a prescribed pore size (300-500 μm).

Prior to *in vivo* implantation, an *in vitro* characterization scheme similar to that performed for PLGA cell-seeded scaffolds (Chapter 6) was instituted for Runx2-modified and control cells seeded on PCL scaffolds. Runx2-modified stromal cells significantly enhanced matrix mineralization in 3-D *in vitro* culture. Furthermore, Runx2-modified and control cell-seeded PCL scaffolds were implanted into critical size craniotomy defects (CSD) in syngeneic rats. Consistent with the subcutaneous results, defects receiving 21 day *in vitro* pre-cultured constructs seeded with Runx2-modified cells demonstrated greater amounts of new bone formation than similarly pre-cultured control stromal cell-seeded scaffolds. However, scaffolds implanted immediately upon cell-seeding demonstrated greater amounts of new bone formation than constructs pre-cultured for 21 days independent of cell treatment, suggesting that the architecture and physical nature of these PCL scaffolds was conducive to bone formation and promoting defect healing in the absence of cell loading in this particular critical size defect model.

MATERIALS AND METHODS

Stromal cell isolation and retroviral transductions

Primary bone marrow stromal cells were isolated from the femora of 6-week-old young adult male Wistar rats (Maniatopoulos et al., 1988) and expanded in culture for 7 days prior to retroviral transduction as described (Chapter 5). Runx2-transducing and control (no Runx2 insert) retroviruses were produced using standard techniques and sub-confluent cultures of target cells were transduced with retroviruses (1-2 x 10^5 cfu/ml viral titer) as detailed (Chapter 4).

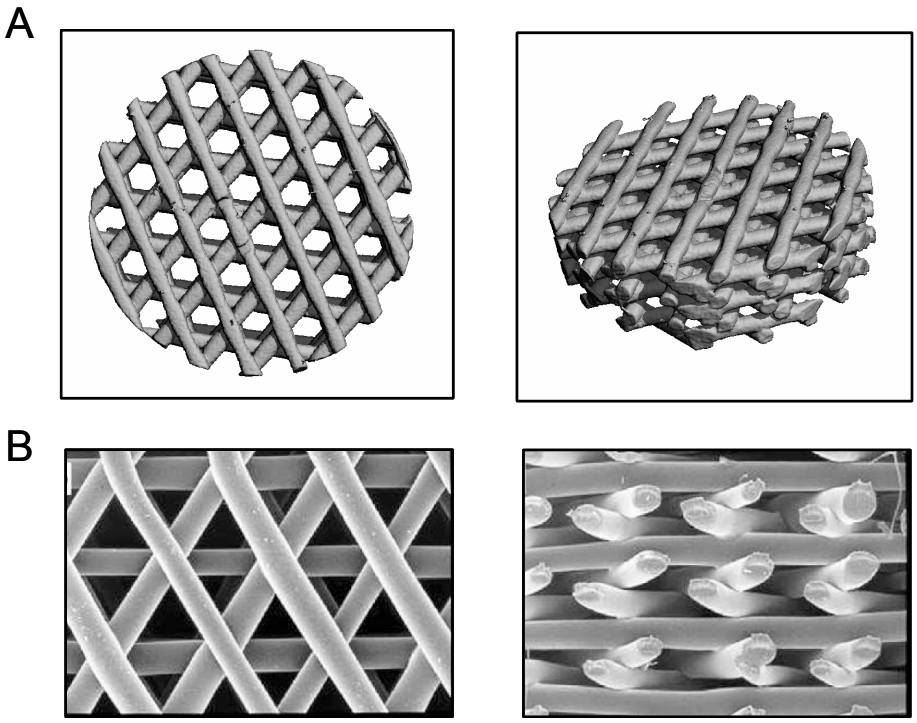

Figure 7-1. Micro-CT and SEM micrographs of fused deposition-modeled polycaprolactone scaffolds. (A) Top-down (left) and angled profile (right) micro-CT images of 8.1 mm × 2.4 mm polycaprolactone disks. (B) Top-down (left) and side (right) SEM micrographs of polycaprolactone scaffolds.

Cell culture and construct preparation

Following transduction, cells were seeded 2 days post-transduction at 5×10^5 cells/scaffold onto fused deposition-modeled PCL scaffolds (8.1 mm diameter × 2.4 mm thick, 300-500 micron pore size, 66% porosity) (Zein et al., 2002). To enhance initial cell adhesion, constructs were pre-coated in a solution of rat plasma fibronectin in PBS (20 μg/mL). During *in vitro* culture, constructs were maintained statically in osteogenic media (α-minimum essential medium, 10% fetal bovine serum, 1% penicillin-streptomycin, 50 μg/ml gentamicin sulfate, and 0.3 μg/ml fungizone, 50 μg/ml L-ascorbic

acid, 3 mM sodium β-glycerophosphate, and 10 nM dexamethasone). Media was changed every other day.

Confocal microscopy

Viability staining was performed on cell-seeded constructs using a calcein-AM/ethidium homodimer Live/Dead assay kit (Molecular Probes, Eugene, OR) according to the manufacturer's instructions, and specimens were viewed on a Zeiss LSM/NLO 510 Confocal/Multi-Photon microscope.

Fourier Transform Infrared Spectroscopy (FT-IR)

FT-IR analyses were performed as described (Bonewald et al., 2003) on bulk phase ethanol-fixed, oven-dried constructs, in which mineralized cultures were gently scraped from the underlying PCL substrate using a small blade and stereomicroscope, and prepared in potassium bromide (KBr) pellets. Spectra, 64 scans acquired at 4 cm^{-1}, were obtained on a Nexus 470 FT-IR spectrometer (ThermoNicolet, Madison, WI) under N_2 purge. A spectral range from 400-2000 cm^{-1} was analyzed for mineral and matrix peaks characteristic of the mineral phase of bone. The bands of interest were those of mineral phosphate (900-1200 cm^{-1}), matrix amide I (1585-1720 cm^{-1}), and carbonate (855-890 cm^{-1}). The mineral to matrix and carbonate to phosphate ratios were computed from the integrated areas of baseline-corrected peaks. Rat calvarial bone, lyophilized, pulverized, and similarly prepared in KBr pellets, served as a positive control.

Scanning Electron Microscopy (SEM)

Following overnight fixation in Karnovsky's fixative (2.0% paraformaldehyde, 2.5% glutaraldehyde, and 0.1 M sodium cacodylate buffer, pH 7.2-7.4), mineralized constructs were rinsed two times in 0.1 M sodium cacodylate buffer and dehydrated in a series of graded alcohol (70%, 80%, 90%, 95%, 100%) for 2×5 min and slowly dried in and hexamethyldisilazane (EM Sciences, Hatfield, PA). Samples were then sputter-coated with gold and visualized using a Hitachi S800 FEG scanning electron microscope.

Craniotomy defect surgeries

Adult male Wistar rats (~250 g, Charles Rivers Laboratories) served as syngeneic recipients of tissue-engineered constructs. All surgical and implantation procedures were performed in accordance to an IACUC-approved protocol. Briefly, animals were anesthetically induced with 4% isoflurane/O_2 gas mixture, and the incision site and surrounding area were shaved and cleaned with chlorhexidine. During surgery, anesthesia was reduced to 2% isoflurane/O_2 or lower as necessary. A midline incision in the skin was made over the cranium from the middle of the nasal bones to the posterior nuchal line. The periosteum was then dissected from the site, and the critical size craniotomy defect was made using a slow speed (500 rpm) Osada Electric Co. dental tool and trephine (8.95 mm O.D.) (Ace Surgical Supply Co., Brockton, MA). The calvarial disks were carefully removed to avoid dural perforation. The implementation of a consistent surgical technique resulted in a high success rate with minimal compromise of dural integrity. The trephine was used to completely perforate the periphery of the defect

in all locations except the rostral and caudal (anterior and posterior) midline sagittal sutures areas. A thin connection of bone remained attached at each of these two locations. A forked periosteal elevator and thin periosteal elevator were then used in tandem to gently pry up the caudal sagittal suture region. Next, the thin elevator was gently slid under the cranial disk and moved slowly toward the rostral sagittal area while downward pressure was applied to the caudal half of the detached cranial disk. After positioning the thin elevator near the only remaining site of attachment, continued downward pressure was applied to the caudal half of the disk while an upward prying motion at the rostral side was used to completely detach the disk. It was consistently observed that progression from the caudal location to the rostral location was the most effective technique to avoid dural perforation.

Residual peripheral bony regions around the periphery were carefully excised with either scissors or forceps, and the defect site was then flushed with saline prior to insertion of the scaffold implant. PCL scaffolds were press-fit into the defect. The subcutaneous tissue was sutured to cover the defect site, and the incision was closed with surgical staples. The relative position and size of the defect as well as the placement of the scaffold within the defect are detailed in Figure 7-2. After 28 days of implantation, animals were euthanized by CO_2 asphyxiation, and defect regions were dissected from the cranium with bone cutters and fixed in 10% phosphate-buffered formalin.

In this study, a total of 6 experimental groups were examined. The first group, termed empty defect, consisted of defects receiving no implanted scaffold. The second group received cell-free PCL scaffold implants. The third and fourth groups were control and Runx2-transduced cell-seeded scaffolds pre-cultured for 1 day, while the fifth and

sixth groups consisted of control and Runx2-modified cell-seeded scaffolds developed *in vitro* for 21 days prior to implantation. The final two sets of experimental groups represent two distinct approaches toward the development of tissue-engineered solutions for bone repair. The first set was designed to evaluate a relatively immature scaffold, similar to the common approach of implanting scaffolds almost immediately after seeding with cells. The second implant time point, occurring after the onset of *in vitro* mineralization at 21 days, was selected to evaluate a more mature construct representative of a mineralized bone repair template.

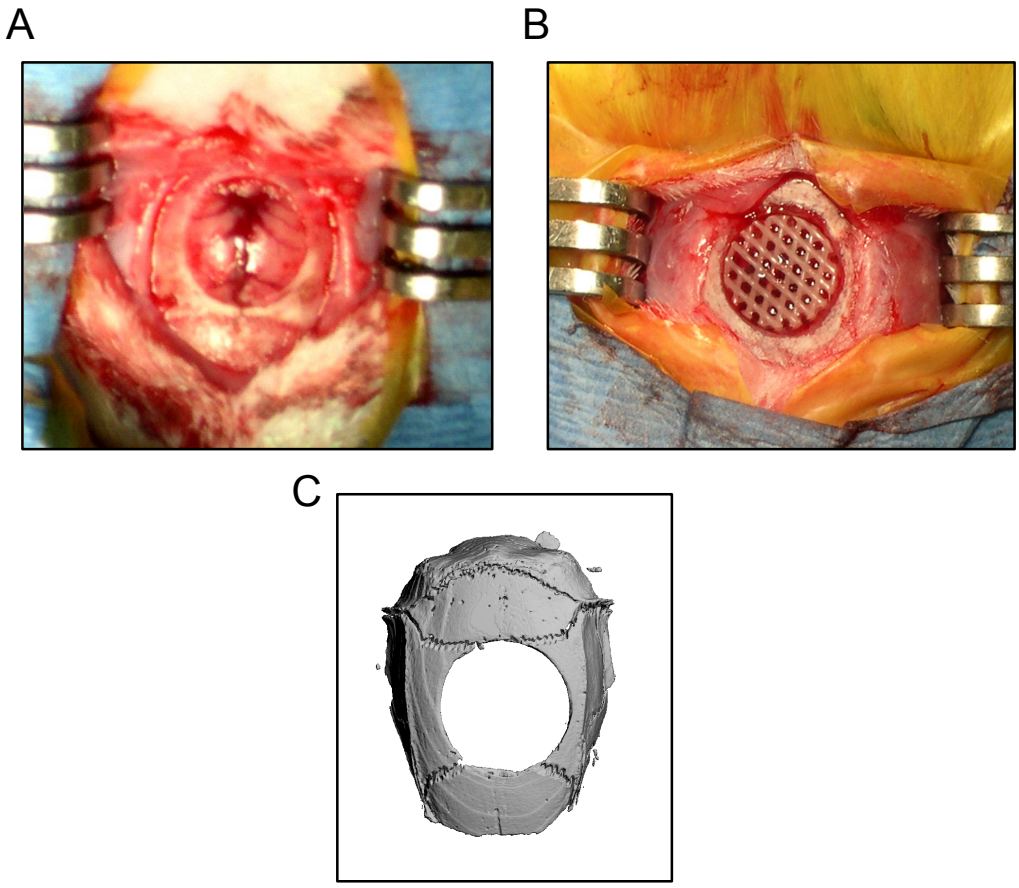

Figure 7-2. Photographs and accompanying micro-CT scans of a craniotomy defect and implanted scaffold at day 0. (A) Photograph detailing a complete defect just prior to implantation. (B) Photograph of a defect containing a PCL scaffold implant just after implantation. (C) Micro-CT scan of defect at day 0.

Microcomputed tomography

In vitro and *in vivo* mineralization of 3-D scaffolds was quantified by high resolution X-ray microcomputed tomography (micro-CT) using a Scanco Medical μCT 40 imaging system (Bassersdorf, Switzerland). Formalin-fixed specimens were scanned in 70% ethanol at 16 μm voxel resolution. *In vitro* cultured constructs were evaluated at a threshold corresponding to a linear attenuation of 0.96 cm^{-1}. Craniotomy explants, however, were evaluated at a threshold corresponding to a linear attenuation of 1.68 cm^{-1}, a threshold selected to evaluate the average attenuation of slightly less mature, new bone formed in healing defect. Evaluation of *in vitro* and *in vivo* specimens used identical filter width (1.2) and filter support (2.0) settings. As a result, of the differences in thresholding, the mineral and bone volume data determined for *in vitro* and *in vivo* constructs, respectively, could not be directly compared. The reconstructed and thresholded 3-D images were evaluated using direct distance transformation methods to calculate mineral volume within each construct (Hildebrand et al., 1999). Data are reported as total mineral volume or total bone volume for *in vitro* and *in vivo* specimens, respectively. Additionally, bone volume fraction data was tabulated for *in vivo* specimens by dividing the new total bone volume detected within the defect by a total average void volume (total pore volume) of 82.1 ± 0.8 mm^3. The individual void volume data set used to calculate the total average void volume was generated from parallel scaffolds (n=12) having an average total volume of 125.7 ± 0.6 mm^3 and a an average PCL polymer volume of 42.6 7 ± 0.3 mm^3 as determined by micro-CT analysis using an evaluation threshold corresponding to 0.40 cm^{-1}.

Histology

Craniotomy defects were bisected along the coronal plane, and one half was decalcified in Surgipath (Surgipath Medical Industries, Richmond, IL), dehydrated in a graded series of alcohol, and embedded in paraffin using standard techniques. Serial sections were stained with either Masson's trichrome or hematoxylin and eosin. Sections were examined to assess host immune and inflammatory response to the implanted cells and polymer scaffold, respectively.

Histomorphometry

Midline sections were examined to assess total new bone formation within the defect area. Quantitative analyses were performed using Image Pro image analysis software to determine the total new bone area and the bone area fraction within the defects. The architecture of the PCL enabled straightforward determination of the polymer area per section, so in order to normalize for any variability associated with scaffold orientation in the defect site, the area devoid of polymer was used to calculate the bone area fraction. Full description and graphic representation of the histomorphometric techniques are detailed in Figure 7-3.

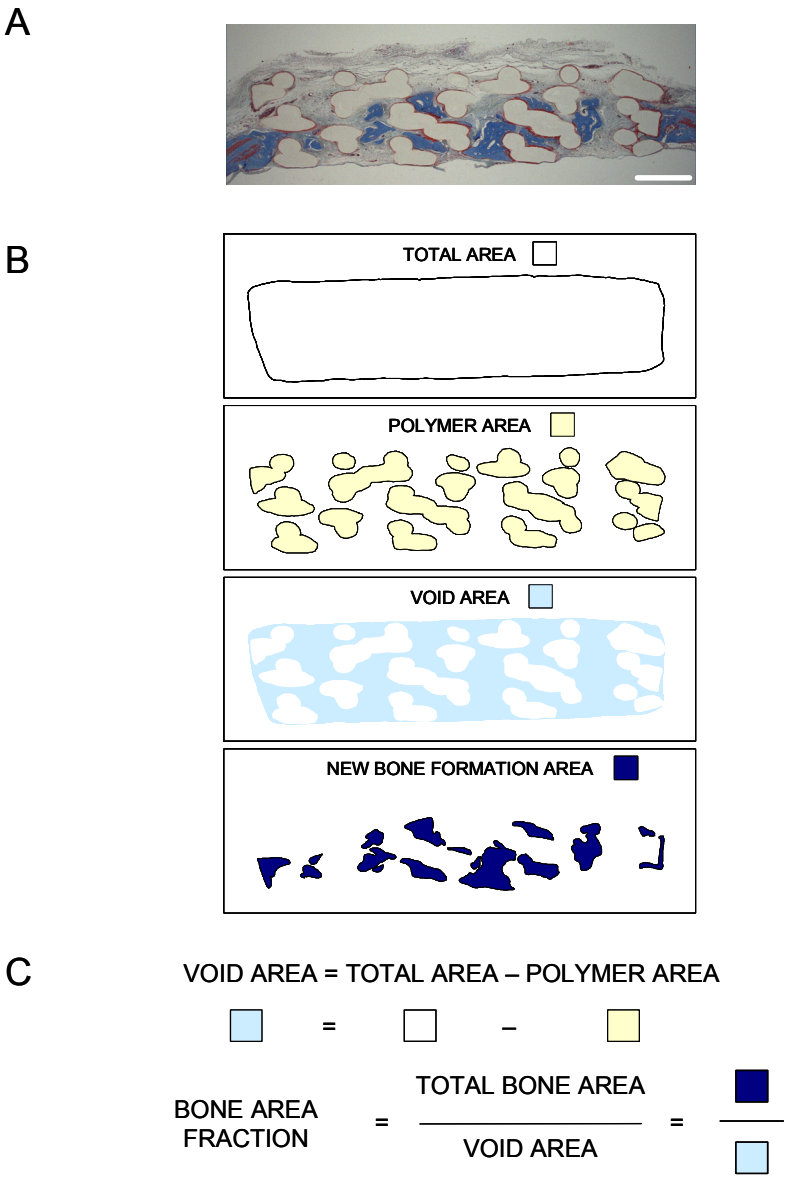

Figure 7-3. Description of methodology for determination of total bone area and bone area fraction from histomorphometrical analyses. (A) Masson's trichrome stain from PCL scaffold implanted into an 8 mm critical size craniotomy defect. (B) Contours were drawn around (i) the total cross-sectional area of the construct, (ii) the areas of polymer present within the cross-section, and (iii) the areas of new bone formation present within the cross-section as indicated by the blue staining component of the trichrome stain. (C) Equations representing the calculations for void area and bone area fraction in the defects.

Data Analysis

Data are reported as mean ± SEM, and statistical comparisons were based on ANOVA and Tukey's test for pair-wise comparisons with a p-value < 0.05 considered significant.

RESULTS

Runx2 expression increases 3-D construct in vitro mineralization

Based on previous 3-D culture experiments (Chapter 6), it was anticipated that Runx2-modified stromal cells would significantly enhance *in vitro* mineralization of PCL scaffolds. As previously described, transduction efficiencies were determined by flow cytometry at the time of scaffold seeding, and levels were equivalent to previous observations (~50%) for both Runx2-transduced and control cells. Quantification of DNA 24 hours after cell seeding demonstrated equal numbers of Runx2-modified or control cells were seeded onto the constructs (data not shown). Scaffold colonization and cellular longevity was examined by a cell viability assay and confocal microscopy at 1, 7, 21, and 56 days post-seeding (Figure 7-3). Observations at 1 day post-seeding indicated cells were sparsely covering the scaffold, yet they attained a rather spread morphology and were fairly well distributed. The scaffolds were typically confluent by 7 days, and cells began bridging struts and in some cases filling large pore voids by 21 days. Demonstrating their ability to be maintained under long term *in vitro* culture conditions, both Runx2-modified and control stromal cells remained viable and had undergone extensive proliferation by 56 days as observed by confocal microscopy. Specifically, a high percentage of the pore structures were occupied by a circular ring of cells which

bridged struts running in multiple directions. Relatively few dead cells were observed at any of the time points examined, and both Runx2-modified and control cells followed similar trends toward scaffold colonization.

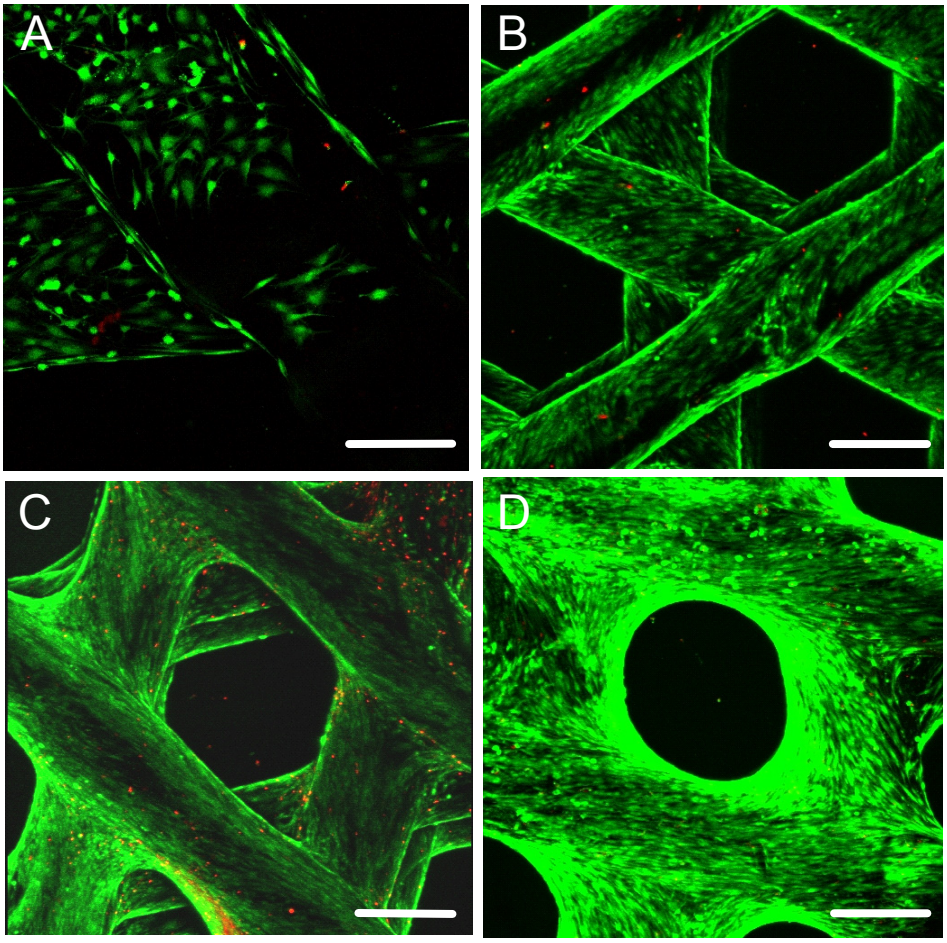

Figure 7-4. Confocal micrographs of Runx2-modified cell-seeded PCL scaffolds at multiple time points. Cell-seeded scaffolds following (A) 1 day, (B) 7 days, (C) 21 days, and (D) 56 days of *in vitro* culture [bar in (A) = 250 μm, bar in (B, C, D) = 500 μm]. Control cell-seeded scaffolds demonstrated similar levels of cellular distribution and proliferation.

Mineralization was quantified weekly by micro-CT beginning at 21 days post-seeding (Figure 7-4). Large quantities of mineralized matrix were already present at 21 days, especially on Runx2-modified cell-seeded PCL scaffolds. In agreement with the cell viability study and the presence of living cells, a steady, linearly increasing amount of mineralization was observed in both Runx2-transduced and control cell-seeded scaffolds. However, the average rate of mineral deposition was significantly higher in Runx2-modified cells compared to control cells ($p<0.02$). Specifically, Runx2-modified cells deposited 1.4 ± 0.1 mm^3 of mineral per week, whereas control stromal cells added on average only 0.9 ± 0.1 mm^3 of mineral per week. This nearly 60% difference in mineral deposition rate indicated that the observed differences in the quantity of mineralized tissue at specific time points was not attributable merely to an acceleration in mineral deposition by Runx2-modified cells. Rather Runx2 overexpression enhanced the overall mineralized matrix-producing potential of stromal cells maintained in the described 3-D environment.

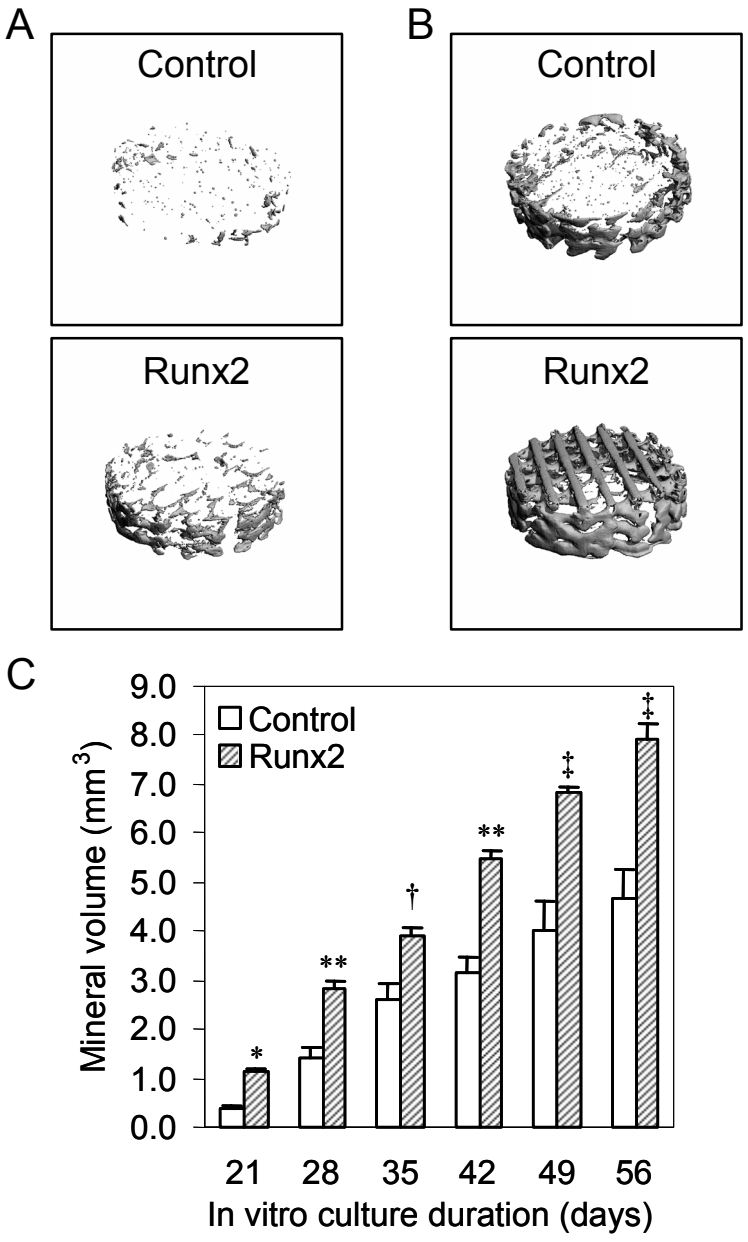

Figure 7-5. Mineralization of 3-D fused deposition-modeled PCL scaffolds by Runx2-transduced and control cells at various time points. (A) micro-CT images of control and Runx2-expressing cell-seeded PCL scaffolds following 21 days (A) and 56 days (B) of *in vitro* culture. (C) Quantification of mineral deposition my micro-CT at various time points [(mean, SEM), n=6]. ANOVA showed differences between treatment and time ($p<0.000001$). Pairwise comparisons between same time point control: * ($p<0.00005$); ** ($p<0.0005$); † ($p<0.01$); ‡ ($p<0.005$).

Examination of micro-CT micrographs confirmed the presence of significantly more mineral present on Runx2-modified cell-seeded scaffolds compared to controls. By 56 days, mineralized regions were clearly visible on all struts of Runx2-modified cell-seeded scaffolds, including those on the periphery and on either face of the construct. In contrast, mineralization on control scaffolds remained primarily confined to peripheral locations. Somewhat surprisingly based on the open architecture of the scaffold and even though ample cell colonization was observed throughout all regions of the scaffold by confocal microscopy, mineralized regions were primarily confined to the outer surfaces of the scaffold. At the outset of the study, it was anticipated that the open macrostructure of the fused deposition-modeled scaffolds would facilitate more homogeneous mineralization due to an anticipated enhancement of localized nutrient transport in the larger pore structures. This response was not observed, however, suggesting the continued persistence of local mass transfer barriers which limit the ability of centralized cells to fully differentiate. Histological analyses confirmed the presence of mineralized regions in peripheral locations similar to those observed my micro-CT, yet the extremely open architecture and *in vitro* culture system resulted in the presence of only small quantities of tissue (data not shown).

Runx2-modified and control cell-seeded scaffolds produce a biologically equivalent, collagen-associated mineralized matrix

FT-IR analysis performed on 56 day *in vitro* constructs revealed Runx2-modified and control stromal cell cultures displayed the amide I and II peaks indicative of protein, a broad phosphate stretching peak near 1100 cm^{-1}, a phosphate bending doublet split at

560 cm^{-1} and 605 cm^{-1}, and a carbonate peak near 870 cm^{-1} (Figure 7-7A). These chemical moieties are representative of a poorly crystalline apatite (Bonewald et al., 2003) and were similar to that observed for a native cranial bone specimen. To further analyze the relative maturity of the matrix, the mineral to matrix and carbonate to phosphate ratios were determined, and no significant differences existed between the treatments or compared to the cranial bone positive control (Figure 7-7B). Taken together, these results demonstrate that exogenous Runx2 expression up-regulates formation of a biologically equivalent mineralized matrix. Examination of cultures by SEM revealed the presence of freshly deposited fibrillar collagen (Figure 7-6A) as well as collagenous meshes containing significant quantities of mineral (Figure 7-6B).

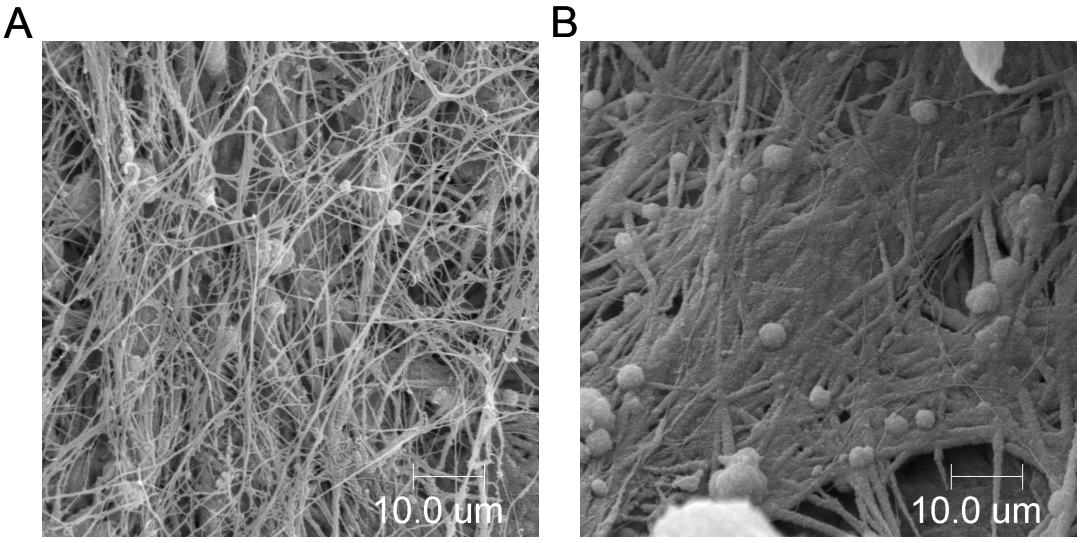

Figure 7-6. SEM micrographs of 56 day Runx2-modified cell-seeded constructs. (A) SEM micrograph detailing a representative region of unmineralized fibrillar collagen, which is actually overlaying mineralized collagen beneath. (B) SEM micrograph showing a region of mineralized collagen, demonstrating association of crystalline mineral with fibrillar collagen.

A

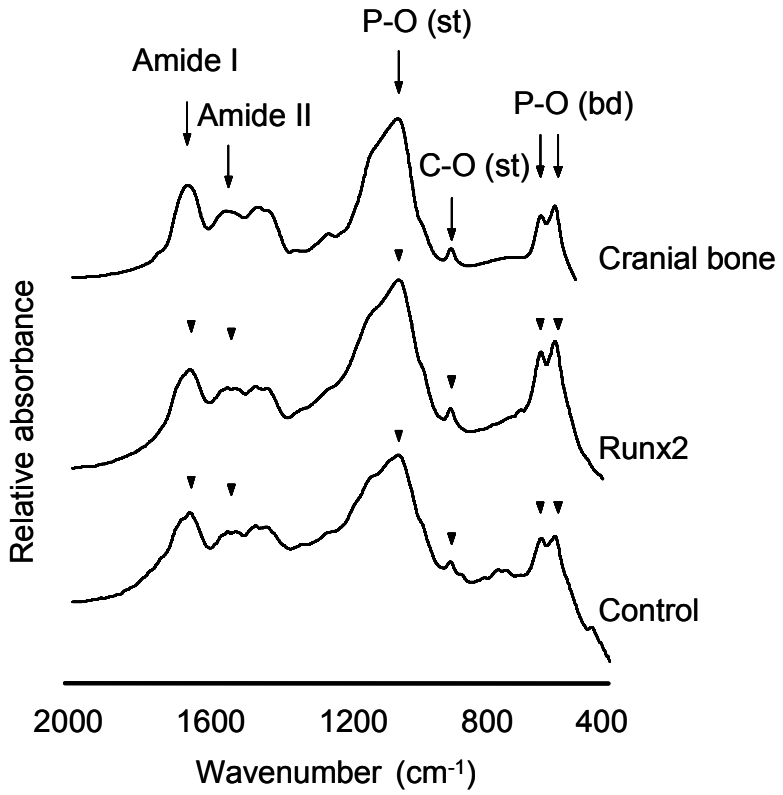

B

	Mineral to matrix ratio	CO_3 to PO_4 ratio
Cranial Bone	5.3 ± 0.1	0.015 ± 0.001
Control	4.9 ± 0.6	0.013 ± 0.001
Runx2	6.3 ± 0.4	0.013 ± 0.001

Figure 7-7. Comparative FT-IR spectra of Runx2-modifed and control bone marrow stromal cells on PCL scaffolds following 56 days of *in vitro* culture. Adult rat cranial bone was included as a positive control. (A) Transmission spectra, generated from bulk phase, ethanol fixed cultures carefully extracted from the underlying PCL scaffold and pressed into KBr pellets, showed bands characteristic of biological hydroxyapatite formation, including phosphate- and carbonate-related vibrations. st: stretching vibrations, bd: bending vibrations. (B) Comparative ratios, including the mineral to matrix (900-1200 cm^{-1} to 1585-1720 cm^{-1}) and carbonate to phosphate (855-890 cm^{-1} to 900-1200 cm^{-1}), were calculated from baseline-corrected, integrated peak areas [(mean,SEM), n=6]. No statistical differences were observed between Runx2 and control specimens compared to that observed in native cranial bone.

Histological evaluation of experimental groups

No severe immune or inflammatory responses were observed in any of the cell-containing groups examined, suggesting that minimal adverse reaction to the implanted cells or PCL scaffold material had occurred (Figure 7-8). Formation of new bone appeared normal, resulting in embedded osteocytes and marrow ossicles, and none of the groups revealed abnormal osteoclastogenesis. Void spaces not filled with new bone were filled with soft connective tissue which lacked any detectable inflammatory cells, including macrophages. As a result of the decalcification, mineralized tissue resident near the scaffold surface/interface of experimental groups containing implanted cells, especially those pre-cultured *in vitro* for 21 days, could not be distinguished from other soft connective tissue present in the void spaces of the PCL scaffold.

Micro-computed tomography and histomorphometric analyses of in vivo scaffolds

Based on the results of *in vitro* studies and the subcutaneous implantation model which revealed a synergistic interaction between Runx2 overexpression and *in vitro* construct development, it was of particular interest to examine similar parameters in an *in vivo* bone healing environment. Following 28 days of *in vivo* implantation, explant constructs were evaluated by micro-CT to determine new bone volume and bone volume fraction data and by histomorphometry to quantify new bone area and bone area fraction data. All experimental groups demonstrated a healing response as determined by both characterization methods (Figures 7-9 through 7-12).

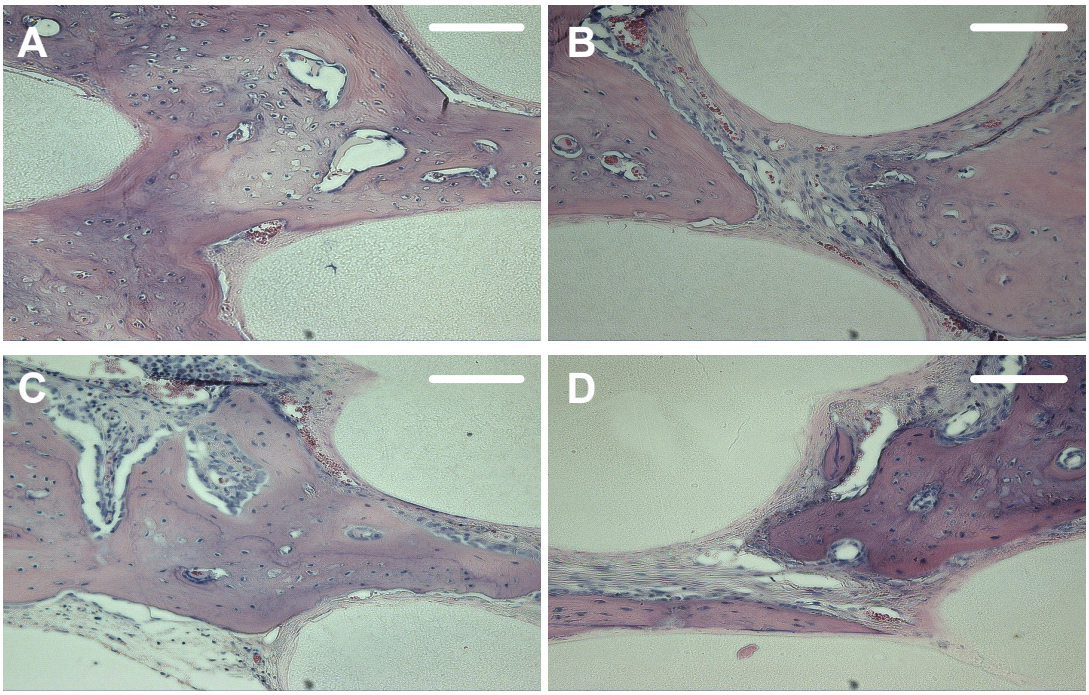

Figure 7-8. Hematoxylin-eosin staining of cell seeded scaffolds following 28 days in vivo implantation. (A) Control cell-seeded scaffold pre-cultured for 1 day prior to implantation. (B) Runx2-modified cell-seeded scaffold pre-cultured for 1 day prior to implantation. (C) Control cell-seeded scaffold pre-cultured for 21 days prior to implantation. (D) Runx2-modified cell-seeded scaffold pre-cultured for 21 days prior to implantation. Similar morphologies were detected in cell-free scaffold implants (data not shown). (bar = 100 μm)

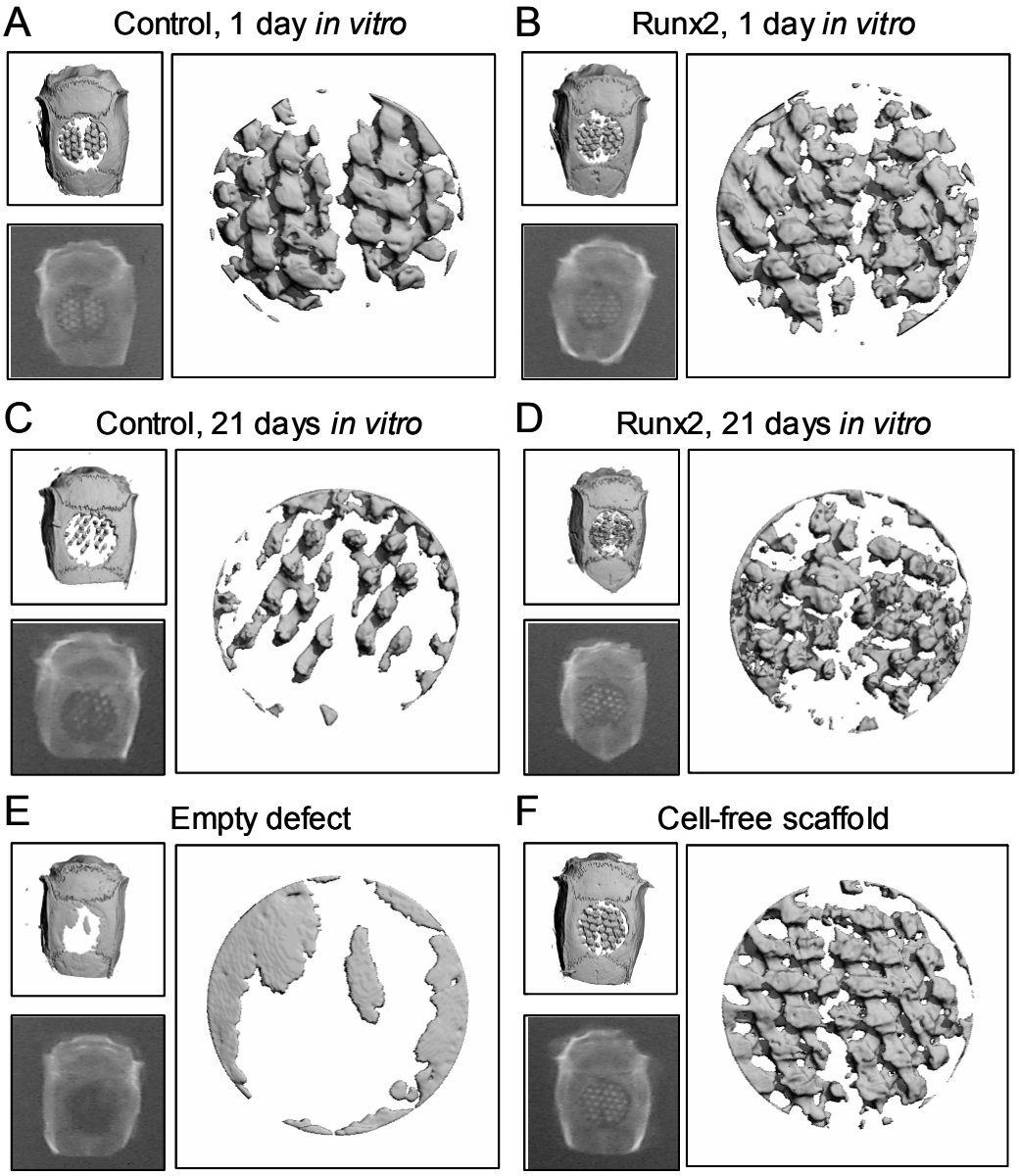

Figure 7-9. Micro-CT and radiograph images of complete skulls and contoured craniotomy defect areas for experimental groups. Contoured regions of the defects from each group were used for quantification of new bone formation by micro-CT. Images shown are representative complete skulls (micro-CT top left, radiographs bottom left) and 0.545 cm^2 (8.3 mm diameter) contoured defects (right), providing an approximate tolerance of 0.2 mm to the diameter of the implanted construct. Groups shown are PCL scaffolds seeded with control (A) or Runx2-transduced (B) stromal cells pre-cultured for 1 day, PCL scaffold seeded with control (C) or Runx2-modified (D) stromal cells pre-cultured for 21 days, or empty defect (E), and PCL scaffold with no cells (F).

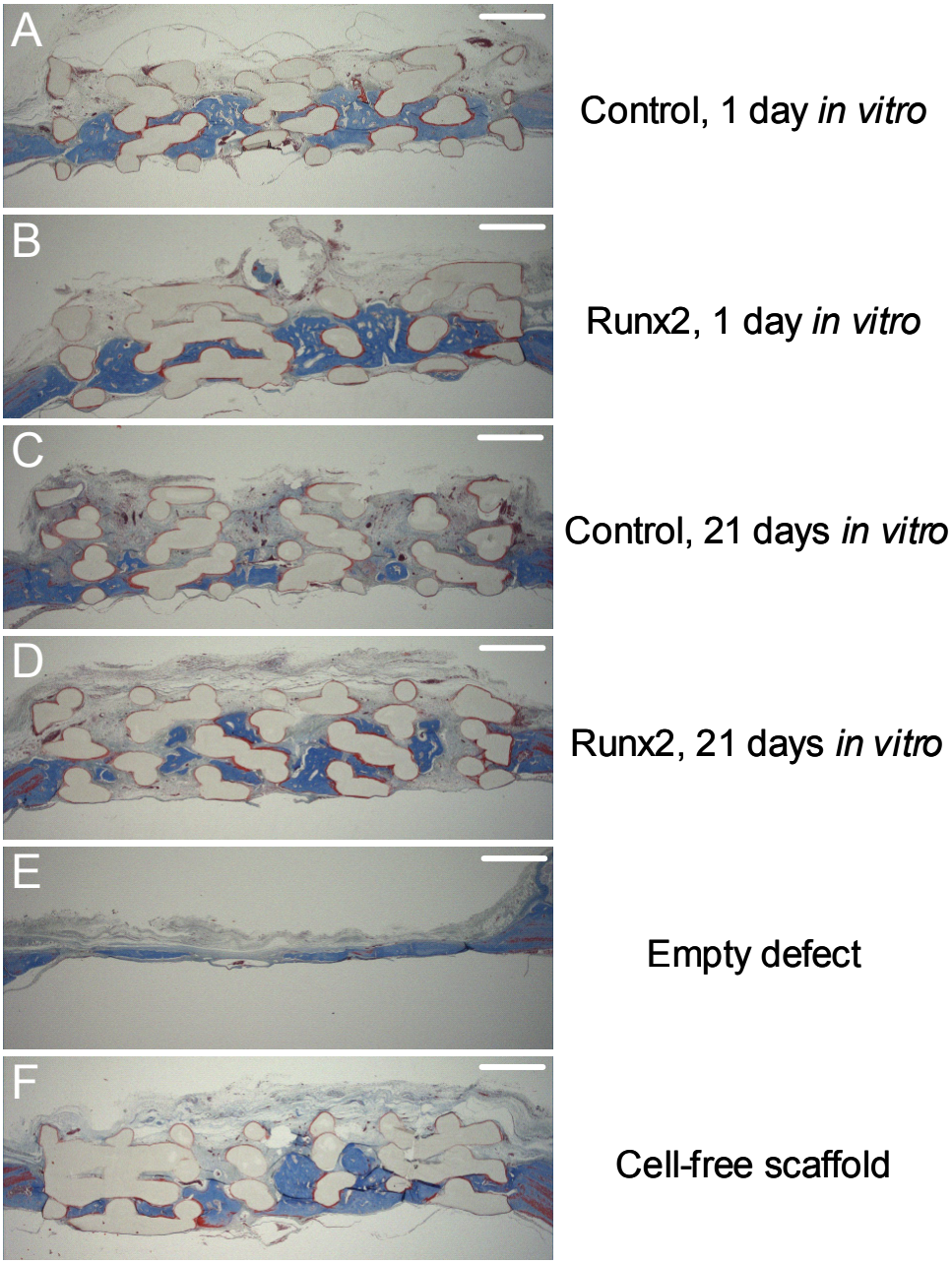

Figure 7-10. Histological micrographs from midline sections of craniotomy defects stained with Masson's modified trichrome. Representative sections from each group were used for histomorphometric analysis, including PCL scaffolds seeded with control (A) or Runx2-transduced (B) stromal cells pre-cultured for 1 day, PCL scaffold seeded with control (C) or Runx2-modified (D) stromal cells pre-cultured for 21 days, empty defect (E), and PCL scaffold with no cells (F) (bar = 1 mm).

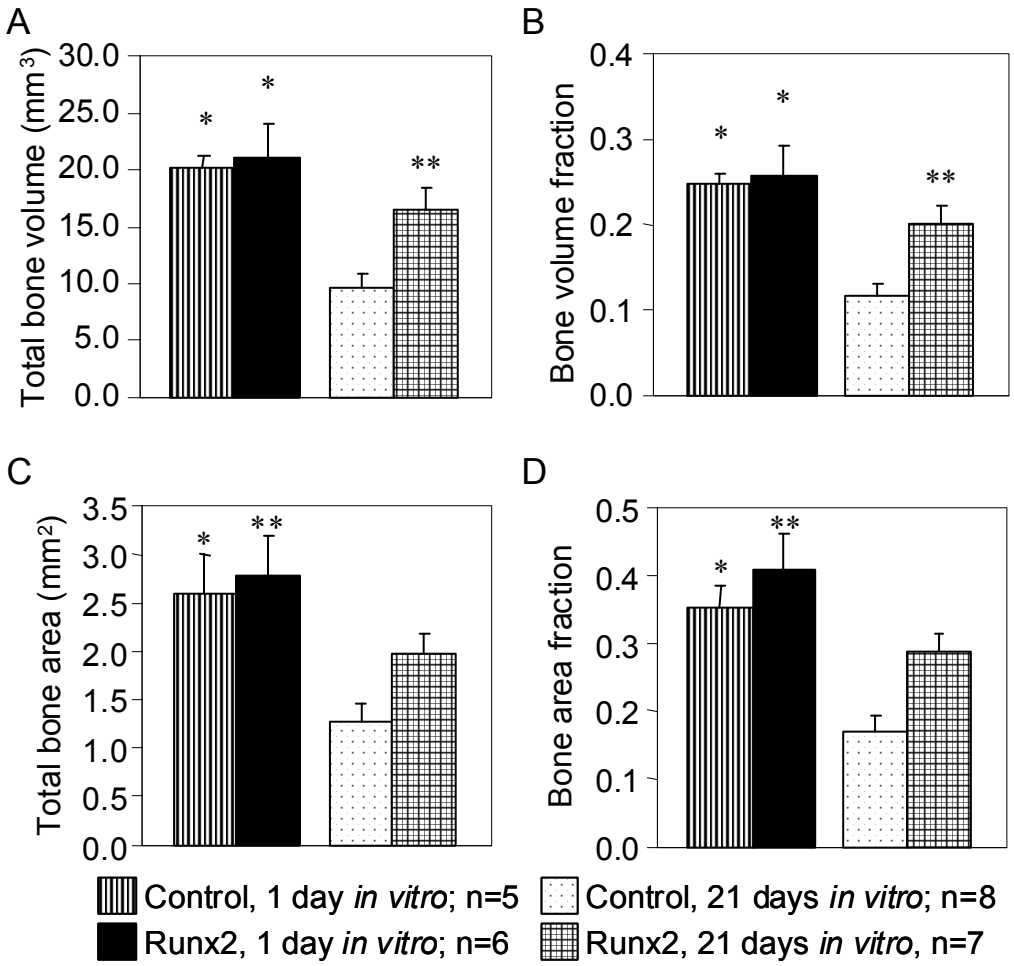

Figure 7-11. Micro-CT total bone volume and bone volume fraction data and histomorphometric total bone area and bone area fraction data from 28 day craniotomy defect explants, including control and Runx2-modified cell-seeded PCL scaffolds pre-cultured for either 1 or 21 days. (A) Total bone volume from micro-CT data (mean, SEM). One-way ANOVA showed differences in groups ($p<0.001$). Pairwise comparisons: greater than control cell, 21 day pre-cultured constructs, * ($p<0.005$); ** ($p<0.05$). (B) Bone volume fraction data determined by normalizing the total bone volume by the average void volume of PCL scaffolds (mean, SEM). One-way ANOVA showed differences in groups ($p<0.001$). Pairwise comparisons: greater than control cell, 21 day pre-cultured constructs, * ($p<0.005$); ** ($p<0.05$). (C) Total bone area from histomorphometry data (mean, SEM). One-way ANOVA showed differences in groups ($p<0.01$). Pairwise comparisons: greater than control cell, 21 day pre-cultured constructs, * ($p<0.03$); ** ($p<0.01$). (D) Bone area fraction data determined by normalizing the total bone area by the void area for each section (mean, SEM). One-way ANOVA showed differences in groups ($p<0.001$). Pairwise comparisons: greater than control cell, 21 day pre-cultured constructs, * ($p<0.01$); ** ($p<0.0005$).

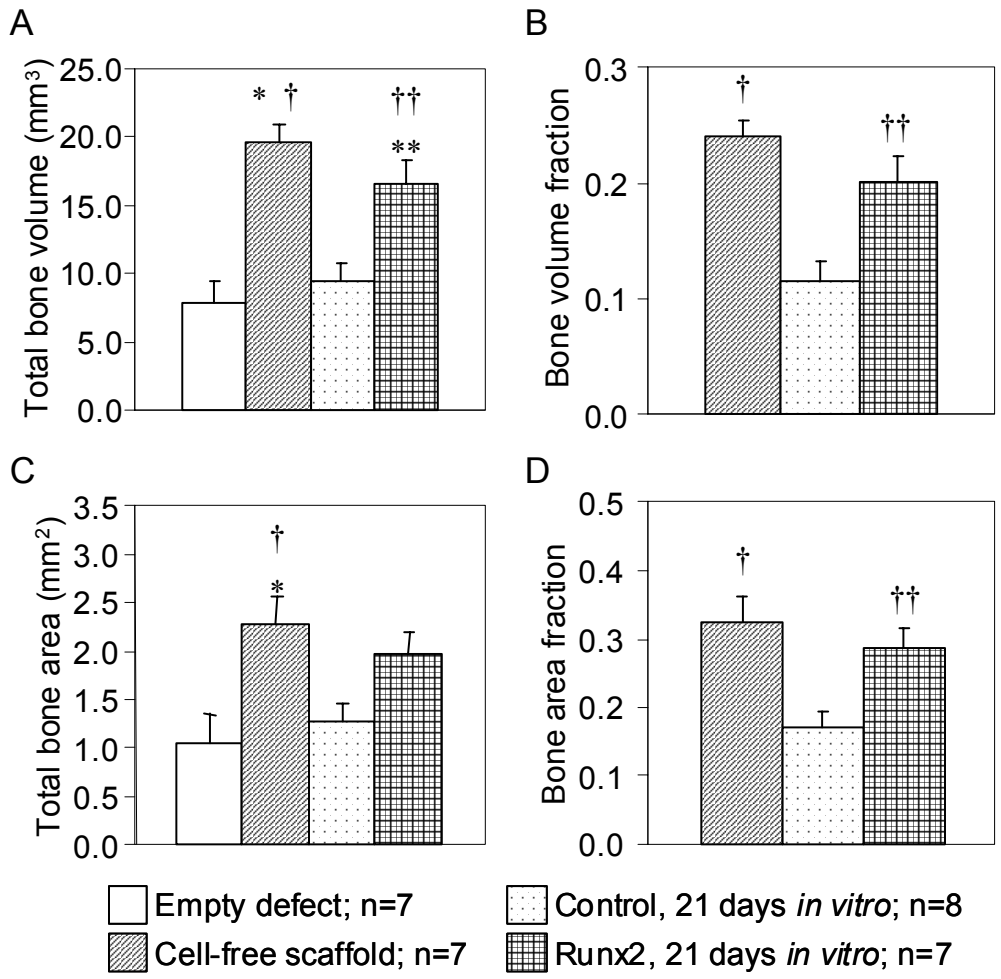

Figure 7-12. Micro-CT total bone volume and bone volume fraction data and histomorphometric total bone area and bone area fraction data from 28 day craniotomy defect explants, including empty defects, PCL scaffolds with no cells, and control and Runx2-modified cell-seeded PCL scaffolds pre-cultured for 21 days. (A) Total bone volume from micro-CT data (mean, SEM). One-way ANOVA showed differences in groups ($p<0.00002$). Pairwise comparisons: greater than empty defect, * ($p<0.0001$), ** ($p<0.005$); greater than control cell, 21 day pre-cultured constructs, † ($p<0.0005$); †† ($p<0.02$). (B) Bone volume fraction data determined by normalizing the total bone volume by the average void volume of PCL scaffolds (mean, SEM). One-way ANOVA showed differences in groups ($p<0.0005$). Pairwise comparisons: greater than control cell, 21 day pre-cultured constructs, † ($p<0.0005$); †† ($p<0.01$). (C) Total bone area from histomorphometry data (mean, SEM). One-way ANOVA showed differences in groups ($p<0.01$). Pairwise comparisons: greater than empty defect, * ($p<0.02$); greater than control cell, 21 day pre-cultured constructs, † ($p<0.05$). (D) Bone area fraction data determined by normalizing the total bone area by the void area for each section (mean, SEM). One-way ANOVA showed differences in groups ($p<0.01$). Pairwise comparisons: greater than control cell, 21 day pre-cultured constructs, † ($p<0.01$); †† ($p<0.05$).

Examination of the effects of *in vitro* pre-culture revealed a quite different result than that observed in the subcutaneous implantation study previously described (Chapter 6). Specifically, defects containing constructs pre-cultured for only 1 day demonstrated the highest total bone volume and bone area independent of cell treatment (Figure 7-11). Furthermore, defects treated with cell-free PCL scaffolds exhibited comparable degrees of healing (Figure 7-12), suggesting that in this particular bone defect model, the open architecture and interconnected structural network of the fused deposition-modeled scaffolds provided a suitable osteoconductive scaffold capable of supporting significant new bone formation by infiltrating host cells. Interestingly, extended *in vitro* pre-culture appeared to have a negative effect on new bone formation in defects treated with constructs containing control stromal cells pre-cultured for 21 days prior to implantation, as this group contained significantly less new bone formation than all other treatments evaluated (Figures 7-11 and 7-12). However, Runx2-modified cell-seeded scaffolds pre-cultured for 21 days contained significantly more new bone volume, nearly 2-fold greater, than similarly pre-cultured control cell-seeded scaffolds. Furthermore, no differences in bone volume or area existed between Runx2-transduced cell-seeded scaffolds pre-cultured for 21 days and the 1 day pre-culture and cell-free groups (Figures 7-11 and 7-12). Although the relative differences in histomorphometric data persisted between the 21 day pre-cultured groups, statistically significant differences in bone area or bone area fraction were not observed. This observation is not entirely unexpected based on the non-uniform distribution of new bone formation as revealed by micro-CT or the potential for slightly offset micro-CT threshold values. These findings suggest that Runx2 overexpression in bone marrow stromal cells is capable of overcoming the

observed inhibitory effect on new bone formation observed in response to *in vitro* pre-culture of constructs containing unmodified stromal cells. The parameters of the current study did not allow for determination of the method by which Runx2-modified cells induced higher levels of new bone formation. The two most likely mechanisms are (i) through cell-mediated secretion of soluble osteoinductive factors subsequent to implantation or (ii) through the development of a more robust osteoinductive, osteoconductive, and biologically active matrix synthesized *ex vivo* prior to implantation.

Finally, the implantation of unmodified 21 day pre-cultured stromal cell-seeded scaffolds, containing cells not exposed to viral treatment, demonstrated levels of new bone formation equivalent to control cell-seeded scaffolds, suggesting a muted immune response to any residual viral particles and proteins (data not shown).

As stated, new bone formation was quite prevalent in defects receiving cell-free PCL scaffolds (Figure 7-12). The mean bone volume and bone area were comparable to that observed in the 1 day pre-cultured cell-seeded experimental groups and significantly higher than that observed in 21 day pre-cultured control cell-seeded scaffolds. Some of the cell-free scaffold implants were pre-cultured for 21 days *in vitro* in parallel with cell-seeded scaffolds, while the remainder were implanted following only 1 day of *in vitro* pre-culture. Importantly, no differences existed in new bone volume between 1 and 21 day pre-cultured cell-free scaffolds, suggesting that *in vitro* pre-culture does not alter the scaffold properties in a manner which impacts its function in this craniotomy defect model. Although none of the empty defects healed completely, a significant amount of new bone formation was formed along the dura in this experimental group (Figures 7-6, 7-7 and 7-9). For reference, total new bone volume in the empty defects was nearly

equivalent to that observed in 21 day pre-cultured control stromal cell-seeded scaffolds. However, direct comparison of total new bone formation in the empty defect group to any of the scaffold containing groups proved inappropriate due to the presence of significant quantities of PCL scaffold material in the dural plane, which greatly reduced the volume/area available for new bone formation.

DISCUSSION

Runx2 overexpression significantly increased mineralization of 3-D constructs following *in vitro* culture. A time series quantitative analysis of matrix mineralization demonstrated more than a 1.5-fold increase in the average mineral deposition rate by Runx2-modified cells. These results indicate that the observed increase in mineral volume at a particular time point is not attributable solely to an acceleration of mineralization by Runx2-modified cells, but rather occurs due to an increase in the mineralized matrix-producing capacity of a stromal cell population undergoing osteoblastic differentiation.

Subcutaneous implantation of Runx2-expressing stromal cells seeded in PLGA scaffolds and pre-cultured *in vitro* for 21 days resulted in a greater than 10-fold increase in mineralization and a 5-fold increase in the average daily rate of mineral deposition compared to controls. However, insignificant quantities of mineral were detected on either Runx2-modified or control cell-seeded constructs implanted following 1 day of pre-culture (Chapter 6). These results indicated a synergistic interaction between Runx2 overexpression and *in vitro* construct development in the subcutaneous environment. It was, therefore, hypothesized that a similar interaction would facilitate healing of a critical

size bone defect. Evaluation of these parameters in a syngeneic craniotomy defect model demonstrated different results than the subcutaneous study, however. Specifically, constructs implanted following 1 day demonstrated the highest levels of new bone formation independent of cell treatment, while defects receiving constructs maintained under *in vitro* culture conditions for 21 days contained less and in the case of control cells, significantly less, new bone formation. These results suggest that in this model, a defect created by the extraction of bone from a site capable of reasonable spontaneous regeneration, *in vitro* pre-culture of stromal cell-seeded constructs is inhibitory to subsequent bone formation. However, as observed in the subcutaneous model, Runx2-transduced stromal cells pre-cultured for 21 days elicited significantly more bone formation compared to these control cell-seeded scaffolds. There are several factors and differences which potentially address the observed disparity in these experimental models.

The first and potentially most pronounced difference exists at the physiologic level of the two models. Bone defect models in general introduce a significant complexity resulting from the presence of endogenous osteoinductive and osteogenic factors present in the defect site. Based on its heterotopic location, these factors are notably absent from a subcutaneous implantation site. As a result, a significant amount of endogenous healing is possible in a bone defect model, and factors such as scaffold selection and species selection can have a profound impact on the clarity of the model and the ability to detect differences among experimental groups. For example, although the rat cranial defect model has been shown to be non-healing out to at least 3 months (Schmitz et al., 1990) and the empty defects in the current study remained nonunions at

28 days, a significant amount of new bone formation was quantified by both micro-CT and histomorphometry. This suggests limited or at least variable functionality of this particular critical size defect model to evaluate the effectiveness of Runx2-transduced stromal cells to facilitate defect healing.

Additionally, the scaffolds used in the two studies were markedly different in physical structure and composition. PLGA is highly porous, possesses minimal mechanical integrity, low interconnectivity, and a relatively high surface area to volume ratio. The fused deposition-modeled scaffolds used in the cranial defect study, on the other hand, contained fewer but larger pores, were mechanically sound and completely interconnected, and had a low surface area to volume ratio. By virtue of the pores being sufficiently large, an exceptional quantity of endogenous signal, in the form of blood born cells and soluble factors, was able to infiltrate the scaffold and potentially initiate substantial localized bone formation in conjunction with progenitor cells present in the dura. This property, coupled with the interconnected architecture of the scaffold and the relatively high rate of spontaneous healing observed in empty defect group, may explain the elevated levels of new bone formation observed in cell-free scaffolds. Furthermore, the comparatively low surface area to volume ratio and large pore structure of the PCL scaffold resulted in a relatively low therapeutic load factor. Specifically, the number of cells, whether Runx2-modified or control, which were introduced into the defect was relatively low compared to alternative scaffolds with higher surface area to volume ratios. This artifact was especially significant for the 1 day pre-cultured scaffolds, in which no differences existed between Runx2-modified and control cell-seeded scaffolds.

A crucial consideration is to clearly identify the attenuating components in the two models. In the subcutaneous explants, the mineral component requires thresholding at a much lower level due to its relative low density compared to that necessary to accurately detect the opaque structure of native bone, specifically, at threshold of 0.96 cm^{-1}, the same threshold used to quantify *in vitro* mineralization of both 3-D PLGA and PCL constructs. Alternatively, the attenuating bone detected in the craniotomy defect was thresholded at 1.68 cm^{-1}, a level above the detection limit of *in vitro* cell-mediated mineralization. As a result, any mineralization present on the PCL constructs prior to implantation or deposited subsequently in the defect following implantation would not have been detected using the selected threshold. Therefore, it is important to maintain the perspective that different physical structures were being quantified by the two different models.

Nonetheless, extended *in vitro* pre-culture reduced the amount of new bone formation observed in control cell-seeded scaffolds pre-cultured for 21 days prior to implantation compared to constructs pre-cultured for 1 day. It is possible that the relatively low therapeutic loading present on 1 day pre-cultured scaffolds actually results in minimal signal from the cellular component, and the observed new bone formation results from the scaffolds closely approximating the cell-free scaffold group, which demonstrated similar levels of new bone formation. Sikavitsas et al. observed a similar trend in response to pre-cultured, stromal cell-seeded titanium meshes (Sikavitsas et al., 2003). Constructs pre-cultured under fluid flow conditions for 1 day demonstrated enhanced defect healing compared to those pre-cultured for 4 or 8 days (Sikavitsas et al., 2003). In the present study, however, scaffold implants containing Runx2-modified cell-

seeded scaffolds pre-cultured for 21 days enhanced new bone formation compared to similarly cultured controls. Taken together, the results of these two studies underscore the importance of matrix maturity and the relative degree of osteoblastic differentiation toward enhancing *in vivo* osteoinductivity of a tissue-engineered matrix.

Examination of bone volume fraction and bone area fraction data (Figures 7-11 and 7-12) revealed a fairly consistent offset between the values, as bone area fraction data was approximately 10% higher for each of the experimental groups. While these differences could be explained by variability in scaffold orientation and section location or the observed non-homogeneity in new bone distribution, an additionally plausible explanation involves the threshold selection for micro-CT evaluation. The value selected, corresponding to a linear attenuation of 1.68 cm^{-1}, although justified in magnitude based on its correlation to the attenuation of the newly formed native bone, may be sufficiently high to exclude less dense or somewhat less mature woven bone that is present in the defect. As histomorphometric analysis was based on visual inspection of histological cross-sections, these subtle differences could be more easily taken into account. Other factors which may contribute slightly to the offset include (i) overestimating the total bone area due to the inability to distinguish osteoid, or the unmineralized portion of the matrix, from that collagenous matrix which was previously mineralized due to the fact that these analyses were performed on decalcified sections, (ii) failing to subtract large marrow cavities from the total bone area, or (iii) conducting the histomorphometric analysis at only one location, in this case the center of the defect rather than doing multiple averaging analysis at several locations. Furthermore, the threshold used was nearly double that selected to evaluate *in vitro* specimens, and

evaluation of *in vitro* scaffolds at this elevated threshold essentially excludes all signal detected under the typical attenuation of 0.96 cm^{-1} used in quantifying mineralization of *in vitro* cultured scaffolds (data not shown). Therefore, in addition to the exclusion of less radio-dense woven bone present in the defect, this threshold restricts the ability to quantify the amount of mineralized tissue deposited by Runx2-expressing or control stromal cells.

Several groups have recently examined the Runx2-responsiveness of selected target cells for bone tissue engineering applications. To date, these reports have provided mixed indications as to the effectiveness of Runx2 overexpression, largely explained by the target cell source or method of Runx2 transduction. Yang et al. examined adenoviral Runx2-expressing pluripotent C3H10T1/2 cells subcutaneously and showed sparse bone and cartilage-like tissue formation at levels considerably lower than BMP-2-expressing cells (Yang et al., 2003). Further supporting this observation that exogenous BMP-2 expression is more effective at promoting bone repair than Runx2, Hirata and colleagues implanted scaffolds seeded with primary skin fibroblasts overexpressing either BMP-2 or Runx2 into craniotomy defects and observed negligible bone-like tissue formation by Runx2-modified cells *in vivo*, whereas BMP-2-expressing fibroblasts demonstrated effective defect healing (Hirata et al., 2003). Both of these studies examined adenoviral gene therapy which admittedly resulted in a rapid decay in transgene expression. It has been proposed that constitutive expression of Runx2 may be required to sustain the osteoblastic phenotype (Prince et al., 2001) and data described herein indicates that sustained Runx2 overexpression enhances differentiation of osteoblastic cells (Chapter 4 and 5) (Byers et al., 2002). As a result, transgene expression duration may have a

profound impact on the overall effectiveness of a genetic engineering strategy involving Runx2 overexpression. Furthermore, it has been clearly shown that Runx2 overexpression alone is not sufficient to direct mineralization of non-osteoblastic target cells (Chapter 4) (Byers et al., 2002) and that supplementation with additional osteoinductive agents, such as dexamethasone, enhances the activity of exogenous Runx2 expression. These results underscore the essential role of Runx2 in osteoblastic differentiation, yet clearly demonstrate the requirement of additional factors which act either in series or in parallel to potentiate Runx2 overexpression. Therefore, an additional underlying limitation associated with the studies of Yang et al. and Hirata et al. in the context of a Runx2 overexpression genetic engineering strategy relates to target cell selection.

The prominence of endogenous healing capacity even in the defects which received no implants suggests that this model may not have been sufficiently rigorous to adequately evaluate the added benefit of incorporating pre-cultured Runx2-modified cell-seeded constructs into the defect site. Alternatively, more challenging models such as a segmental defect study, or perhaps even more appropriately, a spine fusion model, which was initially completely devoid of bone at the site of the fusion may provide even greater insight as to the significance and potential of Runx2-overexpressing stromal cells as a candidate cell source for bone tissue engineering applications.

CHAPTER 8

FUTURE CONSIDERATIONS

Collectively, these *in vitro* and *in vivo* studies have provided a thorough characterization regimen to observe the *in vitro* and *in vivo* performance of Runx2-expressing marrow-derived stromal cells and evaluated their potential as a candidate cell source for bone tissue engineering applications. Furthermore, these analyses provided a novel combination of tissue and genetic engineering techniques toward the development of a Runx2-modified stromal cell/polymeric scaffold composite tissue-engineered bone graft substitutes. There are several key areas to address in order to further develop this technology and these integrated approaches toward the development of mature, biologically active tissue-engineered substitutes.

Based on recent evidence suggesting that constitutive Runx2 expression may actually sustain the differentiated osteoblast phenotype phenotype (Prince et al., 2001), the long term expression duration provided by retroviral systems may be invaluable. However, perhaps the greatest barrier to clinical acceptance of this genetic and tissue engineering strategy is directly associated with the risks of gene therapy techniques, especially retroviral gene delivery. Although insertional mutagenesis is in principle a rare occurrence, inappropriate integration near a proto-oncogene can activate it or integration within a tumor suppressor gene can inactivate it. Short term objectives of this work should likely be the completion of *in vitro* tumorogenicity assays, such as growth on agarose, in order to determine how many if any tumorogenic cells result from this retroviral transduction system. The insertion pattern of a number of retroposons indicate

that these elements are capable of inserting with a high degree of sequence specificity. Long term implications for the gene therapy field and specifically this work might be to identify more advanced retroviral delivery vehicles which have the capacity to preferentially target a safe/dead zones in DNA to even further reduce the risks associated with conventional retroviral mediated gene delivery.

Retroviral gene therapy is only effective in transducing dividing cells, which in principle is acceptable for *ex vivo* genetic modification of stromal cells. However, transduction efficiency and yield of Runx2-expressing cells may be enhanced by the implementation of alternative viral transduction techniques which may offer greater flexibility in target cell identity or stage of mitotic progression, including adeno-associated viruses, lentiviruses, or even adeno-retroviral chimeras (Zheng et al., 2000). Additional areas for improvement include the optimization of transduction efficiency in bone marrow stromal cells. For this particular retroviral packing system, i.e. the ΦNX amphotropic producer line, our results consistently demonstrate transduction efficiencies in the range of 50% for rat bone marrow stromal cells. While our results in demonstrating the effectiveness of Runx2 overexpression in stromal cells are promising even at this level of transduction efficiency, enhancing the transduction efficiency or even the purity of the Runx2-expressing cell population through selection methods may potentiate the osteoblastic phenotypic enhancement capacity of this strategy. This is especially true when examining the transition from a rodent model to the human stromal cells, as the mitogenic properties may vary significantly between species, donor age, etc. Increasing transduction efficiency is the most desirable and perhaps the most practical solution to addressing this issue. Cell sorting/selection techniques while effective in

concept and function are both time consuming and technically demanding. Furthermore, the resulting challenges introduced into cellular system make this a less than optimal solution. Any selection process which reduces the number of viable cells for inclusion in cell-intensive therapeutic applications such as large tissue-engineered bone grafts logistically complicates cell expansion protocols necessary to obtain significant cell numbers. Additionally, the removal of Runx2-negative stromal cells from the population could potentially negatively impact the resulting differentiation capacity of the transduced cell population if requisite support cells are inadvertently removed during the selection process. As suggested by our data examining the Runx2-responsiveness of subcultured stromal cells, a subpopulation of stromal cells remained capable of in vitro nodule formation beyond 15 population doublings, suggesting that dramatic cellular expansion and retention of Runx2-responsiveness to generate significant quantities of cells for tissue-engineered strategies is quite feasible. However, it has been shown that extensive *in vitro* subculture reduces the transducibility of human stromal cells (Bulabois et al., 1998). This observation further underscores the need to optimize transduction efficiency so that the maximum number of potentially Runx2-responsive target cells receive the target gene and are thereby induced toward a more pronounced state of osteoblastic differentiation.

A related concern is the longevity and temporal optimization of exogenous Runx2 gene expression. The requisite expression duration of exogenous Runx2 necessary to maximize the effect of the transgene *in vitro* but more specifically *in vivo* has yet to be determined. Studies have indicated that retroviral promoter silencing/inactivation does occur in stromal cells following extended *in vivo* implantation (Allay et al., 1997).

Further transduction optimization studies would then ideally incorporate long term *in vivo* implantations to observe the efficacy and longevity of the transduced cells and transgene expression. Based on the results of long term *in vivo* studies, further attention could be given to the examination of alternative promoters, including other viral promoters, tissue-specific promoters, or even inducible systems which would allow for enhanced regulatory of Runx2 transgene expression. As reported by several researchers, Runx2 mRNA transcripts have been detected at nearly constant levels throughout the maturation of osteoblasts, in fully mature osteoblasts, and even in nonosseous cells (Prince et al., 2001; Xiao et al., 2001; Shui et al., 2003). The posttranscriptional activity leading to increased Runx2 protein expression observed in these studies has yet to be completely elucidated, but Xiao et al. demonstrate an ablation of an immature splice variant Runx2 transcript and concomitant appearance of the fully mature Runx2 mRNA in C2C12 cells following BMP-2 treatment (Xiao et al., 2001). These results indicate the existence of biological cues and pathways to facilitate Runx2 protein expression and activity independent of Runx2 mRNA transcript levels. As these pathways are determined and the physiologic roadmap of Runx2 expression and activity become evident and more accurately understood, the incorporation of alternative signals or additional inductive mechanisms to facilitate Runx2 activity could be incorporated into this tissue engineering strategy.

From a clinical and biotechnological perspective, the development of a tissue-engineered mineralized bone repair template requires the generation of abundant quantities of biologically-equivalent matrix ideally possessing the osteogenic, osteoconductive, osteoinductive, and osteointegrative capacity of autologous bone grafts.

The studies detailed in the current research form the foundation of a combinatorial genetic and tissue engineering strategy, which may provide a conceivable approach to the creation of a mineralized bone repair template. Specifically, target cells are genetically modified to overexpress an osteoblast-specific transcriptional activator which facilitates their osteoblastic differentiation toward the production of a more robust mineralized matrix *ex vivo*. However, when examining the end result of marrow-derived stromal cells overexpressing Runx2, a product development engineer may not necessarily be concerned with the precise mechanism by which this process occurred, i.e. (i) Runx2 overexpression forces a greater number of stem cells/osteoprogenitors toward osteoblastic differentiation and the concomitant production of tightly regulated quantities of bone-like matrix, (ii) forced Runx2 expression enhances the total average mineralized matrix producing capacity at the level of individual stem/osteoprogenitor cells, or (iii) a combination of these two equally plausible and perhaps equally desirable mechanisms. To this point, the effect of Runx2 overexpression on osteoblastic gene expression and matrix mineralization of stromal cells in both monolayer culture and on 3-D scaffolds has been accessed through quantitative analyses examining the bulk response of a population of Runx2-transduced cells, i.e. quantitative PCR, micro-computed tomography, and histology. As a result, a clear determination of frequency versus total average osteogenic capacity per unit cell has not been determined. Although cell selection protocols and/or limited dilution studies are tedious and time consuming, it would be of significant biological importance to more completely understand the mechanisms by which this genetic engineering technique is functioning in order to so markedly up-regulate the osteoblastic differentiation of target stromal cells.

The transition away from poorly interconnected scaffolds with exceedingly small pores, such as PLGA, to a more macroporous architecture like that of PCL was expected to facilitate a more pronounced and homogenous differentiation of scaffold-seeded cells. It was anticipated that the open architecture of the scaffold would more readily facilitate nutrient transport, waste removal, and soluble growth factor delivery to enhance differentiation and mineralization by cells throughout all of the interstitial regions of the construct. Micro-CT and histological analyses indicated, however, that mineralization persisted at the periphery, and negligible mineralization occurred in the central pore regions, even in the presence of viable cells as indicated by cell viability assays. To address this issue and establish a more homogeneously mature construct would be the implementation of a dynamic culture system to enhance *in vitro* culture parameters of Runx2-modified cell-seeded constructs. A perfusion flow system would likely enhance scaffold colonization and matrix synthesis throughout all regions of the scaffold by reducing the mass transfer limitations associated with conventional static culture.

Based on the outcomes of the present work, the flexibility and robust nature of this genetic engineering strategy to overexpress an osteoblast-specific transcription factor should be implemented in more stringent, higher order animal models and even preliminary *in vitro* analyses of Runx2-tranduced human bone marrow stromal cells or cells of non-osteogenic origin to examine the Runx2-responsiveness of a variety of target tissues, primarily those mesenchymal in origin. The identification of factors such as dexamethasone which potentiate the effects of Runx2 in stromal cell cultures and even seemingly cooperatively enhance its activity suggests in principle that primary cells of

non-osteogenic origin may be capable of forming a bioactive mineralized matrix similar to that deposited by bone marrow stromal cells or other osteoblastic cells.

APPENDIX A

CLONING OF THE RUNX2 RETROVIRAL EXPRESSION VECTOR

The Runx2 sequence was acquired from the pCMV-Osf2 (Runx2) plasmid, a generous gift of Dr. Gerard Karsenty of the Baylor College of Medicine. The focus of this phase of the project was to isolate the Runx2 sequence from the pCMV-Runx2 plasmid and insert into the pTJ66 retroviral plasmid backbone. Initial efforts focused on the restriction endonuclease digestion of the pCMV-Runx2 plasmid using enzymes located at the 5' and 3' ends of the sequence. The Runx2 sequence was inserted into the pCMV5 backbone using the EcoRI/XbaI cloning site. The presence of an internal EcoRI site within the Runx2 required a sequential enzymatic digestion of the plasmid, and ultimately, these efforts proved inefficient. As a result, polymerase chain reaction (PCR) techniques were utilized. Initially, the pCMV-Runx2 plasmid was sequenced in order to design the most efficient primers for amplification of the sequence. The primers used in the sequencing of the pCMV-Runx2 plasmid were optimally designed using Primer Premier, a nucleotide analysis software package. The primers were designed to be approximately 400 base pairs apart in order to ensure sufficient overlap during sequencing. The 1791 base Runx2 sequence (Accession Number: AF010284) described by Karsenty et al. was used in the design of the following primers.

	Primer Name	Primer Sequence
1	mRunx2-334.R	5'- GGC TCA CGT CGC TCA TCT TGC
2	mRunx2-209.F	5'- CGT CAA ACA GCC TCT TCA GCG
3	mRunx2-624.F	5'- CAA GAC CCT GCC CGT GGC
4	mRunx2-1021.F	5'- CCA CGG CCC TCC CTG AAC
5	mRunx2-1412.F	5'- CCA CCT TTA CCT ACA CCC CGC

Note: R=reverse, F=forward

Primers two through five provided sequences corresponding precisely to those reported through base 1791 by Ducy et al. in AF010284. Primer one, mRunx2-334.R, was designed to provide the sequence at the 5' end from base 334 backward as well as the sequence of the plasmid backbone directly proceeding the Runx2 gene. The sequence was identical to AF010284 from base 334 to 81, however, at that point, the sequence diverged. As a result of this sequence divergence, the ATG start codon present at base 205 (corresponding to the methionine at amino acid position 69 of AF010284) was used in the pCMV-Runx2 plasmid rather than the ATG at base 1. This in addition to literature further suggests the amino terminus (amino acids 1-68) are not necessary for a functional protein.

Note: Close observation of the Runx2 sequence indicates that elimination of the first 80 bases of the sequence results in the presence of an ATG start codon (base 90) which would code for a protein that is out of frame; however, a TAA stop codon (base 141) which is in frame with this start codon ensures that the Runx2 protein is translated from the ATG start codon at base 205.

Now that the pCMV-Runx2 sequence including additional bases on the 5' and 3' ends had been determined, primers were designed using Primer Premier in order to amplify the sequence by high fidelity polymerase chain reaction (PCR). The optimized primers selected are indicated in the following table.

	Primer Name	Primer Sequence
1	pCMV-Runx2-197.F	5'- CGA GGG CGT TTA AAT GGT TAA
2	pCMV-Runx2-1928.R	5'- GCC ATG GTT GAC GAA TTT CAA

The pCMV-Runx2-197.F primer included bases 81-97 of the Ducy sequence and four additional nucleotides upstream of that sequence. The pCMV-Runx2-1928.R included bases 1788-1791 of the Ducy sequence and seventeen nucleotides downstream of the Runx2 sequence. As a result of the high GC content in the region from base 300 to 500, the Advantage® -GC 2 PCR system marketed by Clontech Laboratories, Inc. The Advantage-GC 2 enzyme mix contains AdvanTaq™ DNA polymerase as the primary polymerase in addition to a minor amount of proofreading polymerase and the TaqStart™ antibody to the provide the automatic hot start. Additionally, the system utilizes an optimized buffer containing DMSO and GC-Melt that has been shown to improve the amplification of GC-rich sequences [Advantage® -GC 2 PCR User Manual 02/99, p. 3]. The following table indicates the composition of the reaction mixture as well as the run conditions for the thirty-five cycle PCR reaction.

Reagent	Volume per Reaction (μl)
5X GC-2 PCR Buffer (17.5 mM Mg^{2+})	10.0
10 mM dNTP Mix (50 X dNTP Mix)	1.0
100 μM Primer pCMV-Runx2-197.F 5'	0.5
100 μM Primer pCMV-Runx2-1928.R 3'	0.5
50X Advantage-GC 2 Polymerase Mix	1.0
10X GC Melt (5.0 M)	5.0
ddH_2O	31.0
pCMV-Runx2 plasmid DNA (0.250 μg/μl)	1.0
Total	50.0

Event	Temperature (°C)	Time (min)
Initial Activation	94	3.0
Cycle Temperature 1	94	0.5
Cycle Temperature 2	55	0.5
Cycle Temperature 3	68	3.0
Final Extension	68	3.0

A small aliquot of the PCR product was ran on an agarose gel in order to determine purity and relative effectiveness of the PCR reaction, which resulted in a single band present at approximately 1700 base pairs (actual product 1731 base pairs). The PCR product was then purified using a Qiagen QIAquick PCR Purification Kit. The

QIAquick system utilizes special buffers which are optimized for efficient recovery of DNA and removal of contaminants using spin-column technology with selective binding properties of a uniquely-designed silica-gel membrane [QIAquick Spin Handbook 07/97, p.11]. The PCR product was eluted from the column in 50 µl of 10 mM Tris·Cl, pH 8.5.

Isolation of the Runx2 sequence from the pCMV-Runx2 plasmid allowed for cloning of this sequence into a retroviral expression vector. This pTJ66 vector utilizes a retroviral long terminal repeat promoter to express a single, bicistronic mRNA that can produce a therapeutic protein through cap-dependent translation and a zeocin resistance-eGFP fusion protein by translation from an internal ribosomal entry site (IRES). The fusion protein can be used as a selection marker or a monitor of retroviral production and infection efficiency. The plasmid backbone additionally expresses Ampicillin resistance for selection of positively transformed bacteria during culture. The development of the pTJ66 vector is explained in more detail by Abbott and Murphy in a future publication, NFATc1 expression augments cyclosporin-sensitive interleukin-6 gene expression in vascular smooth muscle cells. The therapeutic gene, Runx2 was cloned into the SfiI universal cloning site present in the backbone of the pTJ66 vector, an SfiI site exists at base 1639 and base 1661.

The first step of the cloning process was to blunt end the purified Runx2 PCR product using the Klenow enzyme. The Klenow enzyme (New England Biolabs) functions to fill in 5' overhangs while chewing back 3' overhangs, which are characteristic of PCR. The enzyme was used at a concentration of 1 U/µg DNA, and the following table indicates the other components of the reaction.

Reagent	Volume per Reaction (µl)
Runx2 fragment (0.26 µg/µl)	36.0
2 mM dNTPs	2.0
10X EcoPoI Buffer	5.0
Klenow Enzyme (5 U/µl)	2.1
ddH_2O	4.9
Total	50.0

The reaction mixture was incubated at room temperature for fifteen minutes, and the enzyme was heat inactivated by incubating at 65°C for twenty minutes. The Klenow product was then purified using a Qiagen QIAquick PCR Purification Kit, and the PCR product was eluted from the column in 50 µl of 10 mM Tris·Cl, pH 8.5.

In order to enhance the ligation of the Runx2 fragment into the pTJ66 vector, the blunt-ended Runx2 fragment was kinased, which resulted in the transfer of the γ-phosphate of ATP to the 5' hydroxyl terminus of the DNA. The reaction composition is detailed below:

Reagent	Volume per Reaction (μl)
Blunt-ended Runx2 fragment	50.0
10 mM ATP	10.0
5X Kinase Buffer (Forward Reaction)	20.0
T4 Polynucleotide Kinase (Life Technologies)	2.0
ddH_2O	18.0
Total	100.0

The reaction mixture was incubated at 37°C for thirty minutes, and the enzyme was heat inactivated by incubating at 75°C for fifteen minutes. The Kinased product was then purified using a Qiagen QIAquick PCR Purification Kit, and the PCR product was eluted from the column in 50 μl of 10 mM Tris·Cl, pH 8.5.

In order to clone the Runx2 sequence into the SfiI site of the pTJ66 vector SfiI adapters were ligated to the kinased Runx2 fragment. The SfiI adapters were made from the two oligos having the following sequence: ACE 258 -> 3'-GATCCGGA and ACE 259-> 5'-CTAGGCCTACA, which when kinased together result in an ACA 3' overhang. The reagents necessary to make a 30 μM stock of SfiI adapters are detailed in the following table.

Reagent	Volume per Reaction (μl)
ACE258 (9-30-99) 111 μM stock	27.0
ACE259 (9-30-99) 104 μM stock	28.8
5X Kinase Buffer (Forward Reaction)	20.0
10 mM ATP	10.0
T4 Polynucleotide Kinase (Life Technologies)	2.0
ddH_2O	12.2
Total	100.0

The reaction mixture was incubated at 37°C for thirty minutes, and the enzyme was heat inactivated by incubating at 75°C for fifteen minutes. The reaction was allowed to slow cool to room temperature, and the adapters were then ligated to the kinased, blunt-ended Runx2 fragment in the following reaction.

Reagent	Volume per Reaction (μl)
Kinased, blunt-ended Runx2 fragment	20.0
30 μM SfiI Adapters	20.0
10X T4 Ligase Buffer	5.0
10 mM ATP	2.0
T4 Ligase (New England Biolabs)	2.0
ddH_2O	1.0
Total	50.0

The reaction mixture was incubated overnight at 16°C. This reaction results in the addition of approximately a 100 molar excess of adapters, which if left in the reaction mixture would significantly impede the ligation of the Runx2 fragment into the pTJ66 vector. As a result, the excess adapters were removed from the solution using a Biospin P30 Column (Bio-Rad). The top and bottom of the column were removed and allowed to empty by gravity flow. The column was then centrifuged at approximately 200 g for 1.5 minutes. The reaction mixture was then added to the column which was centrifuged at 200 g for 5 minutes. The small oligonucleotide adapters are adsorbed by the column while the larger Runx2 fragment containing SfiI adapters is eluted from it. 6X loading buffer was then added to the eluent and it was loaded into multiple lanes of 1% agarose gel in order to further purify the Runx2 fragment and ensure that all of the excess adapters were removed. SfiI digested pTJ66 vector was loaded onto another gel. The presence of two SfiI sites on the pTJ66 backbone separated by only 22 bases complicates the digestion process, so in order to ensure that the pTJ66 vector was completely digested, a series of two separate digestions using the SfiIase were conducted. Initially, the 6817 base pair pTJ66 vector was purified from bacterial culture using a Qiagen Plasmid Purification Maxi Kit and resuspended in ddH_2O. The resulting linearized DNA would consist of 6795 bases, as the 22 bases between the two SfiI sites would be removed.

Reagent	Volume per Reaction (µl)
Uncut pTJ66 (0.75 µg/µl)	6.7
10X BSA (1.0 µg/µl)	2.0
10X Buffer 2	2.0
SfiIase (New England Biolabs)	1.0
ddH_2O	8.3
Total	20.0

The reaction mixture was overlayed with 30 µl of mineral oil and incubated at 50°C for one hour. After one hour, additional SfiIase was added (1.0 µl), and the reaction was allowed to proceed overnight at 50°C. Following gel purification to remove uncut plasmid and the 22 base fragment resulting from the digestion using a Qiagen QIAquick Gel Extraction Kit, a second digestion was conducted. The second digestion occurred after some time had passed and all of the initial SfiIase from NEB had been used, so new enzyme from Life Technologies was used in the second digestion.

Reagent	Volume per Reaction (µl)
pTJ66 cut 1 time with SfiIase (0.1 µg/µl)	17.0
10X Buffer 2	2.0
SfiIase (Life Technologies)	1.0
Total	20.0

The reaction mixture was overlayed with 30 µl of mineral oil and incubated overnight at 50°C. Additional SfiIase was added (1.0 µl) the next day, and the reaction was allowed to proceed for an additional hour at 50°C. This SfiI digested pTJ66 vector

was loaded onto a second gel as previously mentioned and both it and the Runx2 fragment containing SfiI adapters were purified using a Qiagen QIAquick Gel Extraction Kit. Each DNA fragment was eluted from the QIAquick spin column with 50 μl of 10 mM Tris·Cl, pH 8.5.

The two key reagents, Runx2 with SfiI adapters and SfiI digested pTJ66, were then available for ligation. Following previous experimental results by others, the Runx2 insert was added to the reaction mixture in approximately 3M excess to the cut pTJ66 vector. This ensured that the Runx2 fragment was not the limiting reagent in the reaction mixture. As previously mentioned, the complete digestion of pTJ66 with SfiIase results in a 6795 base fragment. The addition of the SfiI adapters (8 bases on the 5' end and 11 bases on 3' end) to the Runx2 fragment results in a combined insert approximately 1750 bases in length. Assuming equivalent distributions of nucleotides, the molecular weight of the insert is approximately one-fourth that of the pTJ66 backbone. As a result, it was determined to add equal masses of the two reagents to the ligation reaction, which would provide slightly greater than a 3M excess of the insert.

In addition to the primary ligation reaction necessary to complete the pTJ66-Runx2 vector, a negative and a positive control reaction were conducted. The negative control reaction was conducted in the presence of cut pTJ66 vector with no ligase or insert in the reaction mixture. This would provide insight as to the completeness of the digestion process. If many colonies were present on a plate streaked with bacteria that had been transformed with DNA from this reaction, it would therefore be likely that neither of the SfiI sites had been digested on a large fraction of the pTJ66 vector used in the reaction. Although this was highly unlikely, as the cut plasmid was purified using agarose gel electrophoresis, and supercoiled plasmid DNA will migrate faster in the gel than linearized DNA of the same molecular weight. As a control to monitor this progression, uncut pTJ66 was loaded into the same gels as the digested samples, and in the cases investigated, no uncut pTJ66 remained in the reaction mixture. The positive control reaction was conducted in the presence of ligase and cut pTJ66 vector with no insert in the reaction mixture. This would also provide insight as to the completeness of the digestion process. If many colonies were present on a plate streaked with bacteria that had been transformed with DNA from this reaction, it would therefore be likely that only one of the two SfiI sites had been digested on a large fraction of the pTJ66 vector used in the reaction and it was therefore capable of ligating back together. It should be noted that pTJ66 completely digested with SfiIase is incapable of ligating back onto itself, as this digestion results in the creation of 5'-TGT overhangs at both digestion sites. The following tables indicate the reagents used in the three reactions.

Primary Reaction

Reagent	Volume per Reaction (μl)
Runx2 with SfiI adapters (0.024 μg/μl)	20.0
pTJ66 digested two times with SfiIase (0.030 μg/μl)	16.0
10X T4 Ligase Buffer	5.0
10 mM ATP	2.0
T4 Ligase (New England Biolabs)	1.0
ddH_2O	6.0
Total	50.0

Negative Control Reaction

Reagent	Volume per Reaction (μl)
Runx2 with SfiI adapters (0.024 μg/μl)	0.0
pTJ66 digested two times with SfiIase (0.030 μg/μl)	16.0
10X T4 Ligase Buffer	5.0
10 mM ATP	2.0
T4 Ligase (New England Biolabs)	0.0
ddH_2O	27.0
Total	50.0

Positive Control Reaction

Reagent	Volume per Reaction (μl)
Runx2 with SfiI adapters (0.024 μg/μl)	0.0
pTJ66 digested two times with SfiIase (0.030 μg/μl)	16.0
10X T4 Ligase Buffer	5.0
10 mM ATP	2.0
T4 Ligase (New England Biolabs)	1.0
ddH_2O	26.0
Total	50.0

All three reactions were incubated overnight at 16°C.

The ligation products were then used to transform Top 10 F' bacteria using the following protocol. Bacterial cells were thawed on ice until liquid, and an appropriate number of 14 ml culture tubes were simultaneously chilled. 200 μl of bacterial cells and 50 μl of each respective ligation reaction were added to the chilled tubes. The tubes were then incubated on ice for 30 minutes. They tubes were then transferred to a 37°C water bath for 2 minutes and replaced back on ice for 2 minutes. 800 μl of LB was then added to the cell/DNA mixture and the tubes were incubated in a 37°C bacterial incubator for 1 hour. While the bacteria were incubating, LB agar plates containing the appropriate antibiotics were prepared. In addition to the ampicillin resistance present for bacteria which have been successfully transformed with the pTJ66-Runx2 or a pTJ66 backbone plasmid, the Top 10 F' bacteria are equipped with resistance to tetracycline. As a result, the plates in this study contained both ampicillin (100 μg/ml) and tetracycline (10 μg/ml). After 1 hour, cells were added to the LB agar plates in a series of dilutions in order to simplify the isolation of one colony. The following table details the dilutions prepared for each of the transformations.

	1	2	3
Bacterial Culture	200	20	5
LB	0	180	195
Total	200	200	200

Following addition of the cell solutions, the plates were streaked, and incubated overnight in a 37°C incubator.

The next day, the plates were investigated and individual colonies were isolated in order to obtain one containing the pTJ66-Runx2 plasmid. Both dilution 1 and 2 from the table above were nearly confluent with colonies, while dilution 3 provided distinct colonies which could be easily selected. The negative and positive control samples yielded very little background, indicating that the cloning had likely yielded the appropriate vector. Ten colonies were selected from dilution 3 of the pTJ66-Runx2 plate, and one colony was selected from the dilution 1 plates of both the negative and positive controls. The selected colonies were used to innoculate cultures consisting of 3 ml of LB medium, 3 µl ampicillin (100 µg/µl stock -> 100 µg/ml working), and 12.5 µl tetracycline (5 µg/µl stock -> 20.83 µg/ml working), and the cultures were incubated overnight at 37°C. The following day, the plasmid DNA from each of the colonies was purified using a QIAprep Miniprep Kit. The plasmid DNA was eluted from the column with 50 µl of 10 mM Tris·Cl, pH 8.5.

In order to determine if a pTJ66-Runx2 had been successfully isolated, a diagnostic restriction enzyme digestion was performed on each of the purified samples. As was previously explained, the SfiI digested pTJ66 contains 5'-TGT overhangs, while the Runx2 fragment with ligated SfiI adapters contains 3'-ACA overhangs. This introduces the possibility of the insert being ligated into the pTJ66 cloning in the reverse orientation. The appropriate diagnostic will, therefore, identify whether the insert was ligated into the cloning site and if so was it ligated in the correct orientation. The enzyme selected for the diagnostic was BamHI. A restriction site exists within the Runx2 insert at base 193 and within the pTJ66 backbone at base 3057. As a result, if the insert is ligated in the correct orientation, complete digestion with BamHI would result in two bands, one 5592 bases and the other 2954 bases in length. If the insert was ligated in the reverse direction, one of the bands would be 6957 bases and the other 1589 bases. These two possibilities could be easily distinguished using agarose gel electrophoresis. The following table indicates the reaction components of the diagnostic digestion.

Reagent	Volume per Reaction (µl)
10X BamHI NEB Buffer	2.0
10X BSA (1.0 µg/µl)	2.0
Miniprep purified plasmid DNA	5.0
BamHI (New England Biolabs)	1.0
ddH_2O	10.0
Total	20.0

The reaction mixture was incubated at 37°C for 2 hours, loaded with 6X loading buffer, and ran on a 1% agarose gel. As expected from the previous description, 50% of the colonies provided plasmid in which the Runx2 insert had been correctly ligated, while the other 50% were in the reverse orientation. The colonies isolated from the negative and positive control plates were run in conjunction with a positive control BamHI digestion of uncut pTJ66. The results indicated that both colonies provided bands on the gel that corresponded to linear pTJ66 (6817 bases).

Glycerol stocks (50%) were prepared for the five colonies which appeared to be pTJ66-Runx2, and one was selected to be grown up and harvested for sequencing and any other further diagnostic work. In this innoculation, 0.5 ml of the colony was added to 500 ml of LB containing 500 μl ampicillin (100 μg/μl stock -> 100 μg/ml working), and 1250 μl tetracycline (5 μg/μl stock -> 12.5 μg/ml working), which was cultured overnight at 37°C.

The plasmid DNA was then harvested using the Very Low Copy Protocol contained in the Qiagen Plasmid Maxi Kit. The purified plasmid was verified for correctness and purity by conducting a BamHI diagnostic digest and running the uncut stock and digest samples on a 1% agarose gel.

A portion of the stock plasmid was diluted to a working concentration of 0.2 μg/μl for sequencing, and the same sequencing primers introduced previously were used to determine the sequence of the insert and the regions immediately preceding and following the insert. Following analysis of the sequence chromatograms, it was determined that all of the functional areas of the Runx2 sequence had been correctly polymerized and the sequence appeared to be correct. Two minor variations from the predicted sequence did exist, however. One base on each end of the Runx2 sequence just inside the SfiI adapters was not present, likely indicating they were cleaved during the Klenow blunt-end step of the cloning protocol. The resulting pTJ66-Runx2 plasmid is 8544 bases, consisting of 1587 functional bases (1775-3361 in pTJ66-Runx2) of the Runx2 sequence (205-1791 in AF010284), 127 nonfunctional bases on the 5' end of the Runx2 sequence and 16 nonfunctional bases on the 3' end of the Runx2 sequence, 8 bases on the 5' end and 11 bases on the 3' end of the Runx2 sequence (functional and nonfunctional) resulting from the SfiI adapters, and 6795 bases of the pTJ66 backbone (22 bases were removed by the digestion with SfiIase).

After successfully cloning the pTJ66-Runx2 expression vector, the focus shifted to the packaging of functional retrovirus. A second generation packaging cell line known as the ϕNX helper-free producer line, which function to produce the gag-pol and envelope proteins necessary for encapsulation of the retroviral plasmid, has been developed for the production of retroviruses. The cell line is based on the human embryonic kidney 293T cell line. As is desirable for transient transfection, this cell line is highly transfectable, up to 50% using calcium-based or liposome-mediated transfection protocols. Improvements introduced by this cell line in comparison to previous packaging lines include the ability to monitor gag-pol production through the incorporation of an IRES-CD8 surface marker downstream of the reading frame of the gag-pol construct and the minimization of recombination potential through the use of unique, non-moloney promoters for the gag-pol and envelope constructs. The gag-pol construct was introduced into the cell line with hygromycin as the co-selectable marker while the envelope proteins were introduced with diptheria as the co-selectable marker. The specific ϕNX cell line used in this research is one capable of producing amphotropic retrovirus, and the protocol previously described by Pear et al. for production of amphotropic retrovirus will now be introduced.

ϕNX-ampho cells were plated in 150 mm plates the day prior to transfection at a density of approximately 9.0 x 10^4 cells/cm^2 and incubated for about 24 hours at 37°C in order to establish approximately 80% confluence immediately prior to transfection (2.5 x 10^6 cells per 60 mm plate, 7.0 x 10^6 cells per 100 mm plate, 1.6 x 10^7 cells per 150 mm

plate etc.). The growth media for the ϕNX cells consists of high glucose DMEM supplemented with 10% fetal bovine serum and 1% penicillin-streptomycin. After 24 hours, the cells were refed with 18 ml of growth media + 1/1000 chloroquine (22.5 μl of 25 mM chloroquine stock solution in PBS) and returned to 37°C. The plasmid DNA solution was then prepared. For each plate infected, 90 μg of plasmid DNA (from pTJ66-Runx2 stock solution) was added to sterile ddH_2O to reach a final working volume of 1969 μl. Next, 281 μl of 2 M $CaCl_2$ was added to the DNA solution. Finally, 2.25 ml of 37°C 2X BES solution (50 mM BES, 280 mM NaCl, 1.5 mM Na_2HPO_4) was added to the DNA while vortexing in order to minimize salt precipitation. This transfection solution was then added to the ϕNX cell plates and gently mixed. The plates were incubated at 37°C for 6 hours, the transfection medium was removed, and the cells were refed with 40 ml of fresh growth media and returned to 37°C overnight. The following day, 24 hours after the start of the transfection, the plates were refed with 20 ml of fresh growth media and placed at 32°C. (Note: Kotani et. al. conducted studies using 22 different retroviral vector packaging cell lines in which they discovered a 5- to 15-fold increase in functional vector production at 32°C rather than at 37°C). The media was then collected after 24 hours (48 hours after the start of the transfection), filtered using a 0.45 μm cellulose acetate membrane bottle filter, aliquoted at 6.5 ml per 14 ml Falcon polypropylene test tubes, snap frozen in liquid N_2, and placed in a -80°C freezer for long term storage. Following refeeding with growth media, the plates were replaced at 32°C and two additional harvests occurred in twelve hour increments (60 and 72 hours after the start of the transfection, respectively).

Acquisition of pTJ66-Runx2 retrovirus allowed for the infection of mammalian cells for verification of functionality, while the native pTJ66 retrovirus was used as a negative control. Cell lines investigated include NIH3T3 murine fibroblasts, MC3T3-E1 murine calvarial cells, and primary rat bone marrow stromal cells. On the afternoon prior to the infection, cells were plated in a 6 well plate at a density of approximately 1 x 10^4 cells/cm^2 (1 x 10^5 cells per well) and incubated overnight at 37°C. (Note: any size plate can be used depending upon the application). It should be noted that in order for retroviral infection to be successful, the cells being infected must be replicating, and, as a result, seeding density for infection is cell-specific, i.e. large cells or cells displaying a larger surface area resulting from greater spreading should be seeded at lower densities. For the infection the following day, the growth media was aspirated and 2 ml of retroviral media which had just been thawed from storage in a -80°C freezer was added. Note: do not warm the retroviral media to 37°C, leave it the bath only until it melts. The infection cocktail was completed by adding 20 μl of 100X polybrene (0.8 mg/ml hexadimethrine bromide) directly to the cells, which was followed by incubation at 32 °C for 15 minutes in order to stabilize the pH of the infection medium. (Note: it may be necessary to supplement the infection cocktail with serum or other growth factors depending upon the growth medium required by the cells being infected, as the retroviral infection media is high glucose DMEM supplemented with 10% fetal bovine serum and 1% penicillin-streptomycin.) After 15 minutes, the plates were wrapped with parafilm and centrifuged in a swinging-bucket rotor at approximately 1200 g for 30 minutes at 32 °C. After centrifuging, the retroviral media was aspirated, the appropriate growth media was reapplied, and the cells were returned to incubation at 37 °C. An additional infection was completed 6-12 hours later in order to increase infection efficiency.

REFERENCES

Abbott KL, Friday BB, Thaloor D, Murphy TJ and Pavlath GK (1998) Activation and cellular localization of the cyclosporine A-sensitive transcription factor NF-AT in skeletal muscle cells. Mol Biol Cell 9: 2905-2916.

Abbott KL, Loss JR, Robida AM and Murphy TJ (2000) Evidence that Galpha(q)-coupled receptor-induced interleukin-6 mRNA in vascular smooth muscle cells involves the nuclear factor of activated T cells [In Process Citation]. Mol Pharmacol 58: 946-953.

Allay JA, Dennis JE, Haynesworth SE, Majumdar MK, Clapp DW, Shultz LD, Caplan AI and Gerson SL (1997) LacZ and interleukin-3 expression in vivo after retroviral transduction of marrow-derived human osteogenic mesenchymal progenitors. Hum Gene Ther 8: 1417-1427.

Athanasiou KA, Niederauer GG and Agrawal CM (1996) Sterilization, toxicity, biocompatibility and clinical applications of polylactic acid/polyglycolic acid copolymers. Biomaterials 17: 93-102.

Athanasiou KA, Zhu C, Lanctot DR, Agrawal CM and Wang X (2000) Fundamentals of biomechanics in tissue engineering of bone. Tissue Eng 6: 361-381.

Attard FA, Wang L, Potter JJ, Rennie-Tankersley L and Mezey E (2000) CCAAT/enhancer binding protein beta mediates the activation of the murine alpha1(I) collagen promoter by acetaldehyde. Arch Biochem Biophys 378: 57-64.

Aubin JE (1999) Osteoprogenitor cell frequency in rat bone marrow stromal populations: role for heterotypic cell-cell interactions in osteoblast differentiation. J Cell Biochem 72: 396-410.

Aubin JE and Liu F (1996) The Osteoblast Lineage. In: Bilezikian JP, Raisz LG and Rodan GA (eds) Principles of Bone Biology, pp 51-68. Academic Press, San Diego.

Bae SC, Takahashi E, Zhang YW, Ogawa E, Shigesada K, Namba Y, Satake M and Ito Y (1995) Cloning, mapping and expression of PEBP2 alpha C, a third gene encoding the mammalian Runt domain. Gene 159: 245-248.

Bae SC, Yamaguchi-Iwai Y, Ogawa E, Maruyama M, Inuzuka M, Kagoshima H, Shigesada K, Satake M and Ito Y (1993) Isolation of PEBP2 alpha B cDNA representing the mouse homolog of human acute myeloid leukemia gene, AML1. Oncogene 8: 809-814.

Banerjee C, Javed A, Choi JY, Green J, Rosen V, van Wijnen AJ, Stein JL, Lian JB and Stein GS (2001) Differential regulation of the two principal Runx2/Cbfa1 n-terminal isoforms in response to bone morphogenetic protein-2 during development of the osteoblast phenotype. Endocrinology 142: 4026-4039.

Banerjee C, McCabe LR, Choi JY, Hiebert SW, Stein JL, Stein GS and Lian JB (1997) Runt homology domain proteins in osteoblast differentiation: AML3/CBFA1 is a major component of a bone-specific complex. J Cell Biochem 66: 1-8.

Bareille R, Lafage-Proust MH, Faucheux C, Laroche N, Wenz R, Dard M and Amedee J (2000) Various evaluation techniques of newly formed bone in porous hydroxyapatite loaded with human bone marrow cells implanted in an extra-osseous site. Biomaterials 21: 1345-1352.

Bauer TW and Muschler GF (2000) Bone graft materials. An overview of the basic science. Clin Orthop 10-27.

Baum BJ and Mooney DJ (2000) The impact of tissue engineering on dentistry. J Am Dent Assoc 131: 309-318.

Bellows CG, Aubin JE and Heersche JN (1987) Physiological concentrations of glucocorticoids stimulate formation of bone nodules from isolated rat calvaria cells in vitro. Endocrinology 121: 1985-1992.

Benson MD, Aubin JE, Xiao G, Thomas PE and Franceschi RT (1999) Cloning of a 2.5 kb murine bone sialoprotein promoter fragment and functional analysis of putative Osf2 binding sites. J Bone Miner Res 14: 396-405.

Bianco P, Riminucci M, Gronthos S and Robey PG (2001) Bone marrow stromal stem cells: nature, biology, and potential applications. Stem Cells 19: 180-192.

Boden SD (1999) Bioactive factors for bone tissue engineering. Clin Orthop S84-S94.

Bonadio J, Smiley E, Patil P and Goldstein S (1999) Localized, direct plasmid gene delivery in vivo: prolonged therapy results in reproducible tissue regeneration. Nat Med 5: 753-759.

Bonewald LF, Harris SE, Rosser J, Dallas MR, Dallas SL, Camacho NP, Boyan B and Boskey A (2003) von Kossa staining alone is not sufficient to confirm that mineralization in vitro represents bone formation. Calcif Tissue Int 72: 537-547.

Bortell R, Barone LM, Tassinari MS, Lian JB and Stein GS (1990) Gene expression during endochondral bone development: evidence for coordinate expression of transforming growth factor beta 1 and collagen type I. J Cell Biochem 44: 81-91.

Boskey AL, Guidon P, Doty SB, Stiner D, Leboy P and Binderman I (1996) The mechanism of beta-glycerophosphate action in mineralizing chick limb-bud mesenchymal cell cultures. J Bone Miner Res 11: 1694-1702.

Boyan BD, Hummert TW, Dean DD and Schwartz Z (1996) Role of material surfaces in regulating bone and cartilage cell response. Biomaterials 17: 137-146.

Breitbart AS, Grande DA, Mason JM, Barcia M, James T and Grant RT (1999) Gene-enhanced tissue engineering: applications for bone healing using cultured periosteal cells transduced retrovirally with the BMP-7 gene. Ann Plast Surg 42: 488-495.

Bruder SP, Fink DJ and Caplan AI (1994) Mesenchymal stem cells in bone development, bone repair, and skeletal regeneration therapy. J Cell Biochem 56: 283-294.

Bruder SP and Fox BS (1999) Tissue engineering of bone. Cell based strategies. Clin Orthop 367: S68-S83.

Bruder SP, Jaiswal N and Haynesworth SE (1997) Growth kinetics, self-renewal, and the osteogenic potential of purified human mesenchymal stem cells during extensive subcultivation and following cryopreservation. J Cell Biochem 64: 278-294.

Bucholz RW (2002) Nonallograft osteoconductive bone graft substitutes. Clin Orthop 44-52.

Bulabois CE, Yerly-Motta V, Mortensen BT, Fixe P, Remy-Martin JP, Herve P, Tiberghien P and Charbord P (1998) Retroviral-mediated marker gene transfer in hematopoiesis-supportive marrow stromal cells. J Hematother 7: 225-239.

Busch O, Solheim E, Bang G and Tornes K (1996) Guided tissue regeneration and local delivery of insulinlike growth factor I by bioerodible polyorthoester membranes in rat calvarial defects. Int J Oral Maxillofac Implants 11: 498-505.

Byers BA, Pavlath GK, Murphy TJ, Karsenty G and Garcia AJ (2002) Cell-type-dependent up-regulation of in vitro mineralization after overexpression of the osteoblast-specific transcription factor Runx2/Cbfal. J Bone Miner Res 17: 1931-1944.

Calvert JW, Marra KG, Cook L, Kumta PN, DiMilla PA and Weiss LE (2000) Characterization of osteoblast-like behavior of cultured bone marrow stromal cells on various polymer surfaces. J Biomed Mater Res 52: 279-284.

Centrella M, Horowitz MC, Wozney JM and McCarthy TL (1994) Transforming growth factor-beta gene family members and bone. Endocr Rev 15: 27-39.

Choi JY, Lee BH, Song KB, Park RW, Kim IS, Sohn KY, Jo JS and Ryoo HM (1996) Expression patterns of bone-related proteins during osteoblastic differentiation in MC3T3-E1 cells. J Cell Biochem 61: 609-618.

Crane GM, Ishaug SL and Mikos AG (1995) Bone tissue engineering. Nat Med 1: 1322-1324.

Daga A, Tighe JE and Calabi F (1992) Leukaemia/Drosophila homology [letter]. Nature 356: 484.

Deasy BM, Jankowski RJ and Huard J (2001) Muscle-derived stem cells: characterization and potential for cell- mediated therapy. Blood Cells Mol Dis 27: 924-933.

Doherty MJ, Ashton BA, Walsh S, Beresford JN, Grant ME and Canfield AE (1998) Vascular pericytes express osteogenic potential in vitro and in vivo. J Bone Miner Res 13: 828-838.

Doll B, Sfeir C, Winn S, Huard J and Hollinger J (2001) Critical aspects of tissue-engineered therapy for bone regeneration. Crit Rev Eukaryot Gene Expr 11: 173-198.

Dong J, Uemura T, Shirasaki Y and Tateishi T (2002) Promotion of bone formation using highly pure porous beta-TCP combined with bone marrow-derived osteoprogenitor cells. Biomaterials 23: 4493-4502.

Drissi H, Luc Q, Shakoori R, Chuva De Sousa LS, Choi JY, Terry A, Hu M, Jones S, Neil JC, Lian JB, Stein JL, van Wijnen AJ and Stein GS (2000) Transcriptional autoregulation of the bone related CBFA1/RUNX2 gene. J Cell Physiol 184: 341-350.

Ducy P and Karsenty G (1995) Two distinct osteoblast-specific cis-acting elements control expression of a mouse osteocalcin gene. Mol Cell Biol 15: 1858-1869.

Ducy P, Starbuck M, Priemel M, Shen J, Pinero G, Geoffroy V, Amling M and Karsenty G (1999) A Cbfa1-dependent genetic pathway controls bone formation beyond embryonic development. Genes Dev 13: 1025-1036.

Ducy P, Zhang R, Geoffroy V, Ridall AL and Karsenty G (1997) Osf2/Cbfa1: a transcriptional activator of osteoblast differentiation. Cell 89: 747-754.

Ebara S and Nakayama K (2002) Mechanism for the action of bone morphogenetic proteins and regulation of their activity. Spine 27: S10-S15.

Einhorn TA (1999) Clinically applied models of bone regeneration in tissue engineering research. Clin Orthop S59-S67.

el Ghannam A, Ducheyne P and Shapiro IM (1997) Porous bioactive glass and hydroxyapatite ceramic affect bone cell function in vitro along different time lines. J Biomed Mater Res 36: 167-180.

Enomoto H, Enomoto-Iwamoto M, Iwamoto M, Nomura S, Himeno M, Kitamura Y, Kishimoto T and Komori T (2000) Cbfa1 is a positive regulatory factor in chondrocyte maturation. J Biol Chem 275: 8695-8702.

Fang J, Zhu YY, Smiley E, Bonadio J, Rouleau JP, Goldstein SA, McCauley LK, Davidson BL and Roessler BJ (1996) Stimulation of new bone formation by direct transfer of osteogenic plasmid genes. Proc Natl Acad Sci U S A 93: 5753-5758.

Frendo JL, Xiao G, Fuchs S, Franceschi RT, Karsenty G and Ducy P (1998) Functional hierarchy between two OSE2 elements in the control of osteocalcin gene expression in vivo. J Biol Chem 273: 30509-30516.

Friedenstein AJ (1976) Precursor cells of mechanocytes. Int Rev Cytol 47: 327-355.

Fujiwara M, Tagashira S, Harada H, Ogawa S, Katsumata T, Nakatsuka M, Komori T and Takada H (1999) Isolation and characterization of the distal promoter region of mouse Cbfa1. Biochim Biophys Acta 1446: 265-272.

Galipeau J, Li H, Paquin A, Sicilia F, Karpati G and Nalbantoglu J (1999) Vesicular stomatitis virus G pseudotyped retrovector mediates effective in vivo suicide gene delivery in experimental brain cancer. Cancer Res 59: 2384-2394.

Geoffroy V, Corral DA, Zhou L, Lee B and Karsenty G (1998) Genomic organization, expression of the human CBFA1 gene, and evidence for an alternative splicing event affecting protein function. Mamm Genome 9: 54-57.

Geoffroy V, Ducy P and Karsenty G (1995) A PEBP2 alpha/AML-1-related factor increases osteocalcin promoter activity through its binding to an osteoblast-specific cis-acting element. J Biol Chem 270: 30973-30979.

Gergen JP and Wieschaus EF (1985) The localized requirements for a gene affecting segmentation in Drosophila: analysis of larvae mosaic for runt. Dev Biol 109: 321-335.

Glowacki J (1995) Influence of age on human marrow. Calcif Tissue Int 56 Suppl 1: S50-S51.

Goldstein SA (2002) Tissue engineering: functional assessment and clinical outcome. Ann N Y Acad Sci 961: 183-192.

Gotoh T, Chowdhury S, Takiguchi M and Mori M (1997) The glucocorticoid-responsive gene cascade. Activation of the rat arginase gene through induction of C/EBPbeta. J Biol Chem 272: 3694-3698.

Gronthos S and Simmons PJ (1995) The growth factor requirements of STRO-1-positive human bone marrow stromal precursors under serum-deprived conditions in vitro. Blood 85: 929-940.

Gutierrez S, Javed A, Tennant DK, van Rees M, Montecino M, Stein GS, Stein JL and Lian JB (2002) CCAAT/enhancer-binding proteins (C/EBP) beta and delta activate osteocalcin gene transcription and synergize with Runx2 at the C/EBP element to regulate bone-specific expression. J Biol Chem 277: 1316-1323.

Gysin R, Wergedal JE, Sheng MH, Kasukawa Y, Miyakoshi N, Chen ST, Peng H, Lau KH, Mohan S and Baylink DJ (2002) Ex vivo gene therapy with stromal cells transduced with a retroviral vector containing the BMP4 gene completely heals critical size calvarial defect in rats. Gene Ther 9: 991-999.

Halvorsen YD, Franklin D, Bond AL, Hitt DC, Auchter C, Boskey AL, Paschalis EP, Wilkison WO and Gimble JM (2001) Extracellular matrix mineralization and osteoblast gene expression by human adipose tissue-derived stromal cells. Tissue Eng 7: 729-741.

Harada H, Tagashira S, Fujiwara M, Ogawa S, Katsumata T, Yamaguchi A, Komori T and Nakatsuka M (1999) Cbfa1 isoforms exert functional differences in osteoblast differentiation. J Biol Chem 274: 6972-6978.

Hauschka PV, Lian JB, Cole DE and Gundberg CM (1989) Osteocalcin and matrix Gla protein: vitamin K-dependent proteins in bone. Physiol Rev 69: 990-1047.

Heiple KG, Goldberg VM, Powell AE, Bos GD and Zika JM (1987) Biology of cancellous bone grafts. Orthop Clin North Am 18: 179-185.

Hess J, Porte D, Munz C and Angel P (2001) AP-1 and Cbfa/Runt physically interact and regulate parathyroid hormone-dependent MMP13 expression in osteoblasts through a new osteoblast-specific element 2/AP-1 composite element. J Biol Chem 276: 20029-20038.

Hildebrand T, Laib A, Muller R, Dequeker J and Ruegsegger P (1999) Direct three-dimensional morphometric analysis of human cancellous bone: microstructural data from spine, femur, iliac crest, and calcaneus. J Bone Miner Res 14: 1167-1174.

Hirata K, Tsukazaki T, Kadowaki A, Furukawa K, Shibata Y, Moriishi T, Okubo Y, Bessho K, Komori T, Mizuno A and Yamaguchi A (2003) Transplantation of skin fibroblasts expressing BMP-2 promotes bone repair more effectively than those expressing Runx2. Bone 32: 502-512.

Hollinger JO (1983) Preliminary report on the osteogenic potential of a biodegradable copolymer of polyactide (PLA) and polyglycolide (PGA). J Biomed Mater Res 17: 71-82.

Hollinger JO, Schmitt JM, Buck DC, Shannon R, Joh SP, Zegzula HD and Wozney J (1998) Recombinant human bone morphogenetic protein-2 and collagen for bone regeneration. J Biomed Mater Res 43: 356-364.

Holy CE, Fialkov JA, Davies JE and Shoichet MS (2003) Use of a biomimetic strategy to engineer bone. J Biomed Mater Res 65A: 447-453.

Holy CE, Shoichet MS and Davies JE (2000) Engineering three-dimensional bone tissue in vitro using biodegradable scaffolds: investigating initial cell-seeding density and culture period. J Biomed Mater Res 51: 376-382.

Horwitz EM, Gordon PL, Koo WK, Marx JC, Neel MD, McNall RY, Muul L and Hofmann T (2002) Isolated allogeneic bone marrow-derived mesenchymal cells engraft and stimulate growth in children with osteogenesis imperfecta: Implications for cell therapy of bone. Proc Natl Acad Sci U S A 99: 8932-8937.

Howell TH, Fiorellini JP, Paquette DW, Offenbacher S, Giannobile WV and Lynch SE (1997) A phase I/II clinical trial to evaluate a combination of recombinant human platelet-derived growth factor-BB and recombinant human insulin- like growth factor-I in patients with periodontal disease. J Periodontol 68: 1186-1193.

Hunter GK, Hauschka PV, Poole AR, Rosenberg LC and Goldberg HA (1996) Nucleation and inhibition of hydroxyapatite formation by mineralized tissue proteins. Biochem J 317 (Pt 1): 59-64.

Hutmacher DW, Schantz T, Zein I, Ng KW, Teoh SH and Tan KC (2001) Mechanical properties and cell cultural response of polycaprolactone scaffolds designed and fabricated via fused deposition modeling. J Biomed Mater Res 55: 203-216.

Inada M, Yasui T, Nomura S, Miyake S, Deguchi K, Himeno M, Sato M, Yamagiwa H, Kimura T, Yasui N, Ochi T, Endo N, Kitamura Y, Kishimoto T and Komori T (1999) Maturational disturbance of chondrocytes in Cbfa1-deficient mice. Dev Dyn 214: 279-290.

Ishaug SL, Crane GM, Miller MJ, Yasko AW, Yaszemski MJ and Mikos AG (1997) Bone formation by three-dimensional stromal osteoblast culture in biodegradable polymer scaffolds. J Biomed Mater Res 36: 17-28.

Ishaug-Riley SL, Crane GM, Gurlek A, Miller MJ, Yasko AW, Yaszemski MJ and Mikos AG (1997) Ectopic bone formation by marrow stromal osteoblast transplantation using poly(DL-lactic-co-glycolic acid) foams implanted into the rat mesentery. J Biomed Mater Res 36: 1-8.

Ishaug-Riley SL, Crane-Kruger GM, Yaszemski MJ and Mikos AG (1998) Three-dimensional culture of rat calvarial osteoblasts in porous biodegradable polymers. Biomaterials 19: 1405-1412.

Jankowski RJ, Deasy BM and Huard J (2002) Muscle-derived stem cells. Gene Ther 9: 642-647.

Javed A, Barnes GL, Jasanya BO, Stein JL, Gerstenfeld L, Lian JB and Stein GS (2001) runt homology domain transcription factors (Runx, Cbfa, and AML) mediate repression of the bone sialoprotein promoter: evidence for promoter context-dependent activity of Cbfa proteins. Mol Cell Biol 21: 2891-2905.

Javed A, Guo B, Hiebert S, Choi JY, Green J, Zhao SC, Osborne MA, Stifani S, Stein JL, Lian JB, van Wijnen AJ and Stein GS (2000) Groucho/TLE/R-esp proteins associate with the nuclear matrix and repress RUNX (CBF(alpha)/AML/PEBP2(alpha)) dependent activation of tissue-specific gene transcription. J Cell Sci 113 (Pt 12): 2221-2231.

Jimenez MJ, Balbin M, Alvarez J, Komori T, Bianco P, Holmbeck K, Birkedal-Hansen H, Lopez JM and Lopez-Otin C (2001) A regulatory cascade involving retinoic acid, Cbfa1, and matrix metalloproteinases is coupled to the development of a process of perichondrial invasion and osteogenic differentiation during bone formation. J Cell Biol 155: 1333-1344.

Kadiyala S, Jaiswal N and Bruder SP (1997) Culture-expanded, bone marrow-derived mesenchymal stem cells can regenerate a critical-sized segmental bone defect. Tissue Eng 3: 173-185.

Kagoshima H, Shigesada K, Satake M, Ito Y, Miyoshi H, Ohki M, Pepling M and Gergen P (1993) The Runt domain identifies a new family of heteromeric transcriptional regulators [letter]. Trends Genet 9: 338-341.

Katagiri T, Yamaguchi A, Ikeda T, Yoshiki S, Wozney JM, Rosen V, Wang EA, Tanaka H, Omura S and Suda T (1990) The non-osteogenic mouse pluripotent cell line, C3H10T1/2, is induced to differentiate into osteoblastic cells by recombinant human bone morphogenetic protein-2. Biochem Biophys Res Commun 172: 295-299.

Kenley R, Marden L, Turek T, Jin L, Ron E and Hollinger JO (1994) Osseous regeneration in the rat calvarium using novel delivery systems for recombinant human bone morphogenetic protein-2 (rhBMP-2). J Biomed Mater Res 28: 1139-1147.

Kern B, Shen J, Starbuck M and Karsenty G (2001) Cbfa1 contributes to the osteoblast-specific expression of type I collagen genes. J Biol Chem 276: 7101-7107.

Khan SN, Tomin E and Lane JM (2000) Clinical applications of bone graft substitutes. Orthop Clin North Am 31: 389-398.

Kim IS, Otto F, Zabel B and Mundlos S (1999) Regulation of chondrocyte differentiation by Cbfa1. Mech Dev 80: 159-170.

Komori T, Yagi H, Nomura S, Yamaguchi A, Sasaki K, Deguchi K, Shimizu Y, Bronson RT, Gao YH, Inada M, Sato M, Okamoto R, Kitamura Y, Yoshiki S and Kishimoto T (1997) Targeted disruption of Cbfa1 results in a complete lack of bone formation owing to maturational arrest of osteoblasts. Cell 89: 755-764.

Kotani H, Newton PB, III, Zhang S, Chiang YL, Otto E, Weaver L, Blaese RM, Anderson WF and McGarrity GJ (1994) Improved methods of retroviral vector transduction and production for gene therapy. Hum Gene Ther 5: 19-28.

Krebsbach PH, Gu K, Franceschi RT and Rutherford RB (2000) Gene therapy-directed osteogenesis: BMP-7-transduced human fibroblasts form bone in vivo. Hum Gene Ther 11: 1201-1210.

Kundu M, Javed A, Jeon JP, Horner A, Shum L, Eckhaus M, Muenke M, Lian JB, Yang Y, Nuckolls GH, Stein GS and Liu PP (2002) Cbfbeta interacts with Runx2 and has a critical role in bone development. Nat Genet 32: 639-644.

Laurencin CT, Ambrosio AM, Borden MD and Cooper JA, Jr. (1999) Tissue engineering: orthopedic applications. Annu Rev Biomed Eng 1: 19-46.

Laurencin CT, Attawia MA, Lu LQ, Borden MD, Lu HH, Gorum WJ and Lieberman JR (2001) Poly(lactide-co-glycolide)/hydroxyapatite delivery of BMP-2-producing cells: a regional gene therapy approach to bone regeneration. Biomaterials 22: 1271-1277.

Leboy PS, Beresford JN, Devlin C and Owen ME (1991) Dexamethasone induction of osteoblast mRNAs in rat marrow stromal cell cultures. J Cell Physiol 146: 370-378.

Lecanda F, Towler DA, Ziambaras K, Cheng SL, Koval M, Steinberg TH and Civitelli R (1998) Gap junctional communication modulates gene expression in osteoblastic cells. Mol Biol Cell 9: 2249-2258.

Lee B, Thirunavukkarasu K, Zhou L, Pastore L, Baldini A, Hecht J, Geoffroy V, Ducy P and Karsenty G (1997) Missense mutations abolishing DNA binding of the osteoblast-specific transcription factor OSF2/CBFA1 in cleidocranial dysplasia. Nat Genet 16: 307-310.

Lee JY, Peng H, Usas A, Musgrave D, Cummins J, Pelinkovic D, Jankowski R, Ziran B, Robbins P and Huard J (2002) Enhancement of bone healing based on ex vivo gene therapy using human muscle-derived cells expressing bone morphogenetic protein 2. Hum Gene Ther 13: 1201-1211.

Lee MH, Javed A, Kim HJ, Shin HI, Gutierrez S, Choi JY, Rosen V, Stein JL, van Wijnen AJ, Stein GS, Lian JB and Ryoo HM (1999) Transient upregulation of CBFA1 in response to bone morphogenetic protein-2 and transforming growth factor beta1 in C2C12 myogenic cells coincides with suppression of the myogenic phenotype but is not sufficient for osteoblast differentiation. J Cell Biochem 73: 114-125.

Lee MH, Kim YJ, Kim HJ, Park HD, Kang AR, Kyung HM, Sung JH, Wozney JM, Kim HJ and Ryoo HM (2003) BMP-2-induced Runx2 expression is mediated by Dlx5, and TGF-beta 1 opposes the BMP-2-induced osteoblast differentiation by suppression of Dlx5 expression. J Biol Chem 278: 34387-34394.

Levanon D, Negreanu V, Bernstein Y, Bar-Am I, Avivi L and Groner Y (1994) AML1, AML2, and AML3, the human members of the runt domain gene-family: cDNA structure, expression, and chromosomal localization. Genomics 23: 425-432.

Li J, Tsuji K, Komori T, Miyazono K, Wrana JL, Ito Y, Nifuji A and Noda M (1998) Smad2 overexpression enhances Smad4 gene expression and suppresses CBFA1 gene expression in osteoblastic osteosarcoma ROS17/2.8 cells and primary rat calvaria cells. J Biol Chem 273: 31009-31015.

Lieberman JR, Daluiski A, Stevenson S, Wu L, McAllister P, Lee YP, Kabo JM, Finerman GA, Berk AJ and Witte ON (1999) The effect of regional gene therapy with bone morphogenetic protein-2- producing bone-marrow cells on the repair of segmental femoral defects in rats. J Bone Joint Surg Am 81: 905-917.

Lieberman JR, Le LQ, Wu L, Finerman GA, Berk A, Witte ON and Stevenson S (1998) Regional gene therapy with a BMP-2-producing murine stromal cell line induces heterotopic and orthotopic bone formation in rodents. J Orthop Res 16: 330-339.

Lin AS, Barrows TH, Cartmell SH and Guldberg RE (2003) Microarchitectural and mechanical characterization of oriented porous polymer scaffolds. Biomaterials 24: 481-489.

Liu W, Toyosawa S, Furuichi T, Kanatani N, Yoshida C, Liu Y, Himeno M, Narai S, Yamaguchi A and Komori T (2001) Overexpression of Cbfa1 in osteoblasts inhibits osteoblast maturation and causes osteopenia with multiple fractures. J Cell Biol 155: 157-166.

Livingston T, Ducheyne P and Garino J (2002) In vivo evaluation of a bioactive scaffold for bone tissue engineering. J Biomed Mater Res 62: 1-13.

Locklin RM, Riggs BL, Hicok KC, Horton HF, Byrne MC and Khosla S (2001) Assessment of gene regulation by bone morphogenetic protein 2 in human marrow stromal cells using gene array technology. J Bone Miner Res 16: 2192-2204.

Locklin RM, Williamson MC, Beresford JN, Triffitt JT and Owen ME (1995) In vitro effects of growth factors and dexamethasone on rat marrow stromal cells. Clin Orthop 27-35.

Malaval L, Liu F, Roche P and Aubin JE (1999) Kinetics of osteoprogenitor proliferation and osteoblast differentiation in vitro. J Cell Biochem 74: 616-627.

Maniatopoulos C, Sodek J and Melcher AH (1988) Bone formation in vitro by stromal cells obtained from bone marrow of young adult rats. Cell Tissue Res 254: 317-330.

Marks SC and Hermey DC (1996) The Structure and Development of Bone. In: Bilezikian JP, Raisz LG and Rodan GA (eds) Principles of Bone Biology, pp 3-14. Academic Press, San Diego.

Marsh ME, Munne AM, Vogel JJ, Cui Y and Franceschi RT (1995) Mineralization of bone-like extracellular matrix in the absence of functional osteoblasts. J Bone Miner Res 10: 1635-1643.

Marshall CJ (1995) Specificity of receptor tyrosine kinase signaling: transient versus sustained extracellular signal-regulated kinase activation. Cell 80: 179-185.

McCarthy TL, Ji C, Chen Y, Kim KK, Imagawa M, Ito Y and Centrella M (2000) Runt domain factor (Runx)-dependent effects on CCAAT/ enhancer-binding protein delta expression and activity in osteoblasts. J Biol Chem 275: 21746-21753.

McLarren KW, Lo R, Grbavec D, Thirunavukkarasu K, Karsenty G and Stifani S (2000) The mammalian basic helix loop helix protein HES-1 binds to and modulates the transactivating function of the runt-related factor Cbfa1. J Biol Chem 275: 530-538.

Mehrara BJ, Saadeh PB, Steinbrech DS, Dudziak M, Spector JA, Greenwald JA, Gittes GK and Longaker MT (1999) Adenovirus-mediated gene therapy of osteoblasts in vitro and in vivo. J Bone Miner Res 14: 1290-1301.

Mendelsohn R, Hassankhani A, DiCarlo E and Boskey A (1989) FT-IR microscopy of endochondral ossification at 20 mu spatial resolution [published erratum appears in Calcif Tissue Int 1989 Jul;45(1):62]. Calcif Tissue Int 44: 20-24.

Merriman HL, van Wijnen AJ, Hiebert S, Bidwell JP, Fey E, Lian J, Stein J and Stein GS (1995) The tissue-specific nuclear matrix protein, NMP-2, is a member of the AML/CBF/PEBP2/runt domain transcription factor family: interactions with the osteocalcin gene promoter. Biochemistry 34: 13125-13132.

Meyers S, Lenny N and Hiebert SW (1995) The t(8;21) fusion protein interferes with AML-1B-dependent transcriptional activation. Mol Cell Biol 15: 1974-1982.

Meyers S, Lenny N, Sun W and Hiebert SW (1996) AML-2 is a potential target for transcriptional regulation by the t(8;21) and t(12;21) fusion proteins in acute leukemia. Oncogene 13: 303-312.

Miller J, Horner A, Stacy T, Lowrey C, Lian JB, Stein G, Nuckolls GH and Speck NA (2002) The core-binding factor beta subunit is required for bone formation and hematopoietic maturation. Nat Genet 32: 645-649.

Miyoshi H, Shimizu K, Kozu T, Maseki N, Kaneko Y and Ohki M (1991) t(8;21) breakpoints on chromosome 21 in acute myeloid leukemia are clustered within a limited region of a single gene, AML1. Proc Natl Acad Sci U S A 88: 10431-10434.

Moore WR, Graves SE and Bain GI (2001) Synthetic bone graft substitutes. Aust N Z J Surg 71: 354-361.

Moursi AM, Damsky CH, Lull J, Zimmerman D, Doty SB, Aota S and Globus RK (1996) Fibronectin regulates calvarial osteoblast differentiation. J Cell Sci 109 (Pt 6): 1369-1380.

Mundlos S (1999) Cleidocranial dysplasia: clinical and molecular genetics. J Med Genet 36: 177-182.

Mundlos S, Otto F, Mundlos C, Mulliken JB, Aylsworth AS, Albright S, Lindhout D, Cole WG, Henn W, Knoll JH, Owen MJ, Mertelsmann R, Zabel BU and Olsen BR (1997) Mutations involving the transcription factor CBFA1 cause cleidocranial dysplasia. Cell 89: 773-779.

Murphy WL, Kohn DH and Mooney DJ (2000) Growth of continuous bonelike mineral within porous poly(lactide-co- glycolide) scaffolds in vitro. J Biomed Mater Res 50: 50-58.

Musgrave DS, Bosch P, Ghivizzani S, Robbins PD, Evans CH and Huard J (1999) Adenovirus-mediated direct gene therapy with bone morphogenetic protein- 2 produces bone. Bone 24: 541-547.

Nakamura K, Kawaguchi H, Aoyama I, Hanada K, Hiyama Y, Awa T, Tamura M and Kurokawa T (1997) Stimulation of bone formation by intraosseous application of recombinant basic fibroblast growth factor in normal and ovariectomized rabbits. J Orthop Res 15: 307-313.

Nakashima K, Zhou X, Kunkel G, Zhang Z, Deng JM, Behringer RR and de Crombrugghe B (2002) The novel zinc finger-containing transcription factor osterix is required for osteoblast differentiation and bone formation. Cell 108: 17-29.

Nam YS, Yoon JJ and Park TG (2000) A novel fabrication method of macroporous biodegradable polymer scaffolds using gas foaming salt as a porogen additive. J Biomed Mater Res 53: 1-7.

Ogata T, Wozney JM, Benezra R and Noda M (1993) Bone morphogenetic protein 2 transiently enhances expression of a gene, Id (inhibitor of differentiation), encoding a helix-loop-helix molecule in osteoblast-like cells. Proc Natl Acad Sci U S A 90: 9219-9222.

Ogawa E, Maruyama M, Kagoshima H, Inuzuka M, Lu J, Satake M, Shigesada K and Ito Y (1993) PEBP2/PEA2 represents a family of transcription factors homologous to the products of the Drosophila runt gene and the human AML1 gene. Proc Natl Acad Sci U S A 90: 6859-6863.

Ohgushi H, Dohi Y, Tamai S and Tabata S (1993) Osteogenic differentiation of marrow stromal stem cells in porous hydroxyapatite ceramics. J Biomed Mater Res 27: 1401-1407.

Ohgushi H, Goldberg VM and Caplan AI (1989) Repair of bone defects with marrow cells and porous ceramic. Experiments in rats. Acta Orthop Scand 60: 334-339.

Okubo Y, Bessho K, Fujimura K, Konishi Y, Kusumoto K, Ogawa Y and Iizuka T (2000) Osteoinduction by recombinant human bone morphogenetic protein-2 at intramuscular, intermuscular, subcutaneous and intrafatty sites. Int J Oral Maxillofac Surg 29: 62-66.

Otto F, Lubbert M and Stock M (2003) Upstream and downstream targets of RUNX proteins. J Cell Biochem 89: 9-18.

Otto F, Thornell AP, Crompton T, Denzel A, Gilmour KC, Rosewell IR, Stamp GW, Beddington RS, Mundlos S, Olsen BR, Selby PB and Owen MJ (1997) Cbfa1, a candidate gene for cleidocranial dysplasia syndrome, is essential for osteoblast differentiation and bone development. Cell 89: 765-771.

Owen TA, Aronow M, Shalhoub V, Barone LM, Wilming L, Tassinari MS, Kennedy MB, Pockwinse S, Lian JB and Stein GS (1990b) Progressive development of the rat osteoblast phenotype in vitro: reciprocal relationships in expression of genes associated with osteoblast proliferation and differentiation during formation of the bone extracellular matrix. J Cell Physiol 143: 420-430.

Owen TA, Aronow M, Shalhoub V, Barone LM, Wilming L, Tassinari MS, Kennedy MB, Pockwinse S, Lian JB and Stein GS (1990a) Progressive development of the rat osteoblast phenotype in vitro: reciprocal relationships in expression of genes associated with osteoblast proliferation and differentiation during formation of the bone extracellular matrix. J Cell Physiol 143: 420-430.

Park SR, Oreffo RO and Triffitt JT (1999) Interconversion potential of cloned human marrow adipocytes in vitro. Bone 24: 549-554.

Park YJ, Lee YM, Lee JY, Seol YJ, Chung CP and Lee SJ (2000) Controlled release of platelet-derived growth factor-BB from chondroitin sulfate-chitosan sponge for guided bone regeneration. J Control Release 67: 385-394.

Partridge K, Yang X, Clarke NM, Okubo Y, Bessho K, Sebald W, Howdle SM, Shakesheff KM and Oreffo RO (2002) Adenoviral BMP-2 gene transfer in mesenchymal stem cells: in vitro and in vivo bone formation on biodegradable polymer scaffolds. Biochem Biophys Res Commun 292: 144-152.

Pear WS, Nolan GP, Scott ML and Baltimore D (1993) Production of high-titer helper-free retroviruses by transient transfection. Proc Natl Acad Sci U S A 90: 8392-8396.

Peng H, Chen ST, Wergedal JE, Polo JM, Yee JK, Lau KH and Baylink DJ (2001) Development of an MFG-based retroviral vector system for secretion of high levels of functionally active human BMP4. Mol Ther 4: 95-104.

Perry CR (1999) Bone repair techniques, bone graft, and bone graft substitutes. Clin Orthop 71-86.

Pratap J, Galindo M, Zaidi SK, Vradii D, Bhat BM, Robinson JA, Choi JY, Komori T, Stein JL, Lian JB, Stein GS and van Wijnen AJ (2003) Cell growth regulatory role of Runx2 during proliferative expansion of preosteoblasts. Cancer Res 63: 5357-5362.

Prince M, Banerjee C, Javed A, Green J, Lian JB, Stein GS, Bodine PV and Komm BS (2001) Expression and regulation of Runx2/Cbfa1 and osteoblast phenotypic markers during the growth and differentiation of human osteoblasts. J Cell Biochem 80: 424-440.

Quarles LD, Yohay DA, Lever LW, Caton R and Wenstrup RJ (1992) Distinct proliferative and differentiated stages of murine MC3T3-E1 cells in culture: an in vitro model of osteoblast development. J Bone Miner Res 7: 683-692.

Quarto R, Mastrogiacomo M, Cancedda R, Kutepov SM, Mukhachev V, Lavroukov A, Kon E and Marcacci M (2001) Repair of large bone defects with the use of autologous bone marrow stromal cells. N Engl J Med 344: 385-386.

Quarto R, Thomas D and Liang CT (1995) Bone progenitor cell deficits and the age-associated decline in bone repair capacity. Calcif Tissue Int 56: 123-129.

Reddi AH (1994) Symbiosis of biotechnology and biomaterials: applications in tissue engineering of bone and cartilage [see comments]. J Cell Biochem 56: 192-195.

Robey PG and Boskey A (1996) The Biochemistry of Bone. In: Marcus R, Feldman D and Kelsey J. (eds) Osteoporosis, pp 95-182. Academic Press, San Diego.

Sato M, Morii E, Komori T, Kawahata H, Sugimoto M, Terai K, Shimizu H, Yasui T, Ogihara H, Yasui N, Ochi T, Kitamura Y, Ito Y and Nomura S (1998) Transcriptional regulation of osteopontin gene in vivo by PEBP2alphaA/CBFA1 and ETS1 in the skeletal tissues. Oncogene 17: 1517-1525.

Satomura K, Krebsbach P, Bianco P and Gehron RP (2000) Osteogenic imprinting upstream of marrow stromal cell differentiation. J Cell Biochem 78: 391-403.

Schmitz JP and Hollinger JO (1986) The critical size defect as an experimental model for craniomandibulofacial nonunions. Clin Orthop 299-308.

Schmitz JP, Schwartz Z, Hollinger JO and Boyan BD (1990) Characterization of rat calvarial nonunion defects. Acta Anat (Basel) 138: 185-192.

Shi S, Gronthos S, Chen S, Reddi A, Counter CM, Robey PG and Wang CY (2002) Bone formation by human postnatal bone marrow stromal stem cells is enhanced by telomerase expression. Nat Biotechnol 20: 587-591.

Shors EC (1999) Coralline bone graft substitutes. Orthop Clin North Am 30: 599-613.

Shui C, Spelsberg TC, Riggs BL and Khosla S (2003) Changes in Runx2/Cbfa1 expression and activity during osteoblastic differentiation of human bone marrow stromal cells. J Bone Miner Res 18: 213-221.

Sikavitsas VI, Dolder JJ, Bancroft GN, Jansen JA and Mikos AG (2003) Influence of the in vitro culture period on the in vivo performance of cell/titanium bone tissue-engineered constructs using a rat cranial critical size defect model. J Biomed Mater Res 67A: 944-951.

Simonsen JL, Rosada C, Serakinci N, Justesen J, Stenderup K, Rattan SI, Jensen TG and Kassem M (2002) Telomerase expression extends the proliferative life-span and maintains the osteogenic potential of human bone marrow stromal cells. Nat Biotechnol 20: 592-596.

Sodek J and Berkman FA (1987) Bone cell cultures. Methods Enzymol 145: 303-324.

Sokal RR and Rohlf FJ (1980) Biometry. W.H. Freeman and Company, New York, NY.

Springer ML and Blau HM (1997) High-efficiency retroviral infection of primary myoblasts. Somat Cell Mol Genet 23: 203-209.

Stein GS, Lian JB and Owen TA (1990) Relationship of cell growth to the regulation of tissue-specific gene expression during osteoblast differentiation. FASEB J 4: 3111-3123.

Sudhakar S, Li Y, Katz MS and Elango N (2001) Translational regulation is a control point in RUNX2/Cbfa1 gene expression. Biochem Biophys Res Commun 289: 616-622.

Sudo H, Kodama HA, Amagai Y, Yamamoto S and Kasai S (1983) In vitro differentiation and calcification in a new clonal osteogenic cell line derived from newborn mouse calvaria. J Cell Biol 96: 191-198.

Takeda S, Bonnamy JP, Owen MJ, Ducy P and Karsenty G (2001) Continuous expression of Cbfa1 in nonhypertrophic chondrocytes uncovers its ability to induce hypertrophic chondrocyte differentiation and partially rescues Cbfa1-deficient mice. Genes Dev 15: 467-481.

Ter Brugge PJ and Jansen JA (2002) In vitro osteogenic differentiation of rat bone marrow cells subcultured with and without dexamethasone. Tissue Eng 8: 321-331.

Thirunavukkarasu K, Halladay DL, Miles RR, Yang X, Galvin RJ, Chandrasekhar S, Martin TJ and Onyia JE (2000) The osteoblast-specific transcription factor Cbfa1

contributes to the expression of osteoprotegerin, a potent inhibitor of osteoclast differentiation and function. J Biol Chem 275: 25163-25172.

Thirunavukkarasu K, Mahajan M, McLarren KW, Stifani S and Karsenty G (1998) Two domains unique to osteoblast-specific transcription factor Osf2/Cbfa1 contribute to its transactivation function and its inability to heterodimerize with Cbfbeta. Mol Cell Biol 18: 4197-4208.

Tintut Y, Parhami F, Le V, Karsenty G and Demer LL (1999) Inhibition of osteoblast-specific transcription factor Cbfa1 by the cAMP pathway in osteoblastic cells. Ubiquitin/proteasome-dependent regulation. J Biol Chem 274: 28875-28879.

Tsuji K, Ito Y and Noda M (1998) Expression of the PEBP2alphaA/AML3/CBFA1 gene is regulated by BMP4/7 heterodimer and its overexpression suppresses type I collagen and osteocalcin gene expression in osteoblastic and nonosteoblastic mesenchymal cells. Bone 22: 87-92.

Ueta C, Iwamoto M, Kanatani N, Yoshida C, Liu Y, Enomoto-Iwamoto M, Ohmori T, Enomoto H, Nakata K, Takada K, Kurisu K and Komori T (2001) Skeletal malformations caused by overexpression of Cbfa1 or its dominant negative form in chondrocytes. J Cell Biol 153: 87-100.

Urist MR (1965) Bone: formation by autoinduction. Science 150: 893-899.

Vacanti CA and Bonassar LJ (1999) An overview of tissue engineered bone. Clin Orthop 367: S375-S381.

Wang J and Glimcher MJ (1999) Characterization of matrix-induced osteogenesis in rat calvarial bone defects: II. Origins of bone-forming cells. Calcif Tissue Int 65: 486-493.

Wang SW and Speck NA (1992) Purification of core-binding factor, a protein that binds the conserved core site in murine leukemia virus enhancers. Mol Cell Biol 12: 89-102.

Weinreb M, Shinar D and Rodan GA (1990) Different pattern of alkaline phosphatase, osteopontin, and osteocalcin expression in developing rat bone visualized by in situ hybridization. J Bone Miner Res 5: 831-842.

Wennberg C, Hessle L, Lundberg P, Mauro S, Narisawa S, Lerner UH and Millan JL (2000) Functional characterization of osteoblasts and osteoclasts from alkaline phosphatase knockout mice [In Process Citation]. J Bone Miner Res 15: 1879-1888.

Whang K, Tsai DC, Nam EK, Aitken M, Sprague SM, Patel PK and Healy KE (1998) Ectopic bone formation via rhBMP-2 delivery from porous bioabsorbable polymer scaffolds. J Biomed Mater Res 42: 491-499.

Wijmenga C, Speck NA, Dracopoli NC, Hofker MH, Liu P and Collins FS (1995) Identification of a new murine runt domain-containing gene, Cbfa3, and localization of the human homolog, CBFA3, to chromosome 1p35-pter. Genomics 26: 611-614.

Wozney JM (2002) Overview of bone morphogenetic proteins. Spine 27: S2-S8.

Xiao G, Jiang D, Thomas P, Benson MD, Guan K, Karsenty G and Franceschi RT (2000) MAPK pathways activate and phosphorylate the osteoblast-specific transcription factor, Cbfa1. J Biol Chem 275: 4453-4459.

Xiao G, Wang D, Benson MD, Karsenty G and Franceschi RT (1998a) Role of the alpha2-integrin in osteoblast-specific gene expression and activation of the Osf2 transcription factor. J Biol Chem 273: 32988-32994.

Xiao ZS, Hinson TK and Quarles LD (1999) Cbfa1 isoform overexpression upregulates osteocalcin gene expression in non-osteoblastic and pre-osteoblastic cells. J Cell Biochem 74: 596-605.

Xiao ZS, Liu SG, Hinson TK and Quarles LD (2001) Characterization of the upstream mouse Cbfa1/Runx2 promoter. J Cell Biochem 82: 647-659.

Xiao ZS, Thomas R, Hinson TK and Quarles LD (1998b) Genomic structure and isoform expression of the mouse, rat and human Cbfa1/Osf2 transcription factor. Gene 214: 187-197.

Yang S, Wei D, Wang D, Phimphilai M, Krebsbach PH and Franceschi RT (2003) In vitro and in vivo synergistic interactions between the Runx2/Cbfa1 transcription factor and bone morphogenetic protein-2 in stimulating osteoblast differentiation. J Bone Miner Res 18: 705-715.

Yaszemski MJ, Payne RG, Hayes WC, Langer R and Mikos AG (1996) Evolution of bone transplantation: molecular, cellular and tissue strategies to engineer human bone. Biomaterials 17: 175-185.

Yoshikawa T, Ohgushi H, Akahane M, Tamai S and Ichijima K (1998) Analysis of gene expression in osteogenic cultured marrow/hydroxyapatite construct implanted at ectopic sites: a comparison with the osteogenic ability of cancellous bone. J Biomed Mater Res 41: 568-573.

Zaidi SK, Sullivan AJ, van Wijnen AJ, Stein JL, Stein GS and Lian JB (2002) Integration of Runx and Smad regulatory signals at transcriptionally active subnuclear sites. Proc Natl Acad Sci U S A 99: 8048-8053.

Zein I, Hutmacher DW, Tan KC and Teoh SH (2002) Fused deposition modeling of novel scaffold architectures for tissue engineering applications. Biomaterials 23: 1169-1185.

Zelzer E, Glotzer DJ, Hartmann C, Thomas D, Fukai N, Soker S and Olsen BR (2001) Tissue specific regulation of VEGF expression during bone development requires Cbfa1/Runx2. Mech Dev 106: 97-106.

Zheng C, Baum BJ, Iadarola MJ and O'Connell BC (2000) Genomic integration and gene expression by a modified adenoviral vector. Nat Biotechnol 18: 176-180.